KATHOLIEKE UNIVERSITEIT LEUVEN

FACULTY OF SCIENCE
Department of Chemistry
Division of Coordination Chemistry

Application of optical spectroscopy to distinguish natural, treated and synthetic rubies

by

Thomas SUETENS

Supervisor: Prof. Koen Binnemans
Mentor: Dr. Svetlana V. Eliseeva

Dissertation presented in fulfillment of the requirements for the degree of Master in Chemistry

Academic year 2010-2011

Acknowledgments

I see this masterthesis as a journey. A journey through a rough and relatively unexplored terrain that would not have ended well if I hadn't had the help of many people along the way. I would like to thank all of them:

The first person is my promoter Prof. Koen Binnemans for taking me under his wing when I told him I wanted to do something with minerals. I know there would never have been a topic if I hadn't asked, but he created the opportunity just for me. I would also like to thank him for giving a lot of advice and suggestions and for reading my text multiple times to get the best out of it.
The second person is my mentor Dr. Svetlana V. Eliseeva for teaching me how to work with the instruments, for giving insight in the meaning of the spectra that were collected and for reading my text to filter out all the grammatical errors I couldn't find myself. I also appreciate the long talks in the dark noisy room that helped me stay sane through it all.
All the people who have made their rubies accessible to me. Without those samples I would not have had anyting to write about here. Thank you Guido Crauwels and ACAM, Ivo Quintens, Jan Elsen, Koen Binnemans and Paul Tambuyser.
Prof. Marc Hendrickx for taking the time to look into the spectra of the ruby with me.
Rita Jungbluth for her administrative support.
All of the people in the COC group for accepting me in their group of friends with their many fun activities and for offering support when I needed it.
My friends in the last year of chemistry for the fun note at work, for the many fun nights we had with the caféplan, FIFA-nights and chemika-activities. It was a good final year to conclude our five years together.
My friends at our little comfortable place in the quiet Zevenslapersstraat for the moral support and the many fun times we had. There is one person here that I can't thank enough. Tina, thank you for the unceasing support you kept showing, even when things got tough, thank you for everything.
All the people I have known during my time in Leuven for making me the person who I am now.
And finally, I would like to thank my parents for having confidence in me and for giving me the opportunity to be able to study for these five long years.

Table of Contents

Introduction

This work handles about the distinction of different types of rubies using optical spectroscopy. Different types of measurement were used, including absorption, excitation, emission and decay time measurements. Differences in the spectra between ruby types have been sought and defined as parameters with the single purpose of finding a tool to distinguish different types of rubies by one or more of these parameters.
The optical spectroscopy technique was chosen for this research because it is relatively cheap and underdeveloped. Its possibilities for application were abandoned because spectra with a sufficiently detailed resolution could only be achieved by extreme cooling. This problem is no longer a concern because better equipment made it possible to get the same resolution at room temperature.

The first chapter focuses on situating the problem of natural and synthetic rubies that tend to become harder and harder to identify by the use of traditional techniques such as optical microscopy. A brief introduction in the mineralogical and geological properties of the ruby is given, followed by the history of the development of the synthetic ruby. This is necessary to get a grasp of how many different rubies there are in the world. The chapter is completed by a discussion of the techniques that are used to identify rubies, focusing on the working principle of the technique, along with its availability and cost.
The second chapter gives a detailed description of the instruments that were used along with how each of the measurements is performed.
The third chapter discusses how the data of the measurements are used to collect the parameters of which is thought that they can be used as a tool to differentiate between ruby types.
The fourth and final chapter describes how the parameter values that were obtained in chapter three can be used. Here it is shown that for some parameters, a boxplot graph showing the boxplots of all the measured types for one parameter, can already make a distinction between different geological backgrounds of rubies. It also shows that when two parameters that show a good distinction are used together, area plots can be set up where different origins are spatially separated on the graph.

Chapter 1: Situating the problem

1.1 Natural ruby

1.1.1 Physical properties of ruby

Rubies and sapphires are special varieties of the mineral corundum (Al_2O_3). Because of this, they have the same mineralogical properties as corundum. The only difference between a ruby and normal corundum is that ruby contains Cr-impurities that give the mineral the typical red color. In this case, the Cr^{3+}-ion replaces an Al^{3+}-ion in the crystal structure. Other impurities are also possible, but only stones with the red color are called rubies while stones with other colors are called sapphires. Corundum and all its varieties are classified as oxides in the hematite group.

One of the most important properties of the mineral is its hardness. Corundum is used in the scale of Mohs as a reference species for the value 9. Only a very select amount of minerals have the same or a higher hardness. This high hardness is perfect for the use of these minerals in gemological applications since the material will not be scratched by anything it comes into contact with. This maintains the beauty of the stone while it is used. Some other properties of corundum are given in Table 1.

Table 1. Mineralogical and structural properties of corundum [RalCha11].

Transparency	Transparent, Translucent, Opaque
Cleavage	None observed
Fracture	Irregular/Uneven, Conchoidal
Density (g/cm³)	3.98 – 4.1
Melting point (°C)	2044
Crystal System	Trigonal
Cell Parameters (Å)	a = 4.75, c = 12.982
Unit Cell Volume (Å³)	253.54
Z	6

The Z-value is the amount of times the structural formula of a mineral is repeated in the unit cell.

The structure of corundum is given in Figures 1-3. The red balls are the Al^{3+} -ions and the white ones are the O^{2+} -ions. Figure 1 shows the unit cell. Figures 2 and 3 show

how this seemingly random positioning results in a structure pattern. Figure 2 is a view along the a-axis, while Figure 3 is a view along the c-axis.

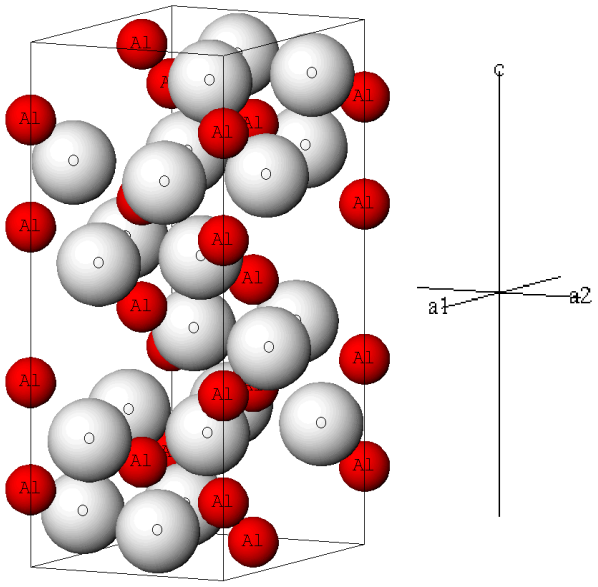

Figure 1. Unit cell of corundum.

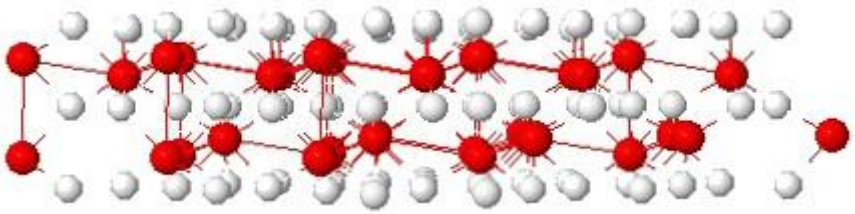

Figure 2. Structure of corundum viewed along the a-axis. Separate layers of O and Al atoms can be seen.

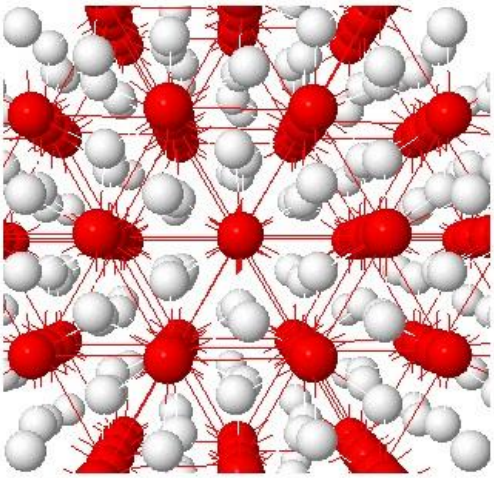

Figure 3. Structure of corundum viewed along the c-axis. Stacking of the O and Al ions can be seen. The difference in the surrounding ions between O and Al is also shown.

Crystals can be divided into two classes according to the way in which they refract light. The first type is the singly refractive crystals which consist of all amorphous and isometric (belonging to the cubic system) materials. All other materials are of the doubly refractive type, including rubies. While entering a doubly refractive gemstone, the light will be split into two perpendicular beams. This will result in different paths through the gem and thus another speed and refractive index for each of the two beams. These two light beams will be absorbed in a different way, resulting in two different colors. This effect is called *pleochroism*. Looking at the gem from another angle results in different coloration of the gem.

Like all crystals of the trigonal system, rubies have an optical axis along the c-axis. Light entering a gem along the optical axis acts as if it passes through a singly refractive crystal, resulting in different optical effects like for instance showing no pleochroism as this is an effect that can only be observed with doubly refractive materials. [Smi08]

Natural gemstones will almost always be cut with the table (the flat top of the gemstone) perpendicular to the optical axis. This is done to minimize the amount of ruby that has to be cut off the rough natural stone. Also, the second color in the ruby originating from its pleochroism is unwanted because it is less pretty. However, the color is extremely important for the value of a gemstone so most gem cutters will try to cut a ruby in the described way. Synthetic ruby is another story.

Synthetic gems are less valuable than natural ones, so the price difference resulting from the color is not that important. The cuts are also made to minimize the amount that has to be cut away, but because of a different orientation of the c-axis the result is different. A Verneuil boule is split through the center along a parting plane to reduce the tension inside this boule before the stone is cut. The orientation of the c-axis of a boule can be chosen by the placement of the seed crystal at the bottom of the boule. For gemological purposes however, this is of less importance. The c-axis will always be in the parting plane of the boule, no matter which orientation is chosen. After the boule has been split, the gems are cut from it as is shown in Figure 4.

The direction of strongest pleochroism in a cut ruby is different for most natural and synthetic rubies as can be seen in Figure 4. This results in a more explicit pleochroism in synthetic cut rubies, where it is often even absent in natural cut rubies when observed through the top facet [Hug97].

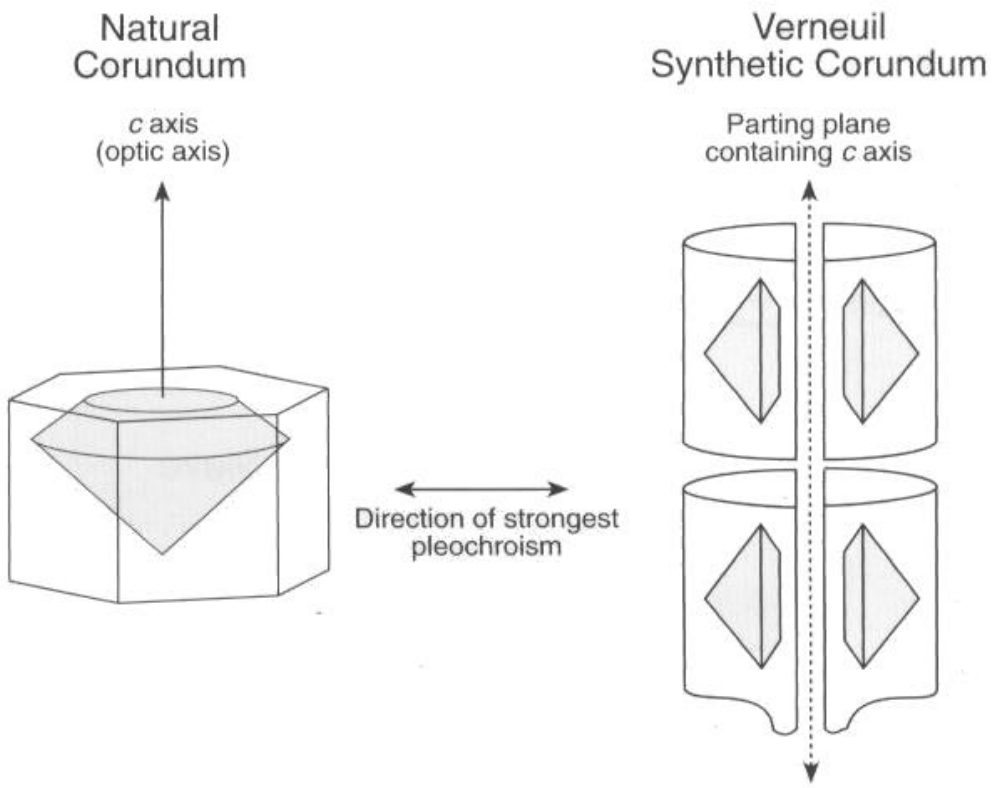

Figure 4. Orientation of the c axis in cut rubies [Hug97].

1.1.2 Geological origin of ruby

The formation of rubies is a rare process, because a lot of conditions have to be met before it can happen. The first condition is a completely silicium-deficient environment. This is because when silicium is present, more abundant minerals like kyanite, feldspars, and micas will be formed instead of corundum [MuhFri98]. Alongside this difficult condition, the correct impurities, the correct pressures, and the right temperatures have to be present. There are three methods of formation known, each one resulting in rubies with slightly different properties. These are basalt-hosted, marble-hosted, and metasomatic rubies.

1.1.2.1 Basalt-hosted rubies

Rubies of this type are found as secondary deposits associated with alkali basalts. How the rubies are formed is not very well understood, but two possible origins have been proposed so far. The first one suggests a mixing of magma at midcrustal levels [GuoORe96a][GuoORe96b], while the other implies on a formation from pegmatite-like crystallization of silica-poor magmas in the deep crust or upper mantle [CoeVic95]. The minerals that have been found around the rubies point out that they were formed in an iron and sulphur rich environment [Coe92]. A higher iron-content than in most other

natural origins is found in this type of ruby. Rubies from Thailand and Pailin (Cambodia) are examples of this type.

1.1.2.2 Marble-hosted rubies

As the name suggests, rubies of the marble-hosted type are found in marbles. It is commonly thought that a regional metamorphism process transformed limestone by heat and pressure into this type of ruby deposits [OkrBun76]. As for the basalt-hosted rubies, the composition in terms of impurities is indicated by associated minerals. Traces of Si, S, K, Ti, V, and Cr are common in these rubies. The level of Fe is low however, resulting in different shades of red in comparison with basalt-hosted rubies [MuhFri98]. Rubies of this type occur at different locations. The most famous rubies are those of Mogok and Mong Hsu (Myanmar), Luc Yen (Vietnam), and also Yegdalek (Afghanistan). Other finding locations of rubies of this type used in this masterthesis are Sagin Town (Myanmar), Qui Chau (Vietnam), and Moragoro (Tanzania).

1.1.2.3 Metasomatic rubies

Metasomatic rubies are rubies that are formed by a metamorphic process in which fluids exchange chemical components of the minerals altering them drastically. In the case of rubies, this is mostly a desilication process that removes Si form the material and leaves the Al and O resulting in the formation of corundum [MuhFri98]. Because this process heavily depends on the rock type in which it occurs, different compositions are achieved. Both low and high Fe contents have been measured. Some marble-hosted rubies like Mogok (Myanmar) are also suggested to be of the metasomatic type [MuhFri98]. Rubies of India, Kenya, Madagascar, Malawi, and Sri Lanka can also be of the metasomatic type.

1.2 Synthetic ruby

1.2.1 History of synthetic rubies

Precious stones have always had a great appeal to man. Their rare nature and beautiful appearance make them interesting for commercial applications. Before transactions were made easier by use of money, traders had to carry precious lightweight products with them, which were valuable regardless of the region they travelled to. Usually silks, gems, spices or precious metals were used for this purpose.

However, because precious stones are so rare, supply could not follow the high demand. This drove man to try and reproduce these stones artificially.

One of the first reported stories about the reproduction of gemstones is the fabrication of lapis lazuli in Egypt. The rich azure hue of this mineral made it very popular in Egypt. However, the source was distant and the production could not meet the demand of the people. A solution was sought by forgers to profit from this growing interest in the material. They began to sell another much cheaper mineral (steatite) that they had glazed blue to make it resemble lapis lazuli. Jewellery that dates back to 4000 BC was found showing these false “lapis lazuli” stones. Of course, these imitations are not really synthetic replications as they are of completely different composition and properties. However, the idea behind the synthesis of synthetic stones was already present. It also shows just how long people have already been thinking about the creation of synthetic gemstones. This is why it can be seen as the “birth” of the synthetic gem industry [Hug97].

Many years have passed since then, and new definitions of synthetic gems have been accepted. A synthetic stone should duplicate multiple properties of a natural gem including chemical composition, crystal structure, mineralogical properties, and appearance. The synthesis of true synthetic gemstones became possible only after the deeper knowledge of chemical composition and structure was achieved as well as new techniques allowing to reach much higher synthesis temperatures were developed. The first time for this to actually happen was in the 19th century AD [Hug97].

The ruby was a gemstone of great interest and the synthesis of ruby has known a long history. Many methods were examined and finally some progress was achieved. The first notable synthetic rubies were those of Edmond Frémy obtained by a flux method. In his experiments, 20-30 kg of an aluminum oxide was heated in a lead oxide melt using a large porcelain container for a period of 20 days. During this period of time, the crystallization occurred and very small crystals were formed. One of his experiments resulted in 24,000 crystals with a total weight of 1200 g. They were formed in a porcelain container of 12 litres. The small dimensions of the stones and the high cost of the production made the technique not very interesting for the commercial production of gemstones. However, this did not prevent some of the larger crystals to be actually used in jewellery [Elw79].

Around 1886 a new type of synthetic ruby appeared on the market out of nowhere. It is still not exactly known where they came from and who made them, but their quality was good enough to pass as natural rubies for a while until some jewelers became

suspicious and had them studied. Tiny bubbles present in the stones hinted at their synthetic origin [Elw79]. These stones were the ‘Geneva’ rubies.

One of the students of Frémy, Auguste Verneuil, was intrigued by the success of these Geneva rubies and started experiments with the synthesis of ruby crystals using another method than used by his mentor: oxy-hydrogen torches. There had already been some experiments with this technique by Gaudin in 1869 to synthesize blue sapphire, emerald and other gem types. Verneuil kept improving this method to create his own process to synthesize rubies.

It is this method that has revolutionized the whole concept of synthetic gem creation. Even now, more than 100 years after it was developed, the overall process remains largely unchanged. Also, at the moment, more than 90% of all the synthetic corundum produced worldwide is synthesized by this method [Hug97].

The most important aspect that makes these ‘Verneuil’ stones so interesting and successful is their extreme purity which results in a clear color and high transparency. They can also be made in quite large sizes and they are cheap.

1.2.2 Advanced synthetic rubies and treatments

After many years, the development in ruby synthesis has continued and many new methods have been developed. These new stones all strive to give the best properties to serve their purpose. Jewelers have developed several methods to distinguish natural from synthetic rubies. For this reason, gem-makers have continued to try to make synthetic gems whose properties more and more resemble natural stones. To do this, the reports that explained the differences between natural and synthetic stones were often used against the technique. Doping with metals occurring in natural stones has been done to make the synthetic stones pass the most recent tests [MuhFri98].

In this chapter, the three main types of synthetic rubies and some of the most common treatments of natural rubies will be discussed.

1.2.2.1 Melt synthesis

The most used method to create synthetic rubies remains the melt up of starting products, mixing to get a perfect blend of Al_2O_3 and the coloring agent and impurities, and solidification of the material into synthetic stones. The Verneuil method is an example of the melt type rubies. The minimum working temperature for making synthetic rubies is above 2044°C when a melt based method is used because this is

the melting point of corundum. A higher temperature is mostly used to make sure that all of the material is present in a molten state before crystallization.

In the Verneuil method, a fine Al_2O_3 powder is melted inside an oxyhydrogen flame along with the coloring agent. The flame itself is directed downward with the Al_2O_3 powder falling through the center of the flame. A gentle tapping of the Al_2O_3 powder container will force powder through a sieve at a steady and controlled pace.

The Verneuil method itself is a textbook example of how innovative thinking can be used to solve the problems of predecessors without giving up on the technique they were using. One of the problems that had to be overcome was the complete melt of the powder in the flame resulting in the formation of a large molten blob of material that would crack when the flames were turned off. This cracked material was not suited for gem use. Verneuil overcame the problem by lowering the temperature of the flame resulting in partially melted powder that forms a sinter cone. When this sinter cone grows, it will eventually reach the hottest part of the flame (2200°C), resulting in the complete melt of the top of the cone. After this has happened, the material that is deposited on top of the cone will also be completely melted. This contact point between melt and support should be kept as narrow as possible to prevent cracking. After the formation of the neck (contact point) the boule is allowed to widen by letting the boule enter the hotter and wider parts of the flame. After that, the supply of powder and the temperature of the flame are increased to get an optimal diameter. As the boule grows, it is simultaneously lowered at a steady pace to keep the formation at a certain height to ensure constant formation conditions. The top of the boule must be closely monitored. When is starts to look as if it is boiling, the flame is too hot, causing gas bubbles to be formed inside the material by the excess O_2 in the flame. Lowering the cone and the temperature of the flame will stop the top from “boiling”.

To release the tension inside the boule it is either split along a parting plane by a gentle tap of a hammer after the process is finished and the system is cooled down, or by rotating and reheating the growing boule. The latter is done only when the boule shape is desired, such as in cover glasses for applications such as watches. The high hardness of the material protects the cover glass from scratching. For the synthesis of gems, the boule shape is not required.

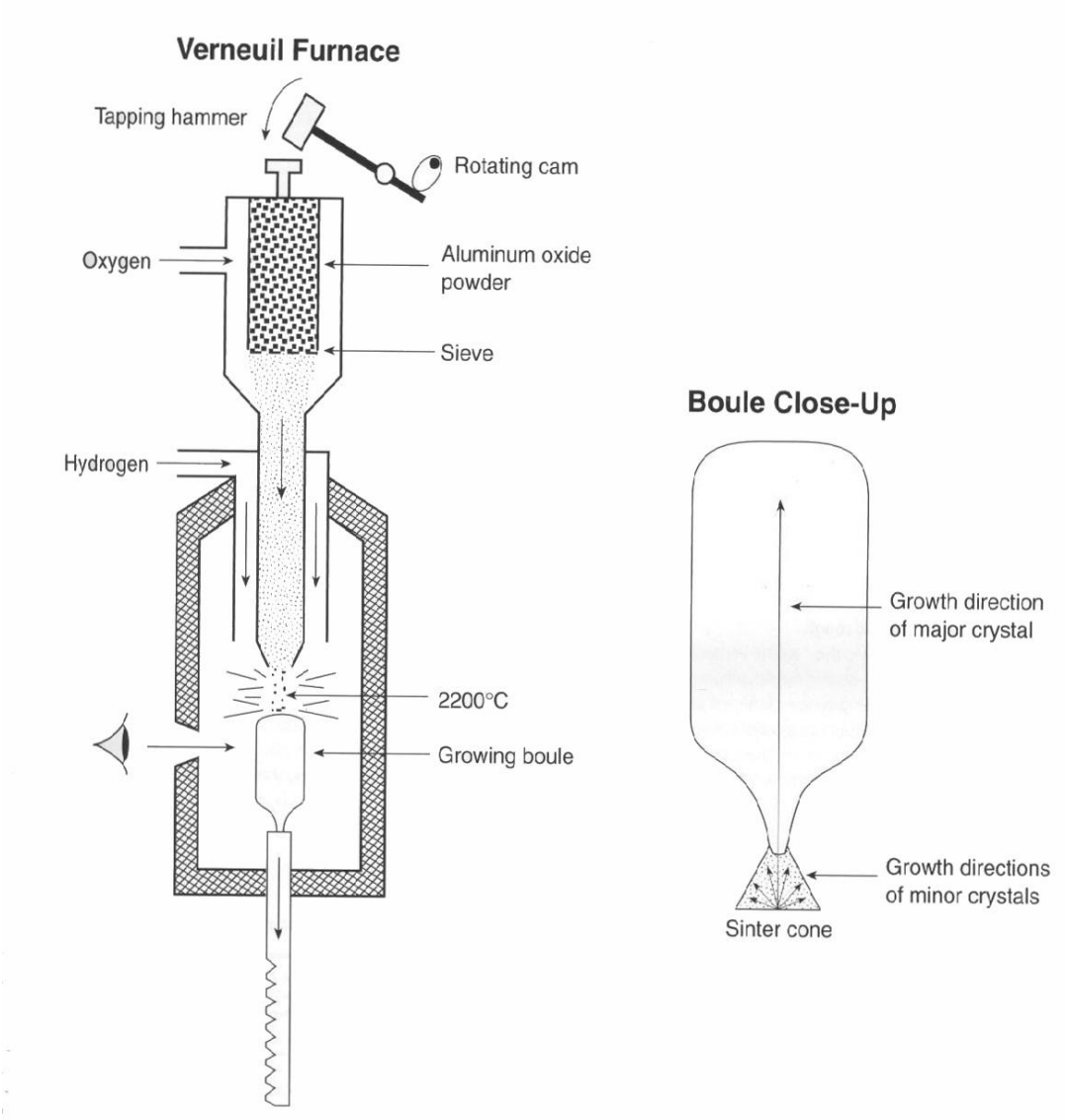

Figure 5. Verneuil method [Hug97].

The stones made by the Verneuil method are not always of a high enough quality. After cooling down, the boules start displaying several cracks and certain impurities like little gas inclusions degrade the optical quality of the material. The laser-market has had growing needs for rubies from the 1960's onward, resulting in a need for long, very pure crystals. These are often created by a technique that was first developed in 1918 by J. Czochralski [Elw79]. In this technique, the synthetic material is pulled in a rotary fashion from the melt to create long rods with identical properties over the entire length (Figure 6).

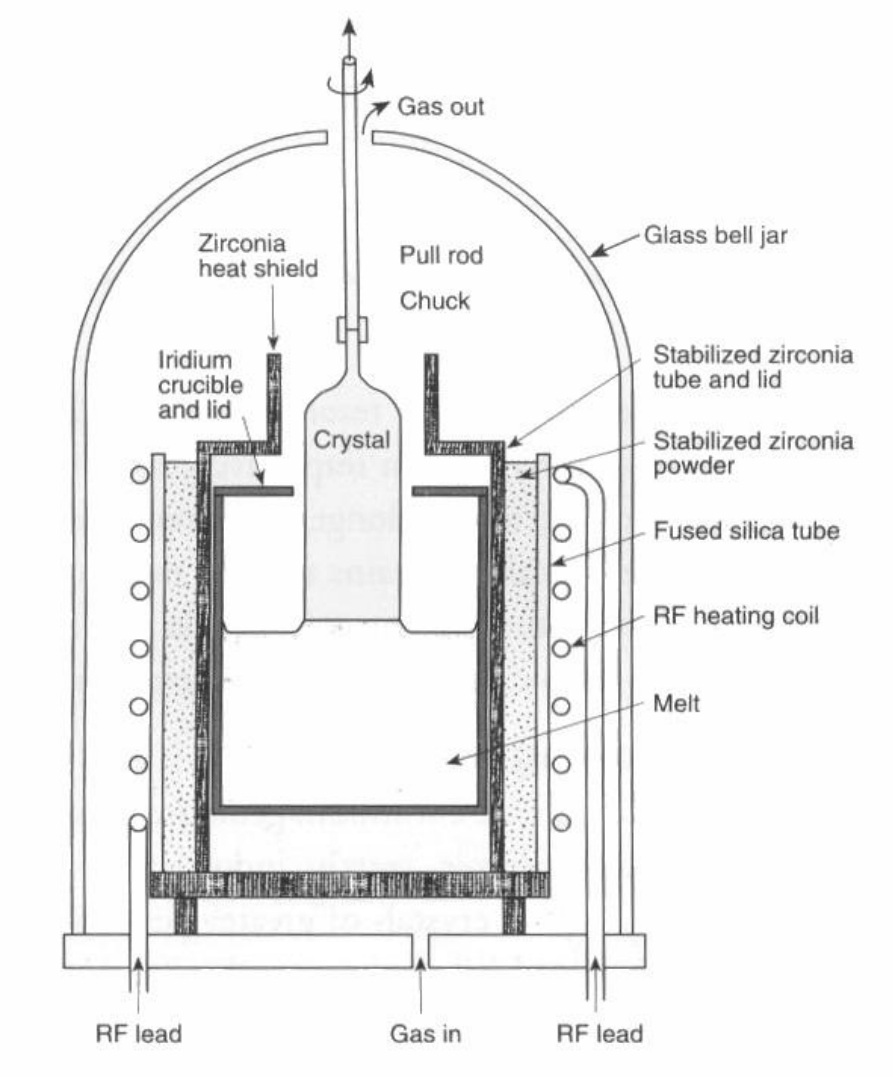

Figure 6. Czochralski method [Hug97].

Another melt based method is the *floating-zone process* (Figure 7). These material made by this method is mostly used for gems. In this technique aluminum and chromic oxides are sintered in a rod. While the whole rod is rotated vertically, the lower end of the rod is partially melted and subsequently lowered through the heating zone. The surface tension keeps the rod together and a ruby crystal is formed after the molten zone has passed. The most interesting part about this method is that impurities tend to remain in the molten zone. This causes the impurities to be filtered out of the rod and collected at the end part resulting in very pure crystals.

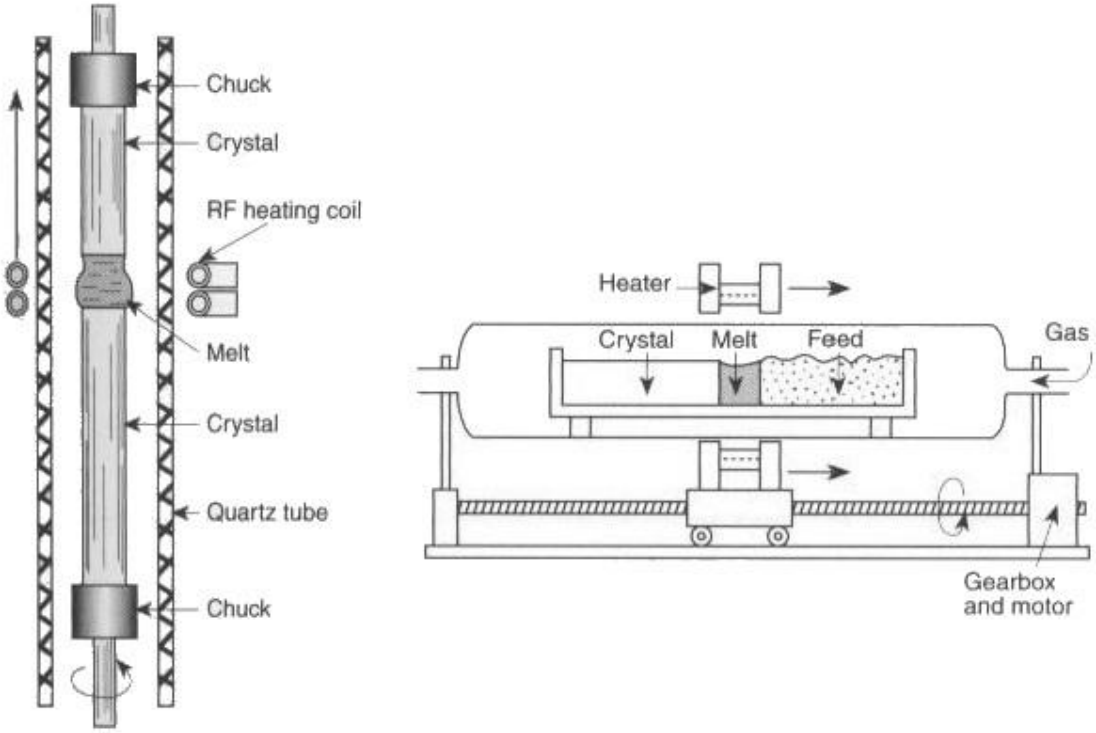

Figure 7. Floating-zone method [Hug97].

1.2.2.2 Flux synthesis

The flux method uses a flux to crystallize new rubies from solution. A flux is a liquid that can dissolve other substances when these are added to the flux. Materials that are solid at room temperature that can become liquid upon heating can also act as a flux. A flux is used to make rubies at temperatures significantly (around 1000°C [Leb11]) lower than the melting point of corundum [Hug97]. The flux and the compounds for the ruby are first mixed so a good distribution of the material over the whole solution is achieved. This happens at a temperature only slightly above the saturation point of ruby in the flux. When the temperature is lowered, the new rubies will crystallize. Depending on the flux used, gems with different properties can be made. The fluxes used by some manufacturers are given in Table 2.

Table 2 Flux composition for different flux method ruby manufacturers [Hug97].

Manufacturer	Flux used
Chatham	Li_2O-MoO_3-PbF_2 and/or $PbO_2Na_3AlF_6$
Douros	Pb-based compound
Kashan	Na_3AlF_6 (cryolite)

Knischka	Li_2O-WO_3-PbF_2 and/or PbO_2: may contain $Na_2W_3O_7$ and Ta_2O_5
Ramaura	Bi_2O_3-La_2O_3-PbF_2 and/or PbO_2
Russia	Lithium tungstate (Li_2O-WO_3)

After the flux has been selected, the choice between using seeds or seedless synthesis has to be made. Using seeds ensures fewer but much larger crystals. Without seeds a lot more crystals of different shapes can be obtained which can be interesting for faceting. Both possibilities have been used in the production of synthetic rubies.

The growth time is quite long for this method, and a waiting period of several months to grow a batch is not uncommon. Chatham has even reported growth times of up to 8 months to get their larger gems. The slow growth and smaller crystals in comparison to melt type stones make this method not suited for the production of rubies for laser-applications. However, the more natural look of these stones and absence of inclusions that strongly suggest synthetic origin make these stones good candidates for gemological applications.

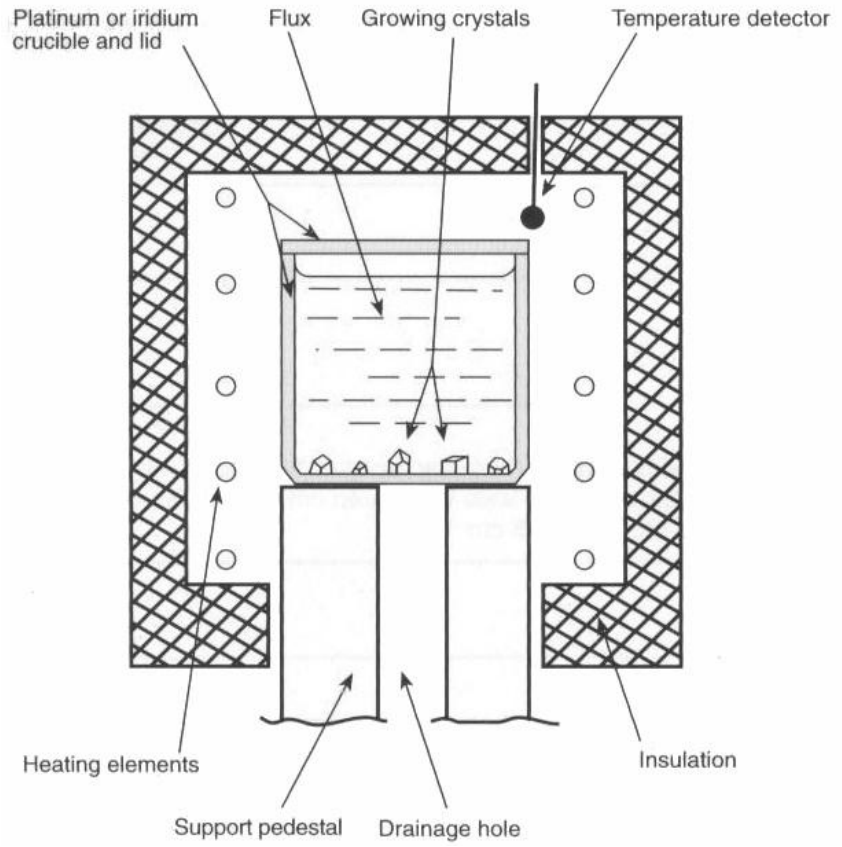

Figure 8. Flux method [Hug97].

1.2.2.3 Hydrothermal synthesis

The hydrothermal method uses autoclaves to dissolve corundum in water at high temperatures and pressures. The dissolved corundum is then to cooler regions of the autoclave where it precipitates onto some crystal seeds. These are small pieces of natural or Verneuil corundum. The technique can be used to create corundum of any color depending on the composition of the starting solution. The conditions in which these synthetic rubies are formed are the most reminiscent to the growth of natural rubies [Hug97].

However, the speed of precipitation of rubies is very slow compared to other techniques. In addition, the hydrothermal method is quite expensive since it requires high temperature and pressure conditions. As a consequence, it is not widely used and production of rubies by the much cheaper Verneuil method is often preferred.

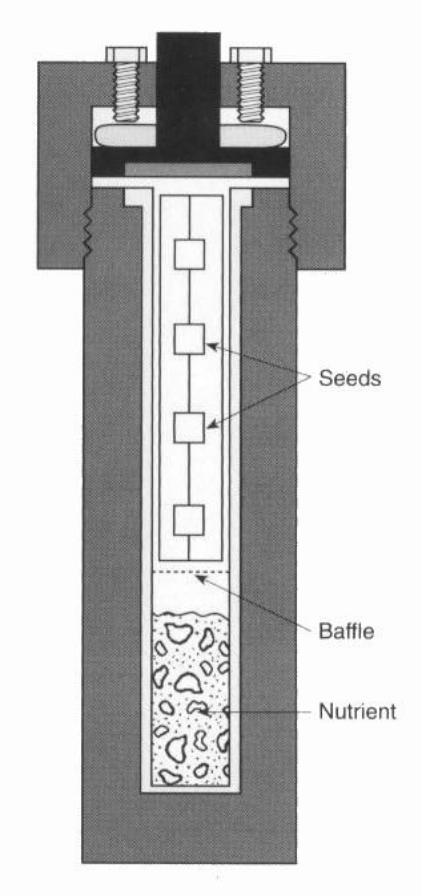

Figure 9. Hydrothermal method [Hug97].

1.2.2.4 Heat treatment

Heating rubies is used to increase the diffusion inside the ruby and to improve its color. Certain impurities of the ruby will be affected in multiple ways. Impurities with transition

elements are chromophoric, adding different hues of color to the stone. When rubies containing impurities that cause unwanted coloration are heated, these impurities may undergo changes that alter their color or even eliminate it altogether. Non-chromophoric impurities can also affect the gemstone under certain circumstances. A good example is solid guest crystals which are quite often found in rubies. They can alter the expansion rate or dissociate or melt when the melting point of the impurity is lower than the temperature to which the ruby is heated [The92]. Using this, heating a ruby to a certain temperature can be used to eliminate unwanted effects of present impurities. A list of possible impurities in corundum is given in Table 3.

Table 3. Chromophoric impurities in corundum, modified from [The92].

Impurity	m.p. (°C)	Notes
Cr_2O_3	2330	In ruby/pink sapphire; partly in orange and yellow-orange sapphire; as color modifier in purple/violet, blue, color change and other sapphires.
FeO	1369	Often in negligible or in minute amounts in ruby/pink sapphire.
Fe_2O_3	1565	Commonly found in rubies and sapphires. It consists of a multitude of iron impurities producing pale bluish to brownish milky-white effect, resembling the color of tea or the color of diesel oil, when the corundum is observed in reflected light. It is commonly known by the colloquial term *diesel-effect.*
TiO_2	1855	Often in rubies and sapphires. It consists of a multitude of needle-like crystals of TiO_2, oriented parallel to the lateral axes of the crystal, intersecting each other at 60°/120°; when examined under suitable lighting conditions, these impurities often impart a so-called *silky* appearance. The silk may appear as short or long needles, thin, thick, dust like, etc.
Ti_2O_3	1877	It exists only in synthetic corundum.
V_2O_3	1970	Present as chromophoric impurity in ruby and usually in color-change sapphire; traces in other sapphires.
Mn_2O_3	1244	Present as traces in some purplish/red rubies and in some sapphires.

Commonly, the heating is used to remove a bluish hue caused by Fe-containing impurities, and thus to improve the quality of the color. The elimination of the needle-like crystals of TiO_2 is one of the best indicators of heat treatment on a stone. The molten crystals result in easily recognizable patterns for a trained eye and a microscope.

1.2.2.5 Borax treatment and lead glass filling

Heating of a ruby may cause damage to the stone. Under heating some parts of the stone may expand slower or faster than the rest of the stone. The strain that is added can lead to small fissures or even to real fractures [The92]. The small cracks strongly reduce the transparency strongly and thus lower the value of the stone. Many natural stones also have these cracks.

The easiest way to improve a stone with these problems is to fill the cracks in the stone with a compound that has optical qualities that are very much alike to corundum. Both borax and lead glass have been used for this purpose because the refraction index of these compounds is very close to that of corundum. The fillings and the cracks they are filling become invisible after the treatment. This improves the quality of the gemstone greatly and can make a relatively worthless stone look like an expensive one.

1.3 Distinction methods

The broad variety of synthetic rubies on the market, with gem compositions increasingly similar to their natural counterparts, lead to really problematic identification using simple and cheap methods [Bos82]. Jewelers don't always know whether a stone is synthetic or not and mistakes happen more and more. This results in people buying stones for much more than their actual value or sometimes much less.

To make matters even worse, most of the gem dealers near the source of the gems even import synthetic gems to sell as authentic stones to increase profits. People who are unaware of these practices are more often than not swindled.

Many methods have been used to make a distinction between synthetic and natural rubies or between different types of natural ones. The properties that are most often used to identify the stones are growth lines, inclusions, chemical composition and interaction with light. Of course, destructive techniques are avoided as much as

possible since we don't want to destroy the gems as they are rare and costly. Some of these methods are explained below.

1.3.1 Optical microscopy

The first way to analyze a gemstone is by use of optical microscopy. This technique is not very hard to perform and does not require expensive machines. Stones fabricated by the Verneuil method have typical slightly curved growth lines that stem from the way the stone is formed. The newly added material is deposited on top of the rounded boule of synthetic ruby which results in curved deposition layers. Natural stones always have straight growth lines.

Another indication of a Verneuil stone is the presence of gas inclusions. When the temperature rises too much, or when the feed of new material is irregular, the top of the boule can start to boil which results in little pockets of gas that are trapped inside the stone when new material is deposited on top of the boule [Hug97].

One always has to be careful when using these kinds of determination steps. The presence of the indicator can tell you if a stone is synthetic, but the absence tells you nothing. The stone might be selected in a way that the most flat growth lines are obtained and no gas inclusions are present.

Natural indicators mostly consist of other minerals that are present as inclusions in the stone on a microscopic level. Small rutile needles are often found in some types of rubies.

The major disadvantage of this technique is that quite a lot of experience is required to find the inclusions and to come to conclusions about the origin of a certain stone. This experience is developed over time and is a personal skill.

1.3.2 Particle Induced X-Ray Emission (PIXE)

In 1989, Tang used the PIXE technique to look into the possibilities of this technique for distinguishing synthetic from natural gemstones [TanTan89]. For the average gemstone, the inclusions present in the stone can be used to define it using simple microscopy. However, as mentioned earlier, some of those synthetic stones present no inclusions and are much harder to determine using visual means.

The particle induced X-ray emission or proton induced X-ray emission technique uses an ion beam to remove electrons from the K-shell, placing the atoms in unstable configurations. Upon relaxation, an electron of a higher shell transfers to a vacant position with emission of an X-ray photon with an energy that is specific to the element.

This can be used to determine which elements are present in the sample and their concentration.

Some interesting observations have been mentioned using PIXE. Namely the absence of vanadium and the very low iron content in the synthetic rubies. These elements are commonly found in the natural stones. Some exceptions have been found for certain origins or synthesis methods as mentioned earlier.

The PIXE is a very powerful technique for non-destructive analysis of gemstones. However, it is very expensive and only available in specialized universities or industry laboratories.

1.3.3 Energy Dispersive X-Ray Fluorescence (EDXRF)

The EDXRF technique was first used by Muhlmeister in 1998 for the distinction of synthetic and natural gemstones [MuhFri98]. Just as the PIXE technique, it determines the nature of the elements present in the sample and their concentrations.

The EDXRF uses an X-ray beam to irradiate the sample after which the emitted X-ray fluorescence is measured. The energies are again element specific as in the case of the PIXE technique.

The EDXRF technique is less expensive and more available in gemological laboratories than the PIXE since doesn't require an ion beam generator. However, despite that the EDXRF is considered as a non-destructive method, the color of a gemstone can be affected during the measurement and the method is still quite expensive.

1.3.4 Optical spectroscopy

Instead of using X-rays to irradiate the samples, the interaction with less energetic UV or visible light can also be studied. Unlike with X-ray fluorescence, the light used in UV-Vis measurements does not have enough energy to excite the inner electrons. The electrons that are affected here are electrons in the valence shell that are more accessible to the environment of the ion. This influences the energy levels that the electrons can have. Cr^{3+} is the main coloring ion in a ruby, so that the UV-Vis spectrum is dominated by the electronic transitions of this ion in the Al_2O_3 matrix. The Cr^{3+} ion is different from Al^{3+} because it is a transition metal and thus has unpaired d-electrons as its valence electrons. D-electrons are more diffuse than the p-electrons of Al^{3+} and are as such more affected by the surrounding ions. For a given ion, the effect that these electrons experience depends on the number of d-electrons and the strength of the

electric field generated by the surroundings. The graphical plots describing this effect are known as the Tanabe-Sugano diagrams. The electron configuration of the Cr^{3+} ion is $[Ar]3d^3$,so the d^3 Tanabe-Sugano diagram describes this system (Figure 10). The principal excitation and emission transitions of the Cr^{3+} ion have are shown in the diagram.

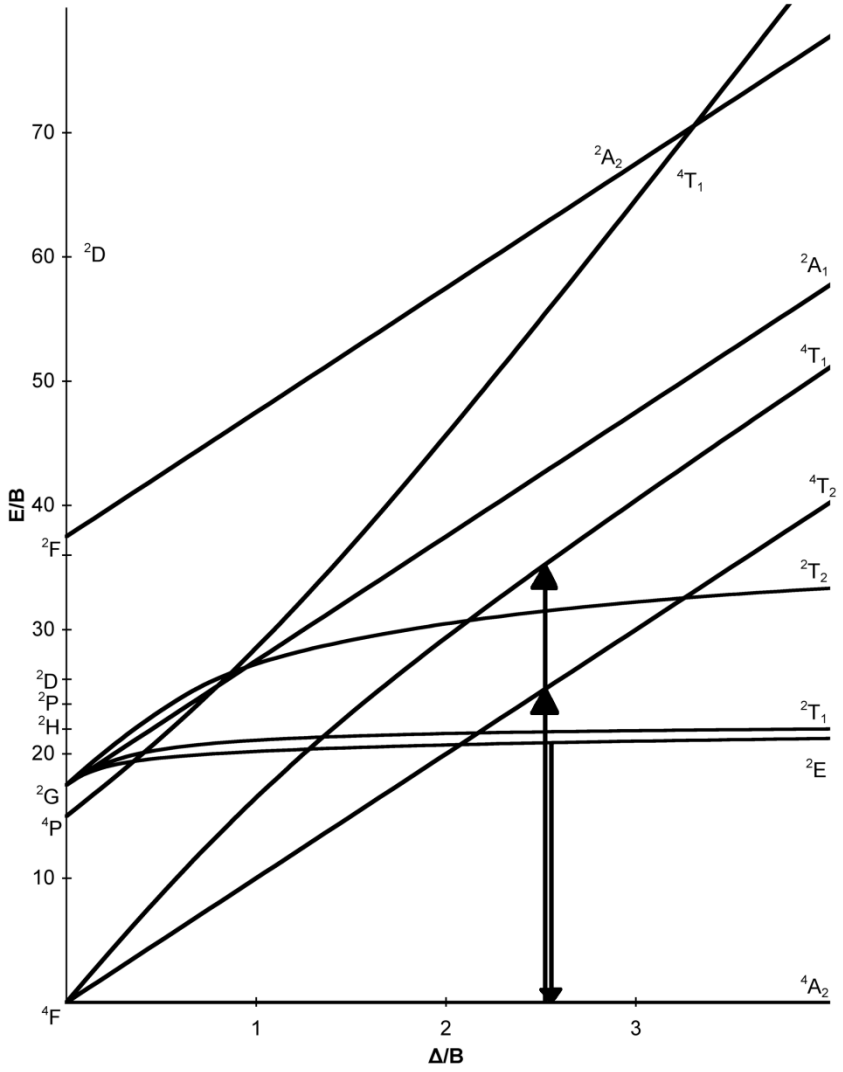

Figure 10. Tanabe-Sugano diagram for the d^3 electron system. The principal transitions in a ruby are shown on the diagram. Figure modified from [Ano11].

Using absorption measurements, the position of the ruby-system on the Δ/B-axis of the Tanabe-Sugano diagram can be found around 2.5. Plotting the energy levels in function of only one point of the Δ/B-axis gives an energy level diagram. The energy level diagram of Cr^{3+} in Al_2O_3 is shown in Figure 11. All absorption bands corresponding to energy levels displayed in this diagram can be assigned to transitions within a single Cr^{3+} ion. Peaks with different energies can originate from special effects like the formation of Cr-Cr pairs [Lapiac91] or impurities of other elements. The

impurities other than Cr^{3+} are present in very low concentrations which makes that their transitions are a lot weaker than those of Cr^{+3}.

Although optical spectroscopy can only give little information about the composition of the stone, the measurements are much cheaper and no X-rays are used. Avoiding the application of X-rays to perform a lot of measurements is always good for health reasons.

Already in 1960, Low investigated the absorption spectrum of ruby in the visible range and found several weak peaks [Low60]. After that, in 1982, Bosshart reported the possible application of absorption measurements to distinguish synthetic and natural gemstones using a special parameter he defined [Bos82]. Later Schmetzer continued the work of Bosshart using absorption measurements [Sch85].

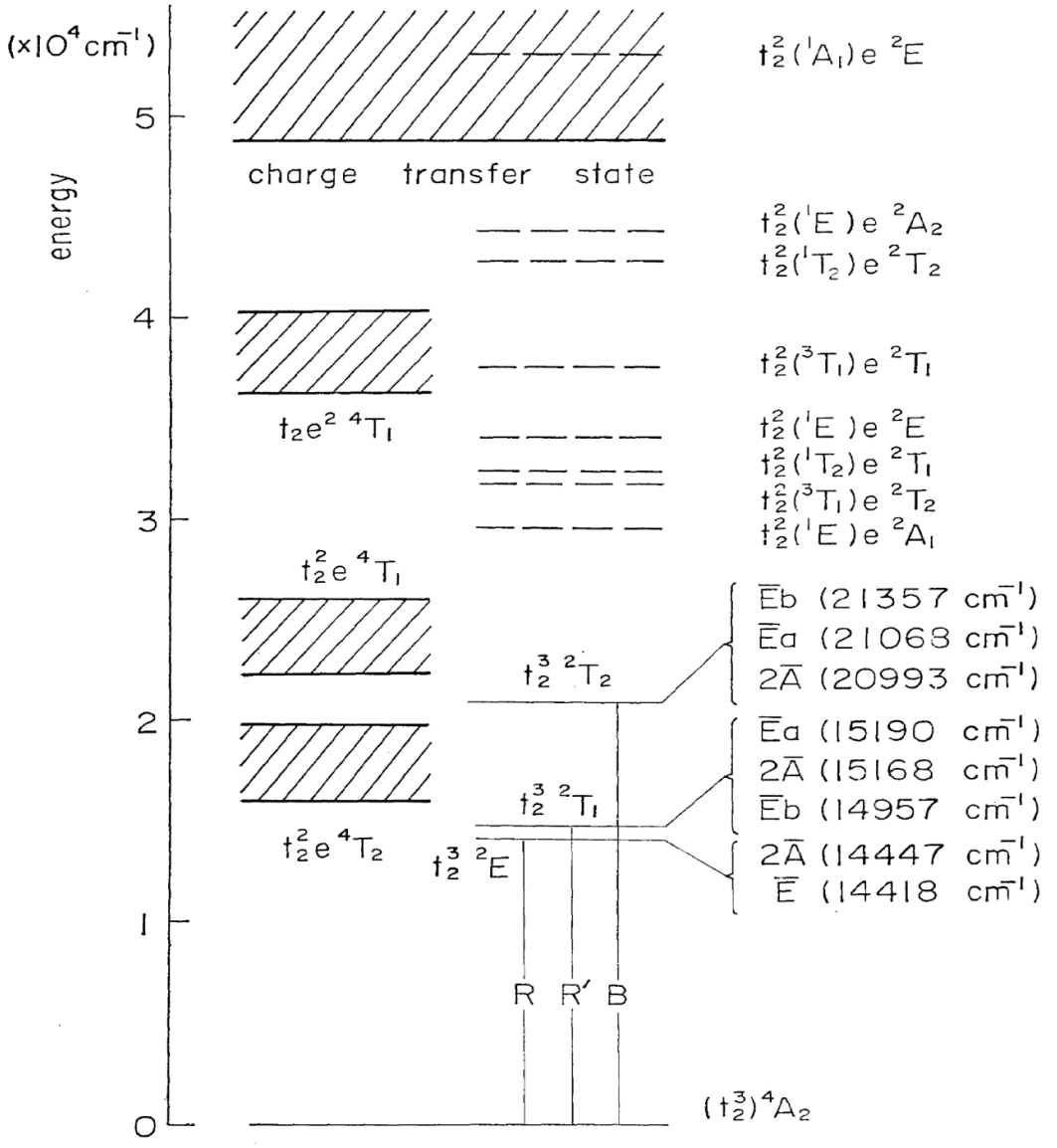

Figure 11. Energy level diagram of ruby, modified from [Kus66].

Emission and excitation measurements have been performed in the past [Sch77], but the resolution of the spectroscopic equipment used was not high enough at room temperature to get sufficient information to make the distinction between different types of rubies. Later, other measurements were done on a range of synthetic rubies to see how the emission peaks change in function of the Cr^{3+} concentration [LapIac91].

1.4 Spectroscopy and rubies

1.4.1 Interaction of rubies with light

Figure 11 gives a very detailed energy diagram that graphically presents where every energy level is situated. Each energy level is labeled using a symbol of the form ^{2S+1}X, where S is the spin multiplicity and X is determined by the degeneracy. When the level is non-degenerate, the symbol A is used for X. When the energy levels are twofold or threefold degenerate, the symbols E and T are used respectively.

For absorption and excitation measurements, the broad bands around 400 and 550 nm can be assigned to the transition of an electron from the $^4A_2$ ground level to the $^4T_1$ and $^4T_2$ levels respectively. These peaks are broadened by vibrational progression. Transition to the ^2E, $^2T_1$ and $^2T_2$ levels is spin-forbidden but is sometimes observed as very small peaks in the absorption spectra. The transitions to the levels of ^2E and $^2T_1$ are situated between 640 and 730 nm, while the transitions to the $^2T_2$ level are situated between 460 and 490 nm.

Electrons in excited states will always revert to their ground state. This can happen by non-radiative or radiative relaxation. Non-radiative relaxation normally occurs when two levels are close together. The energy will be dissipated in the system without emission of photons. When it happens by radiative relaxation, a new photon is sent out with an energy equal to the difference between the excited state and the lower laying state. In rubies, the electrons relax from the broad $^4T_2$ and $^4T_1$ bands to the ^2E level using the non-radiative pathway. The absence of levels between ^2E and the ground level $^4A_2$ causes the radiative relaxation to be the only possible way to return to the ground level. This results in a strong emission of photons of a constant energy when the electrons return to the ground level. The ^2E level is split into two levels because of spin-orbit coupling, the Jahn-Teller effect, and the interaction of the trigonal crystal field [Kus66], which results in a doublet around 694 nm when this emission is measured. Impurities

and special configurations can alter these processes which results in other emission peaks next to the main doublet.

It is the combined effect of the excitation and the emission that gives ruby its characteristic color. The two spin-allowed excitation bands occur in the blue and green spectral region. This causes a ruby to filter out all blue and green light, giving a red color to the stone. In addition, the light that is emitted by the ruby is of lower energy than the light absorbed and is red of color. This effect intensifies the red color of the stone when the stone is illuminated.

Because the transition from ^2E to $^4A_2$ is spin forbidden, it is a relatively slow process. So the time it takes for the sample to return to the ground state is relatively long (in ms range). The measurements can be done by using an ordinary xenon flashlamp for excitation. Photons emitted by the sample are then counted in function of the time after the end of the light pulse. Pure systems tend to have longer decay times because impurities can cause interactions that stimulate the spin-forbidden transition.

A technique that is often used by gemologists is to irradiate a gemstone by UV-light and to observe the luminescence light. The wavelengths of 254 and 366 nm are used for this purpose. Because light at 366 nm is still part of the excitation band around 400 nm, both natural and synthetic rubies light up red when they are excited by this wavelength. The shorter wavelength however does not work in the same way. Light with this wavelength is responsible for the transition from the $^4A_2$ level to the higher laying $^4T_1$ level. Absorption around this wavelength is observable in all samples, but the emission around 694 nm is only strong for synthetic and filling treated stones, untreated natural stones are less active in this way. A higher concentration of impurities such as Fe^{3+} can be the cause of this. These impurities can give rise to extra excited states in the stone, giving an alternative pathway for electrons to fall back to the ground state. This is an easy indicator that already suggests the origin in a very fast and cheap way.

1.4.2 Why using luminescence spectroscopy?

Many researchers have studied the luminescence of rubies and tried to distinguish synthetic and natural rubies, but it has never been used as a method on itself. Some emission bands were used as extra separating parameters when the absorption method was not sufficient to make the distinction [Bos82]. Other unique features were discovered when the spectra were examined however, without any intention to follow the origin of the ruby [LapIac91][HooThe93]. While older papers [Sch77][Bos82] stated that a good resolution can only be obtained when measuring at low temperature, this is

no longer the case. Better monochromators and overall instrument specifications have increased the resolution drastically. This, in turn, greatly improves the simplicity of the measurement as no cooling of the sample is needed to get good results. Moreover, some stones can crack by a thermal shock when they are cooled to liquid nitrogen temperature. Liquid inclusions in rubies (common in hydrothermal synthetic rubies) expand when frozen, resulting in great pressures inside the ruby.

The clearly visible doublet around 694 nm in the emission spectrum of ruby is a good indicator of the resolution. When the slits are set too wide, the doublet will coalesce to a single line.

The higher resolution combined with the simplicity of the measurements might just make this technique unambiguous enough to make good distinctions.

Chapter 2: Experimental part

2.1 Materials and methods

2.1.1 Samples

For this study 203 rubies were measured of which the origin was exactly known.These samples were supplied by Guido Crauwels and ACAM, Ivo Quintens, Jan Elsen, Koen Binnemans, and Paul Tambuyser. For the natural stones, we had access to stones from Pailin (Cambodia) (15), Thailand (1), Luc Yen (Vietnam) (21), Mogok (Myanmar) (18), Mong Hsu (Myanmar) (12) (all treated with borax), Moragoro (Tanzania) (10), Qui Chau (Vietnam) (10), Sagin Town (Myanmar) (12), Yegdalek (Afghanistan) (12), Chimwadzulu (Malawi) (11), India (12), Kenya (10), Madagascar (21), and Sri Lanka (2). It was more difficult to get a set of synthetic stones of the same type because they are hard to come by and sometimes very expensive for rare productions. The big exception to that rule is the Verneuil synthetic as these are the most common synthetic rubies on the market. The following synthetic stones were measured: Chatham (3), Douros (3), Kashan (4), Knischka (3), Lechleitner (1), Ramaura (4), Tairus (2), Pinky Trade (hydrothermal) (2), Pinky Trade (floating zone) (2), Czochralski (1), USA (1), and Verneuil (10).

Both cut and uncut rubies were measured, and no differences were observed between measurements of these two types. Obviously, the positioning of the cut stones required more finesse because these stones were cut in a way to increase the path of the light inside the ruby resulting in unwanted side effects for the measurements.

The samples were named after the person who provided them. A complete list of the samples can be found in Appendix 1. When there were multiple stones of the same type, an additional letter was added to the sample name to keep them separated.

2.1.2 Spectrofluorimeter Edinburgh Instruments FS920

The most often used instrument for this research is the spectrofluorimeter FS920 of Edinburgh Instruments. It was used to collect emission spectra, excitation spectra and decay times. The system consists of a Xenon arc lamp, a microsecond flashlamp, two monochromators, a sample compartment and a photomultiplier detector. All these components are separated from each other by manually adjustable slits. The exact arrangement and labeling can be seen in Figure 12 and Table 4 respectively.

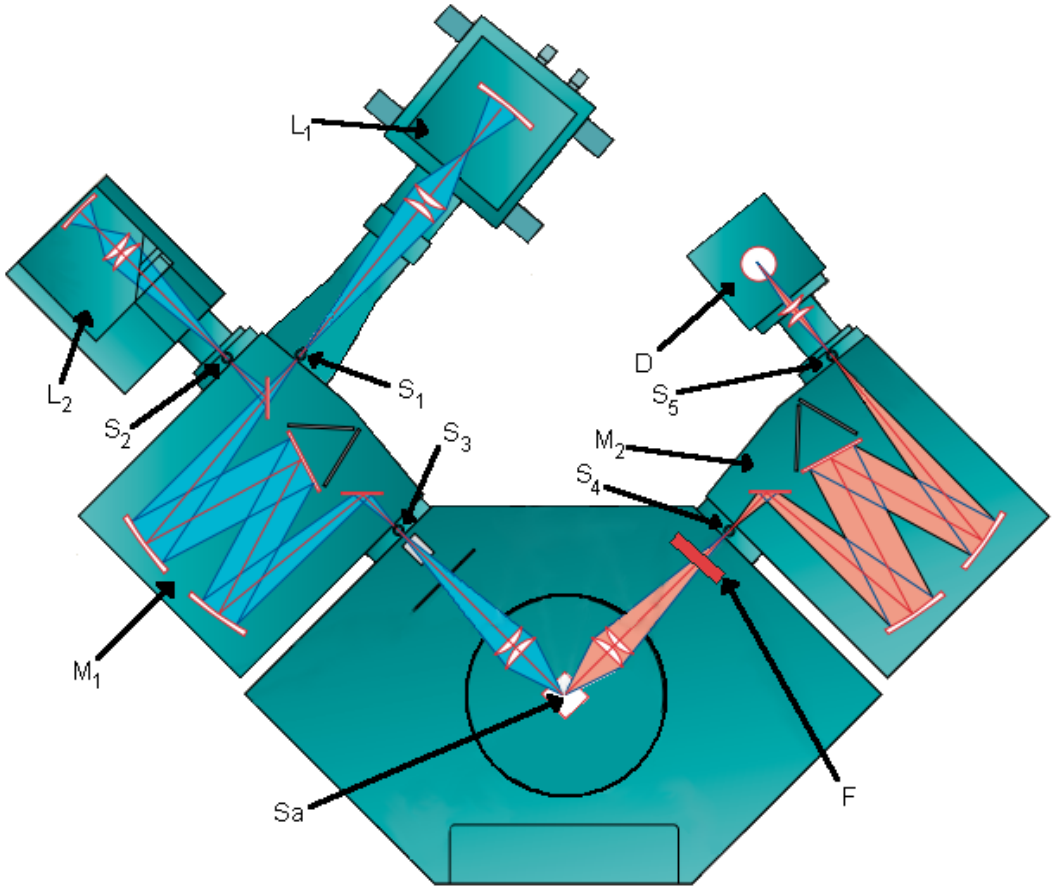

Figure 12. Schematic representation of the optical bench of the Edinburgh Instruments FS920 spectrofluorimeter, picture modified from [EdiIns03].

Table 4. Instrument components of the Edinburgh Instruments FS920 spectrofluorimeter

L1	Xenon Arc Lamp (Xe900)	S1-5	Adjustable slits
L2	µs flashlamp (µF900H)	Sa	Sample room
M1-2	Monochromators	F	Longpass filter of 550 nm
D	Photomultiplier tube (S900)		

The main light source is a 450W continuous xenon arc lamp (Xe900), giving a continuous radiation from 190nm to 2600nm and a good intensity from 230nm to 1000nm [EdiInsXe900].

The second lamp is a 50W pulsed xenon microsecond flashlamp (µF900H). It produces intense optical pulses at repetition rates up to 100Hz [EdiIns03]. The µF900H lamp is only used for lifetime measurements because the lamp is still much less intense than the Xe900 xenon lamp. For lifetime measurements, the pulsed character of the lamp is necessary, but the lower light intensity can cause problems when the light is no longer strong enough to collect the luminescence spectra with a good signal-to-noise ratio.

Before a measurement, the light source can be selected via the F900 software. The light will then pass the first monochromator which is referred to as the excitation monochromator as it selects the wavelength used for the excitation during the measurement. The monochromator uses a grating with 1800 grooves per mm which can give a resolution of 0.05 – 18nm depending on how wide the slits are opened [EdiInsM300] The instrument used for the measurements differs slightly from the schematic in Figure 12 as it has a second monochromator placed right after the first one to further reduce stray light.

The light exiting the monochromator is shone upon the sample. The light can cause the electrons in the sample to become excited. To return to their normal states, these excited electrons will send out photons containing their excess energy. The light sent out perpendicular to the incoming beam is then captured in the second monochromator after going through a longpass filter of 550nm. The filter is important because second order light passing the excitation monochromator could cause unwanted peaks. The filter makes sure that only the wanted signals are measured.

The second monochromator is identical to the first one, but this one serves to select the wavelength that is sent to the detector out of the light emitted from the sample. Analogously to the excitation monochromator, this one is referred to as the emission monochromator.

The intensity of the light beam leaving the monochromator is then measured using the red sensitive Hamamatsu R2658P detector. This detector is a photomultiplier tube (PMT) that is sensitive from 200 nm to 1010 nm. To decrease the background noise of the system, the detector has to be cooled to -20°C. This reduces the ‘dark counts’ (counts from background noise or dark current) from 2000 at 20°C to 100 at -20°C. Cooling is based on a Peltier-element cooling system which surrounds the PMT [EdiInsS900].

A PMT is a detector that is typically used for optical measurements. The PMT used here consists of a photosensitive cathode, nine dynodes and a collection anode.

The amount of electrons generated by one photon depends on the instrument used [IngCro88]. For the Hamamatsu R2658P detector, the gain is about 1×10^7 [EdiInsS900]. These electrons generate a current that can be measured. The high amplification of the small signal makes it possible to count each photon separately. The total amount of counts per amount of time is constantly displayed to the operator.

This high sensitivity of the detector is not constant for the whole sensitive range however. Near the edges of the sensitivity range the intensity of the measured signal is much lower than the actual signal. To overcome this problem, the signal is automatically corrected by the software. A similar defect can be observed at the edges of the xenon lamp spectrum. This lower emission of light can also be corrected using the software.

2.1.3 Cary 5000 UV-Vis-NIR spectrophotometer

The other instrument, the Cary 5000 UV-Vis-NIR spectrophotometer, was used to perform absorption measurements on all samples that allowed transmission of light. The system consists of a lamp, an out-of-plane double Littrow monochromator, a beamsplitter for the creation of a sample and a reference beam, a sample room with a lockdown system and a detector. The monochromator and the beamsplitter are separated by an adjustable slit to arrange resolution. The exact arrangement can be seen in Figure 13 and the meaning of the labels in Table 5.

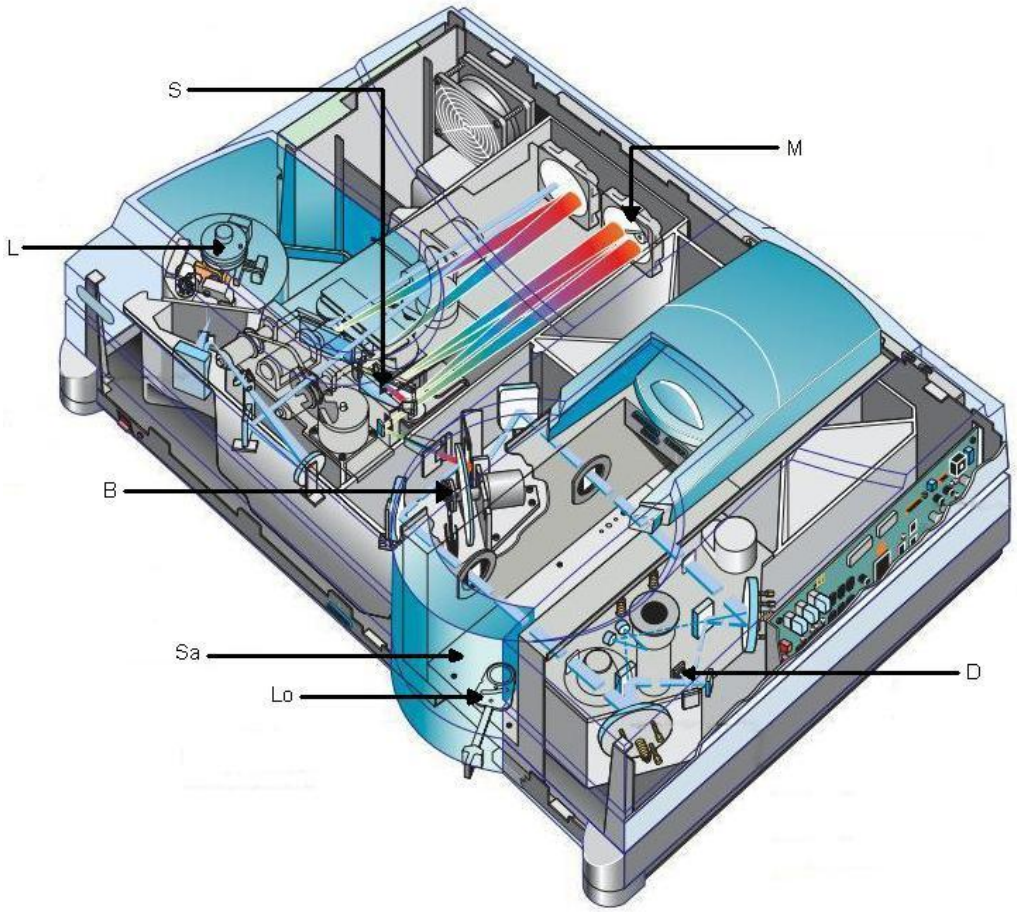

Figure 13. Cary 5000 diagram, picture modified from [AgiTec04].

Table 5. Instrument components of the Cary 5000 UV-Vis-NIR spectrophotometer.

L	Lamp	B	Beamsplitter
S	Slit	Sa	Sample room
M	Monochromator	Lo	Lockdown system
D	Detector		

This instrument is a standard Cary 5000. It has both a tungsten filament and a deuterium lamp. The software that drives the instrument gives the possibility to manually adjust at which wavelength the filter is switched. During measurements, the collection of data will be paused automatically when a change of filter has to be made. After the change, the measurement continues automatically.

The slit-width is not manually adjustable but is also managed automatically by the instrument with the possibility to change the settings in the software.

The beamsplitter ensures that two beams with identical properties are accessible. One of the beams is going through a sample while the other one serves as a reference beam. In this way, fluctuations in the lamp intensity are taken into account.

The sample room makes use of a special lockdown system that helps to put the sample holders in exactly the same place to ensure easy reproducibility of the measurements. The sample holder used in these measurements is an aluminum plate with a small hole in the center. The ruby can be mounted at the center of this hole by using Apiezon grease while making sure that no light can pass alongside the stone. An empty sample holder is placed in the reference path.

The Cary 5000 has a UV-VIS and a NIR detector. The UV-VIS detector is a Hamamatsu R928 photomultiplier tube. The NIR detector is a Peltier cooled PbS photocell [AgiTec02]. This type of detector takes advantage of the semiconductor properties of PbS. A thin layer of this semiconductor is deposited on a non-conducting substrate. The absorption of NIR photons promotes electrons from the non-conducting layer to a higher energy state. This changes the conductivity in the detector. These variations can be measured and translated to a digital signal [SkoWes04].

2.2 Measurements

For every sample an excitation spectrum, four emission spectra, and three decay time measurements were collected. The measurement of three different decay times is

necessary to calculate an average to get a statistically significant value. In addition, for samples that would transmit light, three absorption spectra were recorded. For some samples excitation-emission maps were also measured.

2.2.1 Excitation, Emission, and Decay Time Measurements

The samples were always first mounted in the FS920 spectrofluorimeter in a way so that the maximum luminescence signal is achieved. To do this, in the signal rate window of the F900 software, the Xe900 lamp is selected, the excitation monochromator is set to 400 nm, and the emission monochromator to 694 nm. These are the settings for the most intense luminescence. After that, the excitation slits are adjusted so that the radiation that is shone on the sample has an intensity of about one million counts per second. Two emission slits can then be opened equally to ensure a good resolution of the spectrum. The intensity on the detector should not exceed one million counts per second to prevent damage of the detector. If the luminescence of a second sample is much higher than a previous sample, the emission slits can be further closed. This will only improve the resolution of the measurements.

To find the best place for the sample, one has to move the sample holder in all directions and rotate it around to find the maximum. In the signal to rate window, the intensity can be seen and as long as this screen is active, the light beam can be seen to position the ruby.

When the instrumental parameters are chosen to measure rubies and only very low emission is observed, the sample might be a spinel stone. Spinel ($MgAl_2O_4$) is a mineral that has a variety that strongly resembles ruby and is found in the same conditions as a genuine ruby. In the mines, these two minerals can occur next to each other. To test if the stone is a ruby or not, the emission slits can be widened so that a signal of at least 100,000 counts per second is achieved. Thereafter, an emission spectrum can be measured with a reasonable signal-to-noise ratio. When the luminescence spectrum looks like the one in Figure 14, the sample is a spinel. This typical spinel spectrum is called the *"organ-pipe" spectrum*. When the general envelope of the spectrum resembles the one in Figure 15, it is simply a ruby with a weak emission. More examples of these emission spectra can be found in Appendix 2.

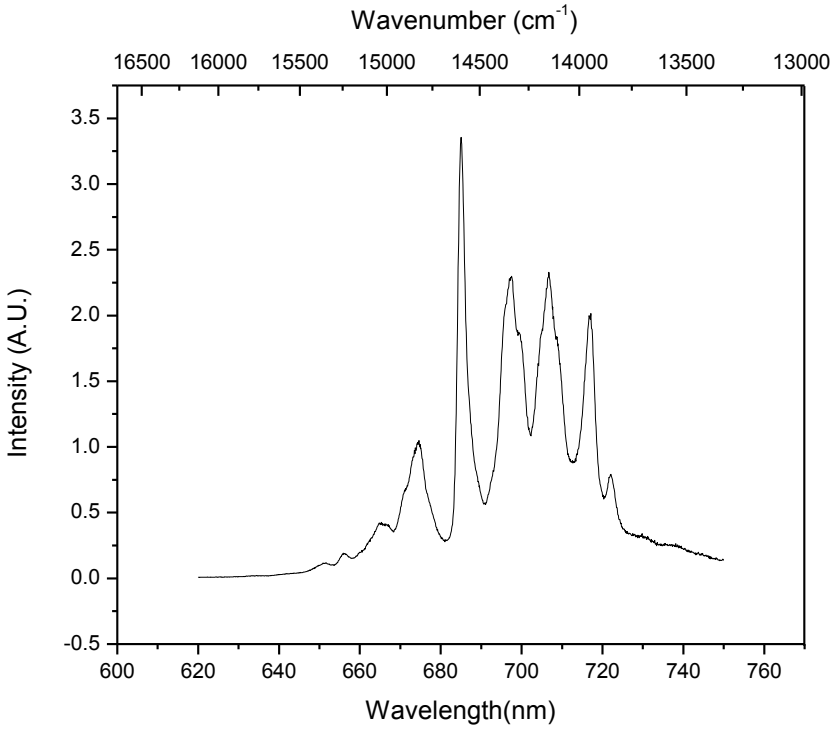

Figure 14. Typical emission spectrum of a spinel, the so-called "organ-pipe" spectrum.

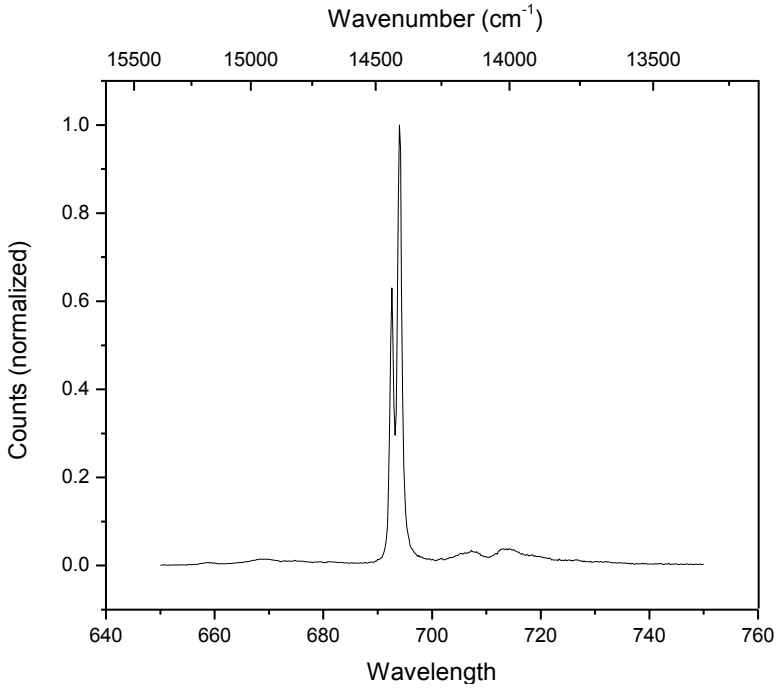

Figure 15. Typical emission spectrum of a ruby (IQ06C: Mogok).

After finding an optimal position for the sample, an excitation spectrum is recorded. Besides the information that can be collected from this measurement for the distinction between different gem types, this measurement also reveals if the position is really optimal. Depending on how the optical axis of the stone is oriented in relation to the incoming light, different effects can be observed. Other abnormalities can also be

observed when the path of the light inside the gem is too long. This effect is mostly seen in cut gems as they are cut just for the purpose to increase the path of the light inside the gem and to direct all outgoing light in one main direction.

Figure 16 shows how the effect of the shape of the gem and its positioning influences the excitation spectrum. Both peaks of the black curve are not complete as part of the light that would form the peak did not exit the stone in the direction of the detector because it was reabsorbed by the stone. Integration of the peaks in this spectrum will give poor results. Simply turning the sample a little bit can markedly affect the result.

The red curve in Figure 16 shows the envelope of the excitation spectrum when the ruby is placed in the most ideal position and the light is not reabsorbed. Usually, excitation spectra of rubies present two slightly overlapping peaks of almost perfect Gaussian shape. To extract the correct values of the peak areas, the excitation spectrum has to be fitted with a Gaussian model.

When an excitation spectrum of this shape had been found, the stone is perfectly placed and the emission spectra and the decay time measurements can be collected.

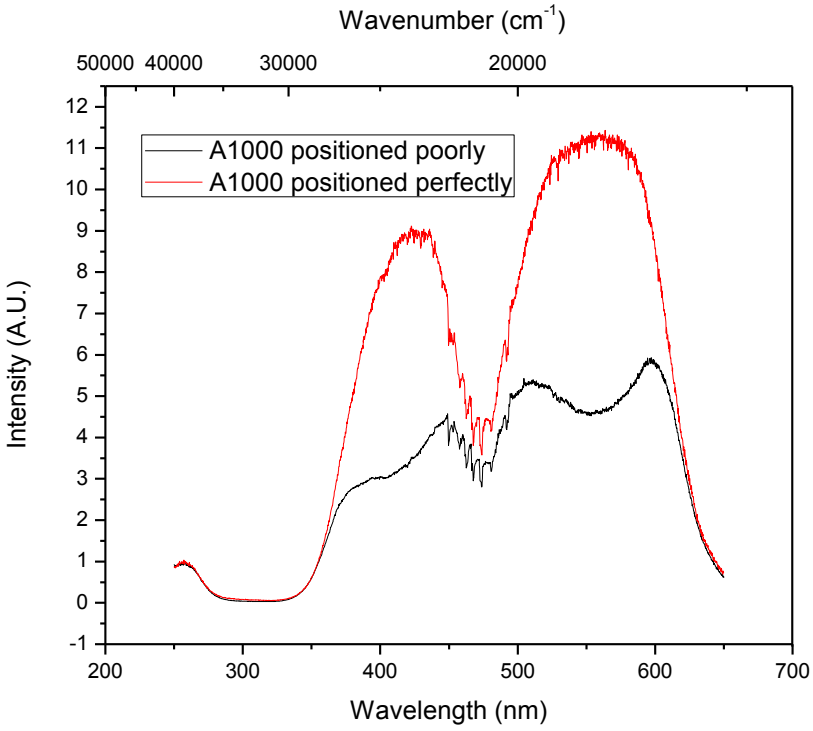

Figure 16. Normalized excitation spectra of the same ruby showing the effect of the positioning of the stone on the excitation measurement (A1000: Verneuil).

However, it is not always possible to find an ideal position for the sample in the excitation beam. Figure 17 shows the excitation spectrum affected by reabsorption, but with a lower impact. The positioning of the stone is not perfect, but the overall shape of

the curve is maintained. Moreover, the peak areas calculated using a Gaussian model have the same (within experimental errors) values as in the case of ideal measurements. So, such excitation spectra can be considered as acceptable in case an ideal position of the sample could not be found. More examples of excitation spectra can be found in Appendix 3.

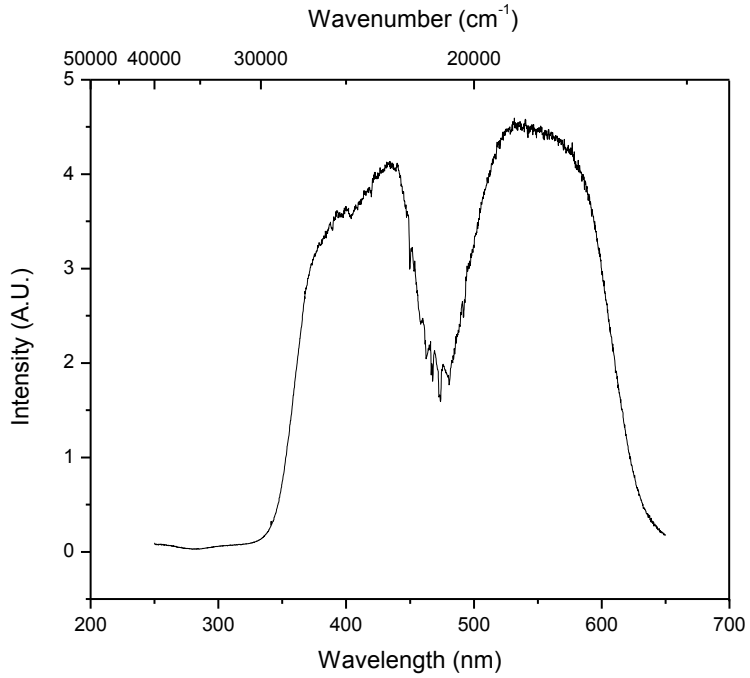

Figure 17. Excitation spectrum of ruby showing slight deformation of the peaks because of reabsorption of the light inside the gem. (A955C: Qui Chau).

The instrument settings for each type of measurements can be found below.

Excitation spectra

Start: 250.00 nm

Stop: 650.00 nm

Step: 0.200 nm

Dwell time: 0.10 s

Lamp: Xe900

Fixed/offset: 694 nm

Emission spectra

Start: 650.00 nm

Stop: 750.00 nm

Step: 0.200 nm

Dwell time: 0.10 s

Lamp: Xe900

Fixed/offset: 254, 366, 400, 570 nm

Decay time measurement

Lamp: µF900H
Lamp frequency: 20.0 Hz
Excitation wavelength: 400 nm
Emission wavelength: 694 nm
Time range: 40 ms
Channels: 4000
Lamp trigger delay: 0.005 ms
Stop conditions: time: 300 s
Sweeps: 6000

2.2.2 Excitation-Emission Maps

Instead of taking four separate emission measurements, multiple emission measurements can also be collected in one setting and combined into one excitation-emission map. The emission spectra are measured in the same way as before, but instead of manually setting the excitation wavelength before each measurement, the software does this automatically. Only a starting and ending excitation wavelength and the excitation wavelength interval between two measurements must be chosen as extra parameters. The time needed to record an excitation-emission map is much longer than for the four separate measurements as it consists of considerably more measurements. Therefore, after all the information available in the maps was found, the less time consuming option was used. The settings that were used for the excitation-emission map measurement are given below.

Excitation-Emission Map spectra

Excitation Start: 250.00 nm
Excitation Stop: 630.00 nm
Excitation Step: 10.00 nm
Emission Start: 650.00 nm
Emission Stop: 750.00 nm
Emission Step: 0.200 nm
Dwell time: 0.10 s
Lamp: Xe900

2.2.3 Absorption Measurements

The absorption spectra have been recorded using the Varian Cary 5000 Spectrophotometer. The cut stones are placed with their table pointing away from the light source into the sample holder as described earlier. Since these stones are cut to

reflect most light back to the table, placing them with the table facing the light would decrease the transmission of light needlessly. To position uncut stones, there are no specific guidelines.

A good positioned sample should result in an absorption spectrum like the one shown in Figure 18. More examples of absorption spectra can be found in Appendix 5.

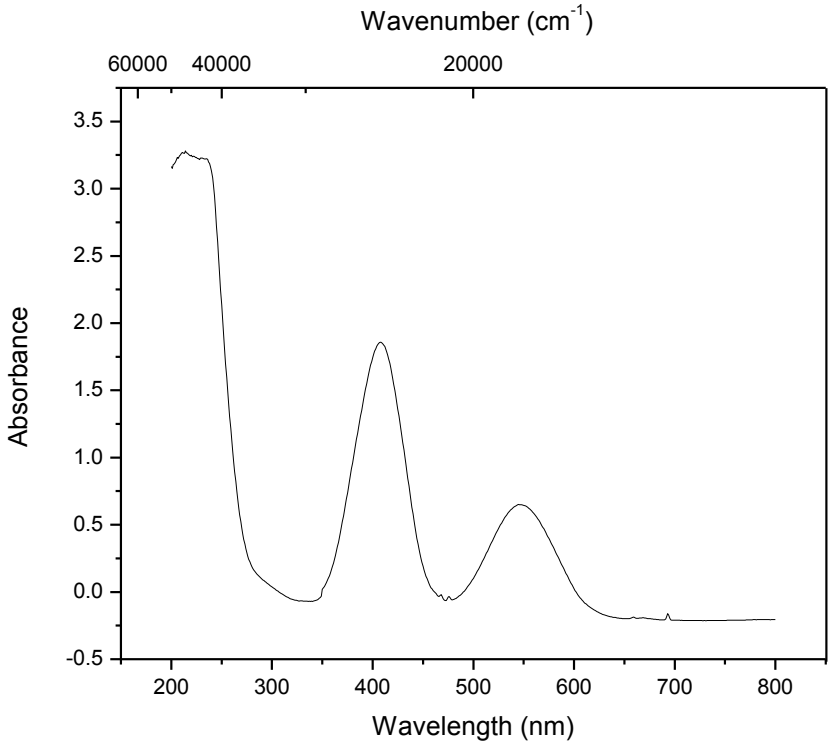

Figure 18. Typical complete UV-Vis absorption spectrum of a clear transparent ruby (A1628: Verneuil).

The instrument settings for each type of measurements can be found below.

Complete absorption spectrum

Start: 800.00 nm

Stop: 200.00 nm

Data interval: 1.000 nm

Dwell time: 0.100 s

Source changeover: 350.00 nm

Absorption detail 1

Start: 490.00 nm

Stop: 460.00 nm

Data interval: 0.050 nm

Dwell time: 0.100 s

Slit width: 0.500 nm

Source changeover: 350.00 nm

Absorption detail 2

Start: 730.00 nm

Stop: 640.00 nm

Data interval: 0.050 nm

Dwell time: 0.100 s

Slit width: 0.500 nm

Source changeover: 350.00 nm

Chapter 3: Results

3.1 Excitation spectra

T. Toyoda et.al have applied photoacoustic spectroscopy to study optical absorption of synthetic rubies with different Cr content and concluded that the intensity ratio between the peaks around 410 and 565 nm is concentration-dependent [ToyObi98]. Excitation peaks can be considered as the absorption peaks multiplied by the quantum yield (amount of photons emitted divided by the amount of photons absorbed) at each wavelength. So, the effects observed by photoacoustic spectroscopy could be expected to be present in the excitation measurements. Therefore, the analysis similar to the one discussed in [ToyObi98] was performed.

After excitation spectra have been collected, the peaks around 410 and 565 nm are fitted using a Gaussian model and the ratio between corresponding areas is estimated. This value is the first parameter that can be used for the characterization of rubies. All fittings are performed by using the Origin Pro 8 software package. Results of this fitting should look like Figure 18.

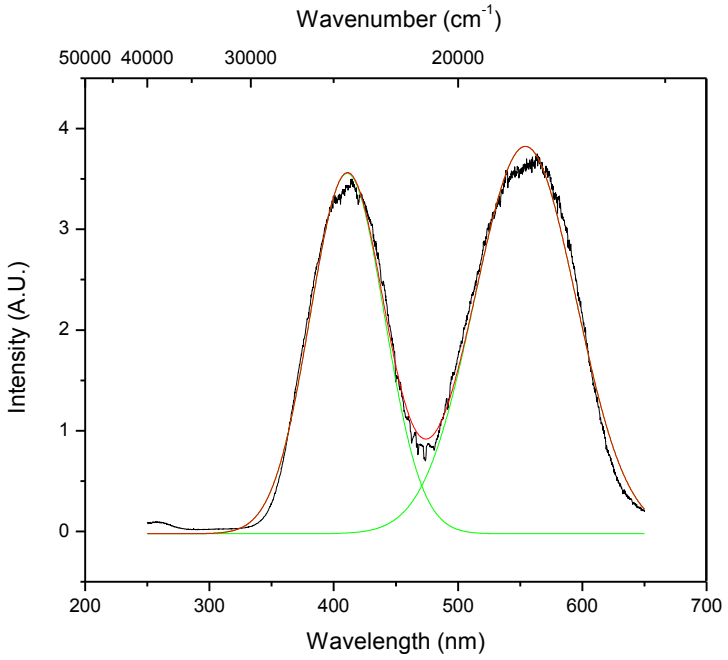

Figure 19. Excitation spectrum fitted with a Gaussian model to determine the peak areas (G016B: Mogok).

3.2 Emission spectra

The absolute intensity of emission measurements varies according to slit widths, positioning of the stone and the potency of a given stone for luminescence. To get data that can be compared, the four measurements have to be normalized. This can be achieved by combining the data of the four measurements in one datasheet and dividing every value by the maximum value of all four measurements. This is a task that is easily performed using Microsoft Excel.

As all rubies have the strong doublet peak around 694 nm when excited at 400 nm, this is a feature that will give no extra information. The details that can be used were found in the smaller side peaks. When looking at the emission spectrum excited at 570 nm, two small peaks can sometimes be observed at 701 and 705 nm as can be seen in Figure 20. These can be attributed to the interactions of neighboring Cr^{3+} ions acting as "dimers" [LapIac91][ToyObi98]. To get parameters out of this detail, the peak height is derived by subtracting the emission value at the base of the peak from the top of the peak for both peaks. The values were also multiplied by a factor of 100 to get more practical and eye-catching parameters, but this is not necessary.

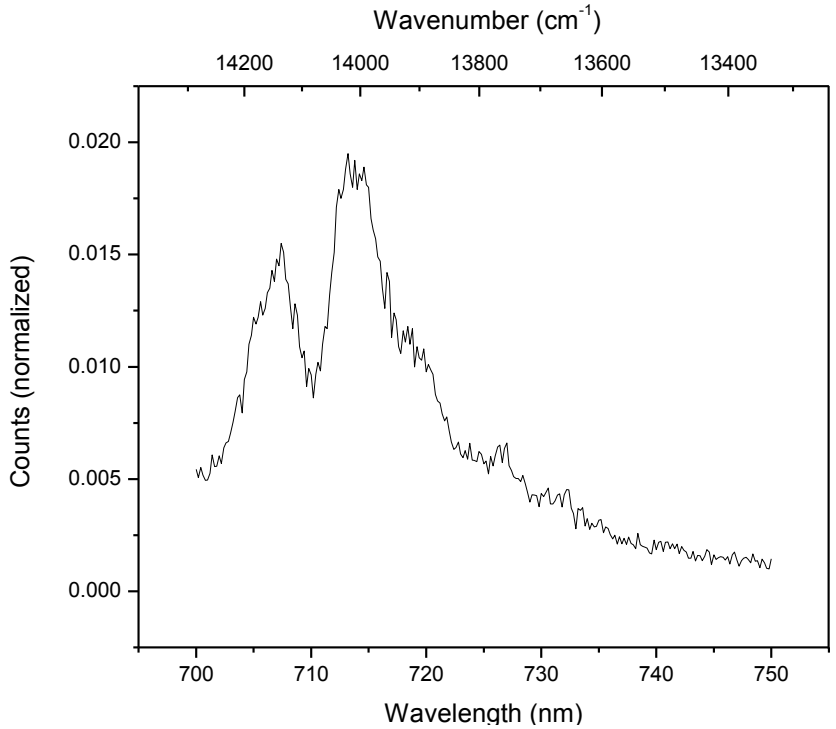

Figure 20. Enlargement of the emission spectrum of a ruby without characteristic peaks from Cr-Cr pairs (G015A: Madagascar). (Excitation wavelength: 570 nm).

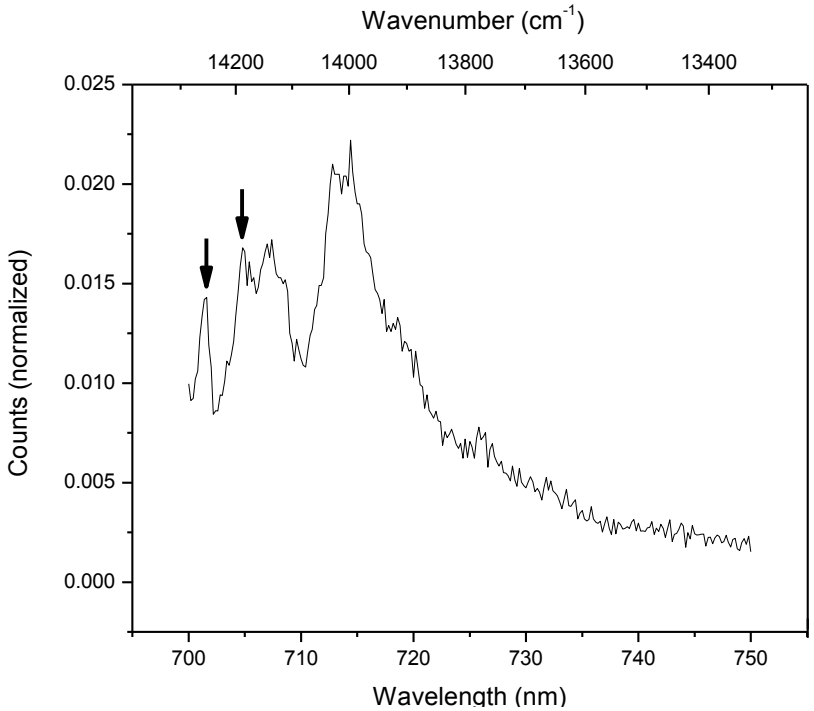

Figure 21. Enlargement of the emission spectrum of a ruby exhibiting Cr-Cr interactions, peaks indicated by arrows (IQ16A: Douros). (Excitation wavelength: 570 nm).

Another interesting detail is the peak height at 694 nm at the excitation wavelength of 254 nm. This peak is present in almost all stones, but the intensity differs greatly: from hardly recognizable among background noise to very intense peaks. Even at the beginning of this work, it became clear that almost all synthetic rubies had a much stronger emission at 694 nm when excited at the short wavelength of 254 nm. Treated rubies with borax filled cracks to hide the imperfections demonstrate similar behavior. This can be explained by partial melting of the edges of the cracks upon borax treatment due to the high temperatures. During the cooling of the gem, the borax with molten ruby crystallizes and forms a sort of synthetic ruby material inside the crack. To get a value for this parameter, the maximum of the normalized measurement at 254 nm is taken.

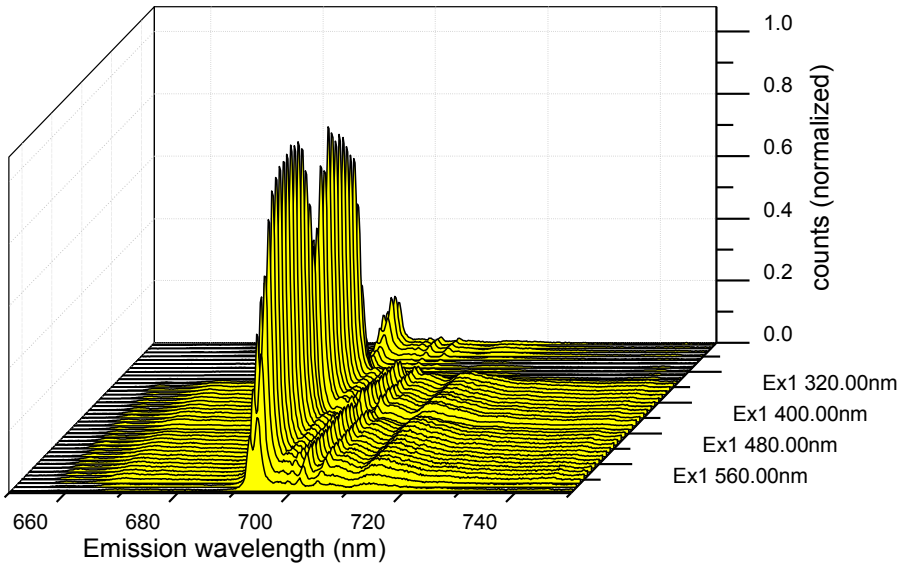

Figure 22. Excitation-Emission map clearly showing the emission peak upon excitation at a short wavelength (A1964: Verneuil). More excitation-emission maps can be found in Appendix 6.

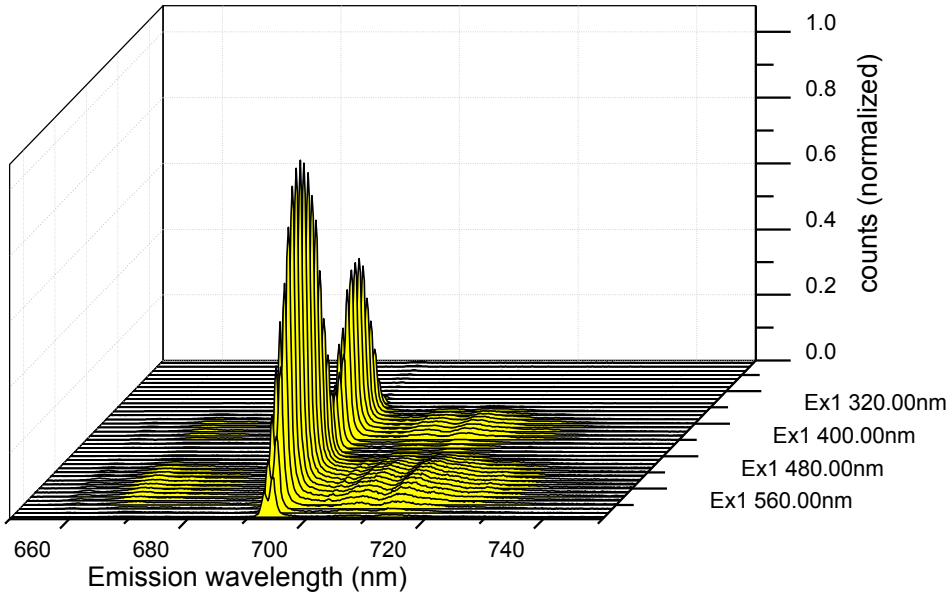

Figure 23. Excitation-Emission map showing no emission peak at short excitation wavelength (G005: Madagascar).

3.3 Decay Times

After a decay curve has been collected, it can be fitted to an exponential decay using the Edinburgh Instruments software. The fitting uses the following exponential function:

$$Fit(t) = A + \sum_{i=1}^{4} B_i \times e^{-t/\tau_i} \quad (1)$$

where A is the background value, B_i are the pre-exponential factors, and τ_i are the decay times. An impact of each τ_i to the total decay curve can be calculated.

The software automatically fits the decay curve by equation (1) after the number of terms has been set. The residuals are also shown. When these show a different pattern then a straight line, another term should be added to the fit to improve the shape of the fit. Along with the residuals, the χ^2-value is given, giving a measure of the quality of the fit. Mono-, bi- or tri-exponential functions have been used for fitting depending on the type of the stone.

Two examples of these measurements and their fitting can be found in Appendix 4.

To compare different gemstones the average decay times have been calculated according to equation (2).

$$\tau_{av} = \frac{\tau_1\% \times \tau_1^2 + \tau_2\% \times \tau_2^2 + \tau_3\% \times \tau_3^2}{\tau_1\% \times \tau_1 + \tau_2\% \times \tau_2 + \tau_3\% \times \tau_3} \quad (2)$$

3.4 Absorption spectra

Three different absorption spectra were measured for each sample. The first one is the overall spectrum from 800 to 200 nm. This measurement shows the position of the large absorption peaks and their shape and is shown in Figure 18. The other two measurements are detailed measurements of the spin-forbidden peaks between 460 and 490 nm (Figure 24) and between 640 and 730 nm (Figure 25). These are the spin-forbidden transitions to the $^2T_2$ and to the ^2E and $^2T_1$ levels respectively. After measuring different stones, a difference was detected in the intensity of the peaks at 475 and 476.5 nm. To get a value that can be used to compare different samples, the spectrum is firstly corrected for the background by fitting the data with a second order polynomial while masking the peaks. This polynomial is then subtracted from the data resulting in a dataset with three peaks on a flat background. These data are then smoothed to remove the noise from the measurement. The smoothed line can be used to get estimated peak heights. The value received by dividing the peak height of the peak at 475 by that of the peak at 476.5 gave another parameter to distinguish between types of rubies. However, in literature [Low60] the ratio of these peaks was already reported as dependent on how the sample is placed in the light beam. So, even

though a variation can be determined between different types of rubies, this is not a parameter that can be used as it gives no information inherent to the sample.

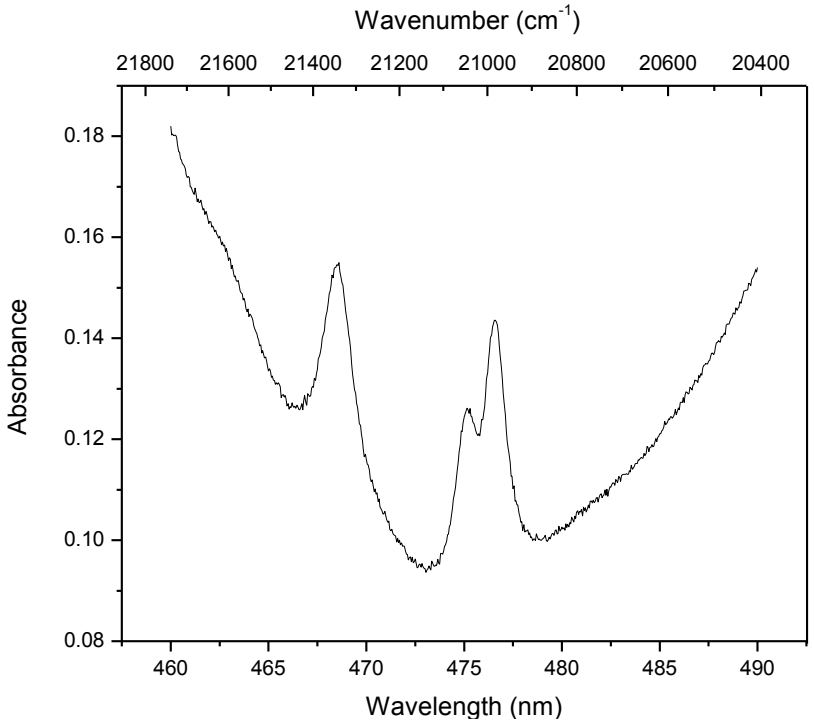

Figure 24. The first detail absorption spectrum of the ruby from Figure 18.

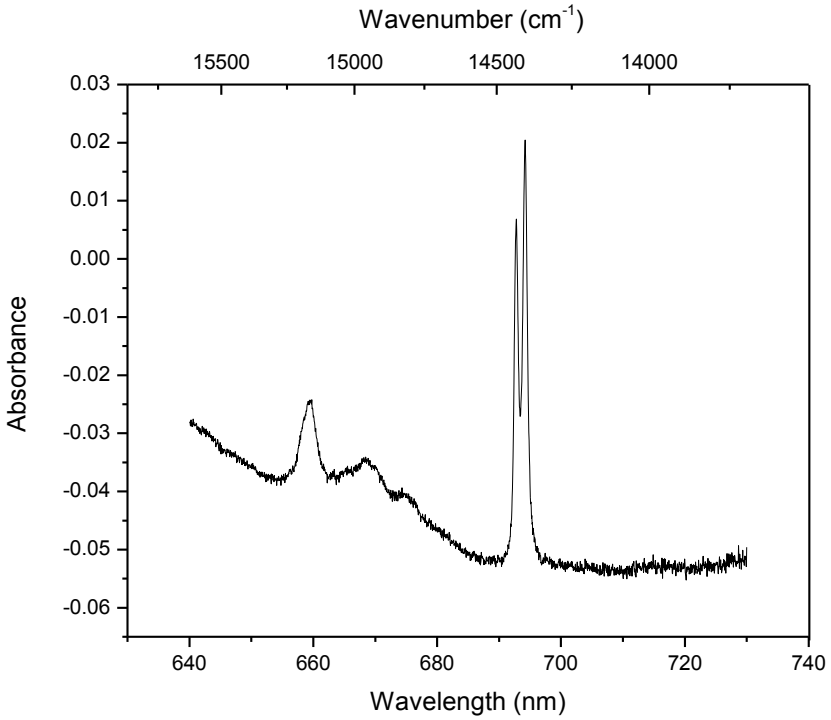

Figure 25. The second detail absorption spectrum of the ruby from Figure 18.

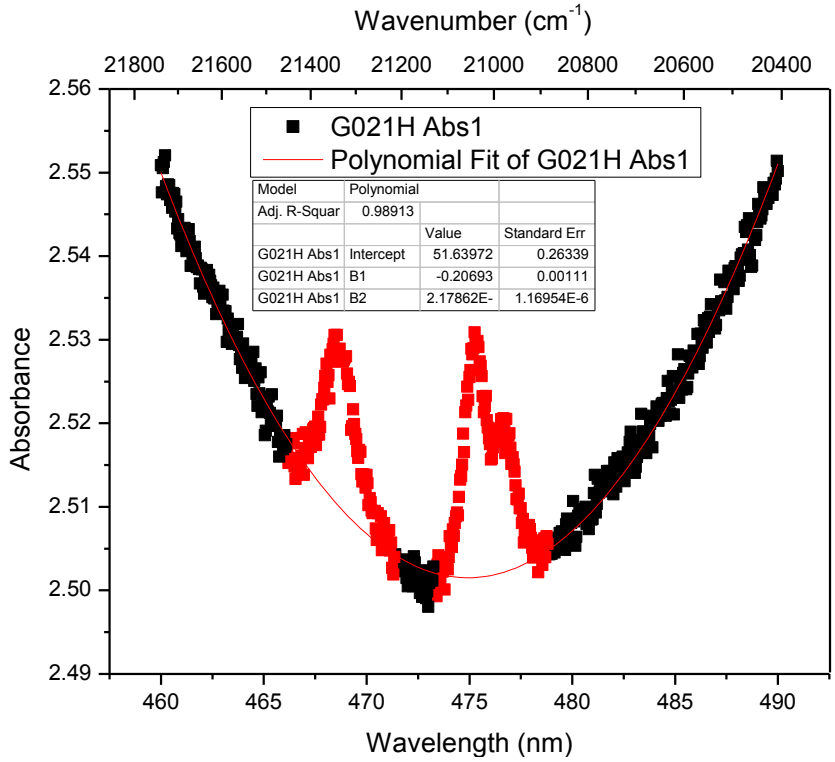

Figure 26. Absorption detail measurement showing the three spin-forbidden transition peaks between the two main absorption bands. (G021H: Qui Chau).

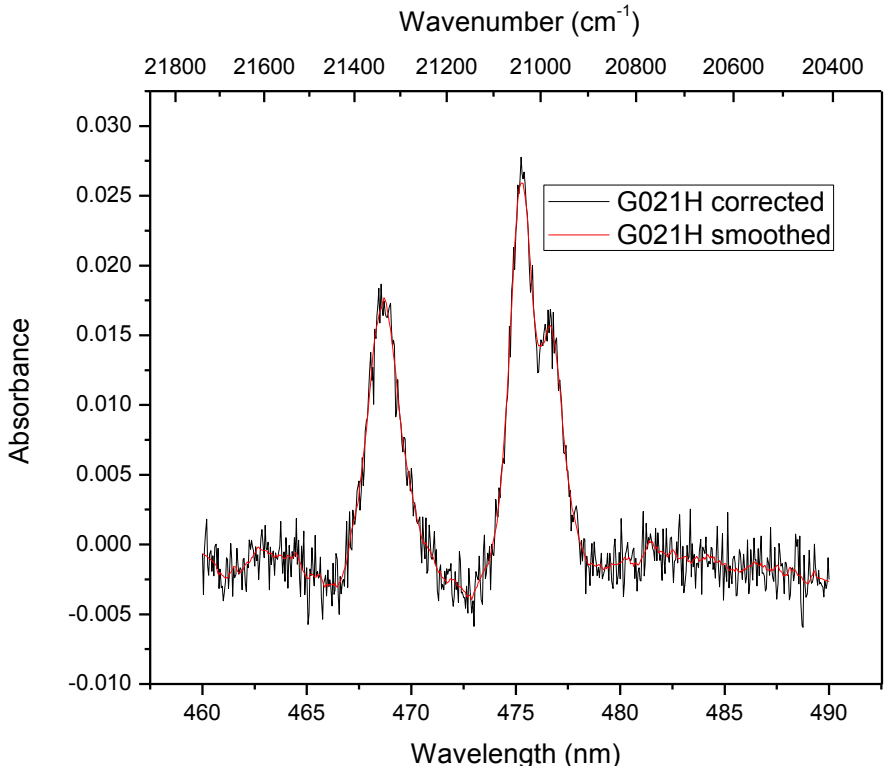

Figure 27. The background-corrected (black) and smoothed (red) absorption spectrum from Figure 23.

Chapter 4: Discussion

4.1 Analysis of results

A very large amount of data was collected from all these samples and to be able to draw conclusions, a good method of presenting the results had to be found. It soon became clear that for one parameter at a time, the use of boxplots to situate the results of a certain type of ruby in the total range of results was very clarifying. A standard example of a boxplot with instructions for reading is given in figure 25. The minimum and maximum values are the first and the last measured values respectively that are not outliers. A measurement is considered an outlier when it is 1.5 times further than the *interquartile range* (IQR = the distance between the upper and the lower quartile, 25 and 75% markers, respectively) from the upper or lower quartile. The plots for all five parameters are given in this chapter and will be discussed on their value and meaning.

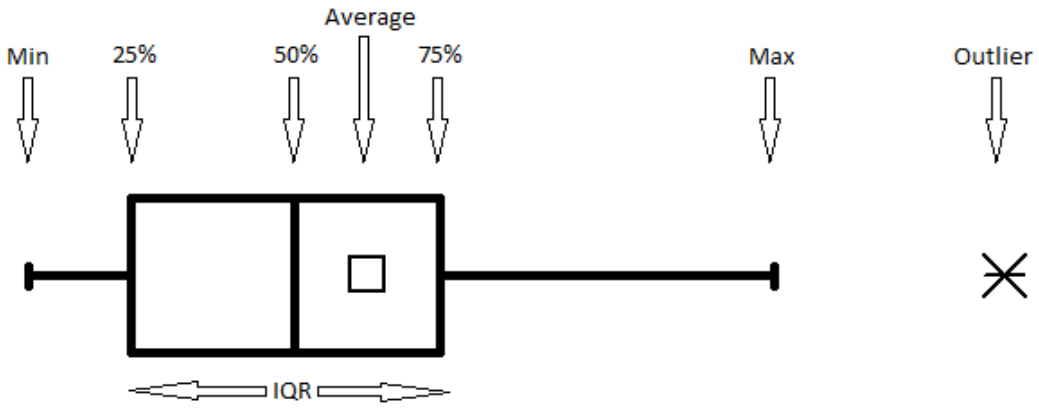

Figure 28. Standard boxplot layout.

Another way of displaying the data is an area plot where the results for one parameter are plotted in function of another. When all data are plotted in this way, areas can be outlined and some types of stones can be separated.

For both types of analysis, the larger set of data for each type of rubies, the better the reliability of the suggested parameter. Therefore, the synthetic samples will be pooled into more general types according to their formation method: (1) the Chatham, Douros, Kashan, Knischka, Lechleitner, and Ramaura samples under the flux type, (2) Tairus and Pinky Trade (hydrothermal) as the hydrothermal type, and (3) Pinky Trade (floating zone), Czochralski, USA (floating zone), and Verneuil in the melt type.

In the boxplot graphs, each geologic formation type is made visible by a color code. This is done because a separation between different types of the same geologic origin is not always possible, for instance Mogok (Myanmar) and Luc Yen (Vietnam), both marble-hosted, but the separation by different geologic origin sometimes is.

4.2 Peaks resulting from the Cr-Cr pair

Figure 26 and 27 show the boxplot graphs of the emission measurement parameters regarding the peaks at 701 and 705 nm. At a first glance, a stronger signal is observed for the synthetic than for the natural rubies with the hydrothermal stones in particular. This indicates that a higher Cr^{3+} concentration is present in the synthetic rubies or that, because of their different way of formation, the occurrence of Cr-Cr pairs is more likely. An imperfect mixing of the aluminum and chromium oxides could cause zones enriched in Cr that promote this pair formation. Natural systems are much better mixed and crystallize over much longer time periods giving diffusion of unequally distributed Cr^{3+} a larger time frame for occurring.

Another striking fact is that the graphs of both the parameter at 701 and 705 nm are very much alike. This is normal because it was previously stated [LapIac91] that both peaks result from the same origin. If this was truly the case, a direct relation between both parameters should be expected (Figure 28).

A nice linear relationship can be observed with a little offset to the right indicating that the peak at 701 nm is expressed faster than the peak at 705 nm. The linear relation also confirms that the origin of these two peaks is the same.

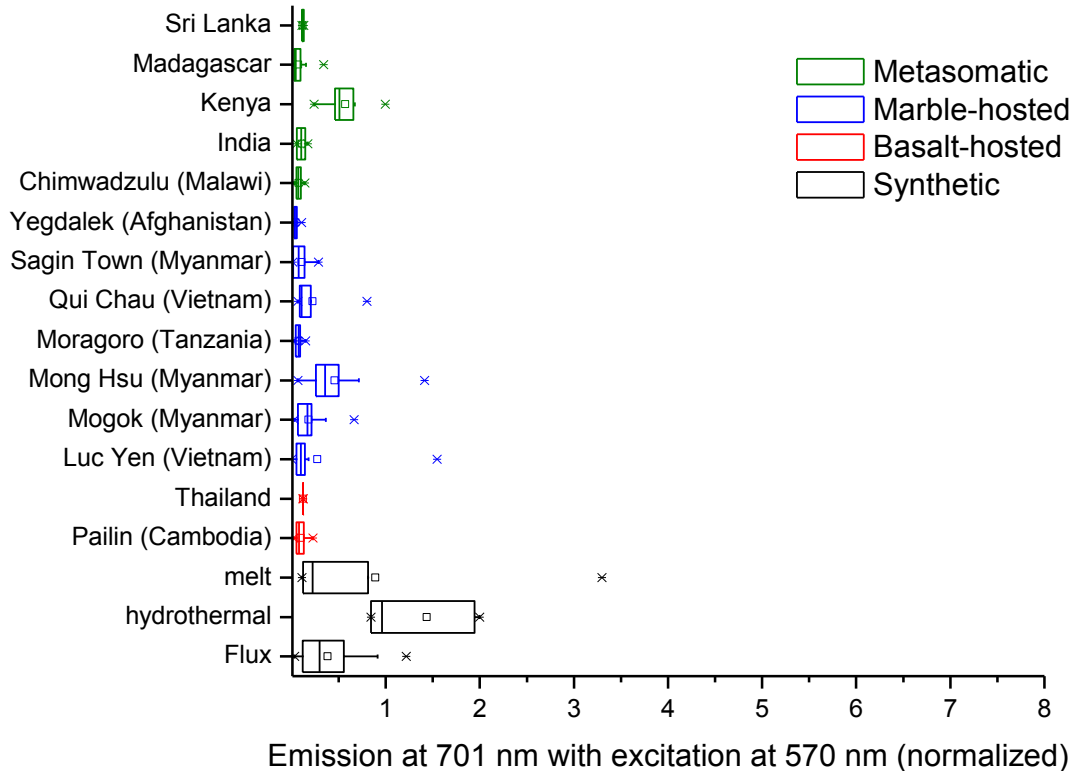

Figure 29. Boxplot graph of the first Cr-Cr pair parameter.

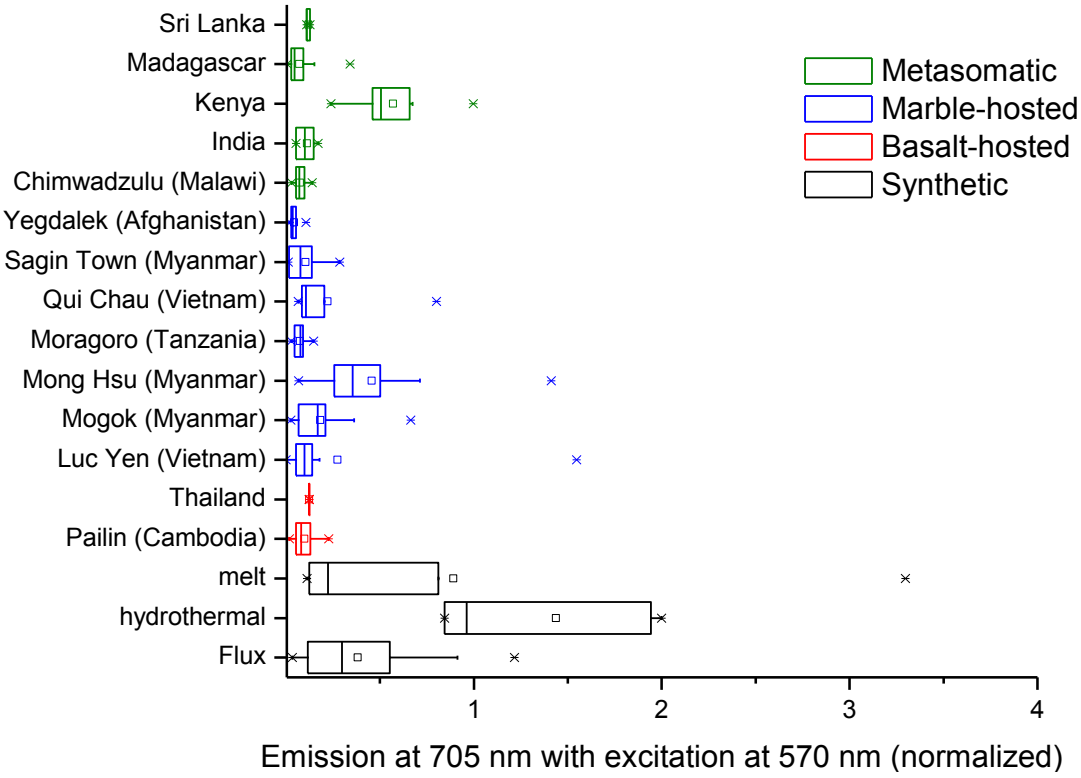

Figure 30. Boxplot graph of the second Cr-Cr pair parameter.

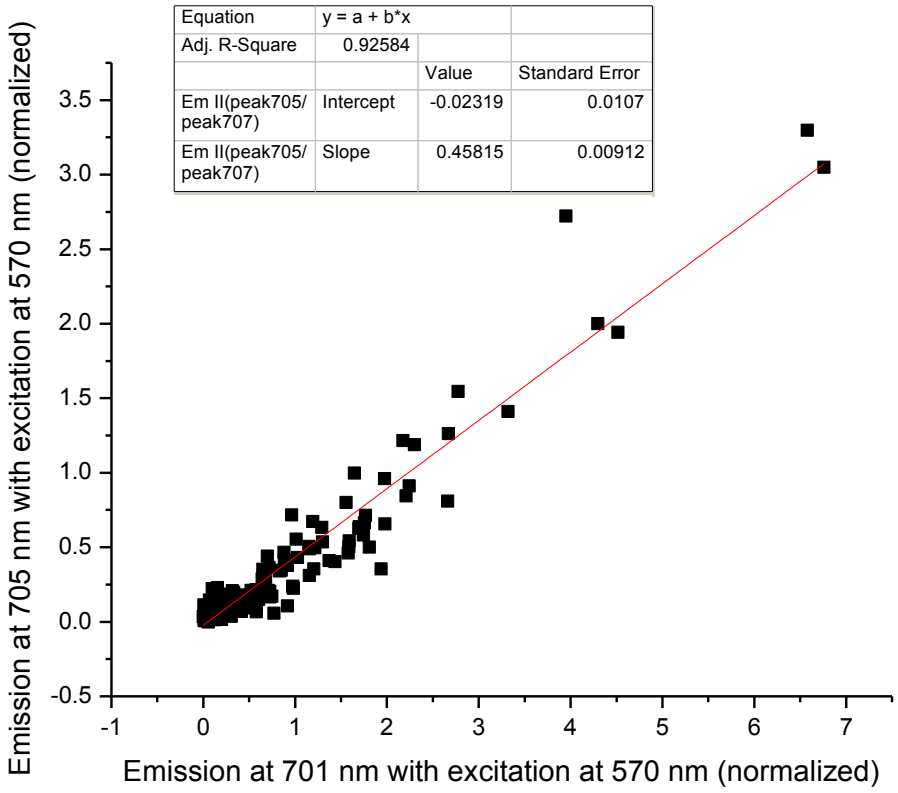

Figure 31. Relation between the first and the second Cr-Cr pair parameters.

4.3 The emission by excitation at 254 nm

One of the most important observed parameters during the study was the emission peak at 694 nm when the sample was excited at 254 nm (further referred to as “the 254 nm parameter”). Where most natural rubies showed very low to no intensity, almost all synthetic rubies showed high intensity for this peak. When we plot this parameter on a logarithmic scale as shown in Figure 29, the even the difference between different geological origins becomes visible. The marble-hosted rubies turn out to have a peak that is one order of magnitude more intense than that of other natural rubies with the exception of Sri Lanka rubies. Synthetic rubies however have peaks that are one order of magnitude larger still than the marble-hosted rubies.

The Mong Hsu rubies seem to be outliers compared to the rest of their geologic origin, but these were all treated with borax, making them partly synthetic.

The flux-type rubies span a wide range of values. This is because the composition of the stone is strongly dependant on the flux used. Since different methods use a variety

of fluxes, the composition of flux stones can differ greatly. To demonstrate this, a detail boxplot graph is shown in Figure 30 in which all flux types have their separate boxplot.

Using only this parameter, some distinction can already be made.

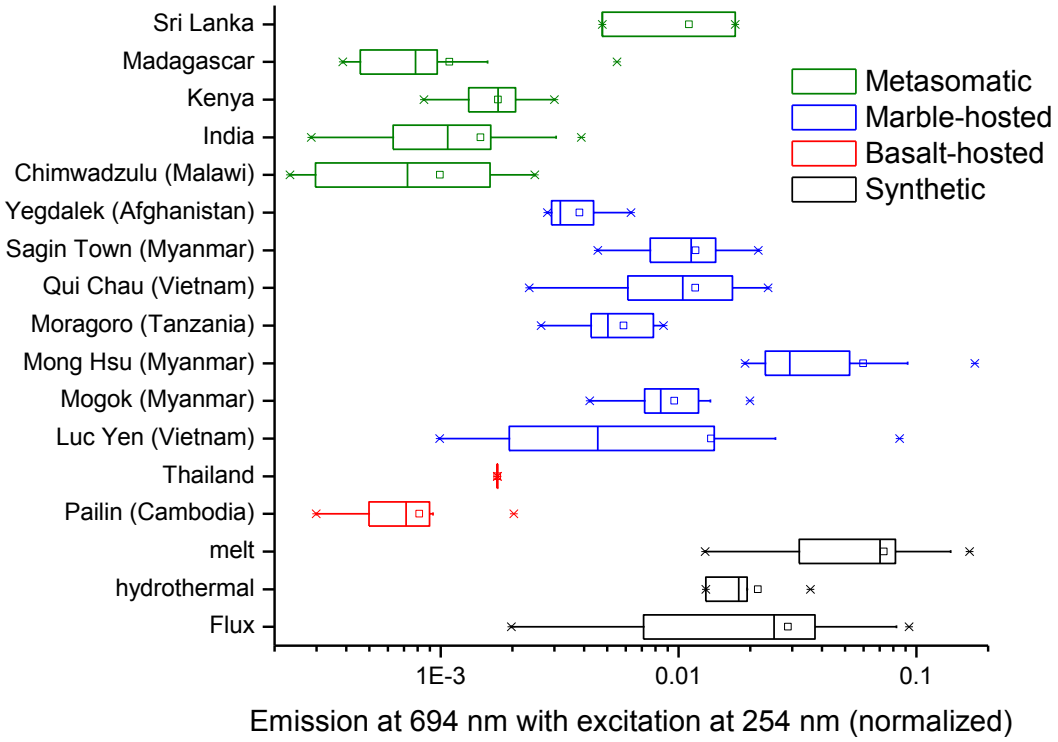

Figure 32. Boxplot graph showing the intensity of the emission peak at 694 nm under excitation at 254 nm (logarithmic scale).

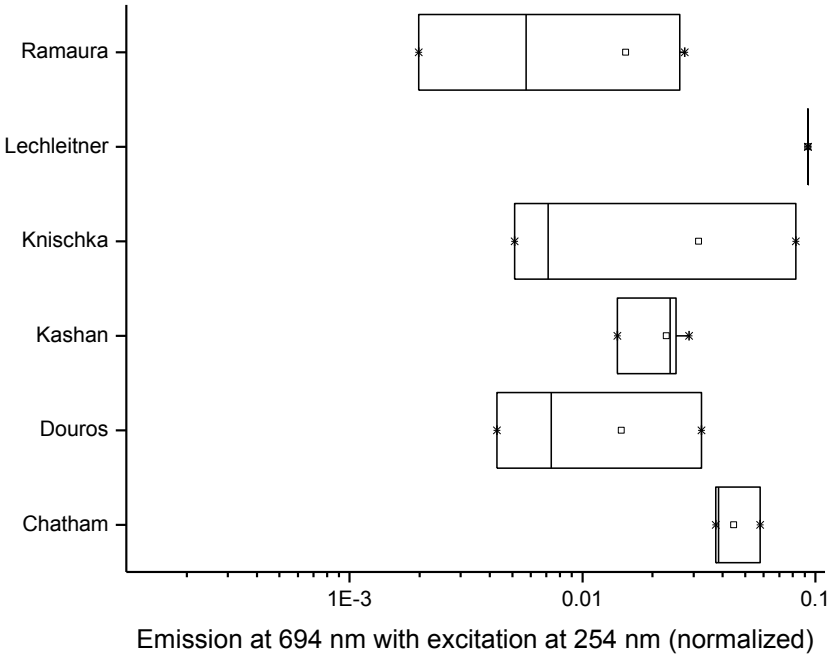

Figure 33. Detailed boxplot graph showing the intensity of the emission peak at 694 nm under excitation at 254 nm for all flux type methods (logarithmic scale).

4.4 The excitation parameter

Even though this parameter came from an interesting theory and the peaks did show different proportions, at the end only slight separation can be found between certain types of rubies. Some marble-hosted types tend to have a higher ratio than others for instance (Figure 31).

Overall, this turns out to be a parameter that cannot really be used to differentiate between different types of rubies.

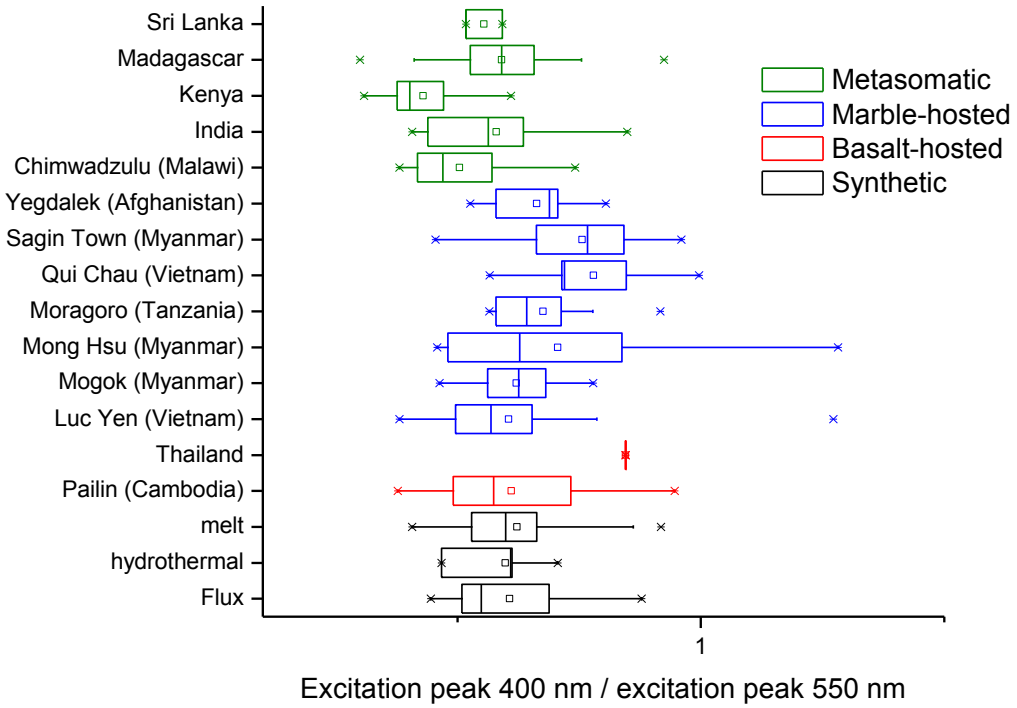

Figure 34. Boxplot graph showing the excitation parameter.

4.5 Decay time parameter

Just like the 254 nm parameter, decay time measurements gave the most important results. There is a clear difference between the basalt-hosted rubies on one side and marble-hosted and synthetic on the other side as can be seen in Figure 32. The metasomatic rubies lay somewhere in between with Kenya acting a lot like the basalt-hosted rubies and the Sri Lanka rubies more like the marble-hosted.

Since the basalt-hosted rubies have been reported to have much higher Fe-concentrations than the other natural types [MuhFri98], it is believed that it is indeed the Fe present in these rubies that shortens the decay time. This would also explain why the more pure melt type synthetic stones tend to have longer decay times and why the hydrothermal stones have shorter decay times as they are created in extreme conditions in an autoclave. Under these extreme conditions, contamination from the autoclave cannot be entirely prevented.

The theory also holds for the metasomatic rubies. As mentioned previously, the composition of these rubies strongly depends on the environment and the rock formation they are formed in. Because of this, both metasomatic rubies with low and high iron-concentration have been measured. This diversity can clearly be seen in the boxplot graph.

As a parameter on itself, the decay time appears to be able to give a good idea of what kind of ruby was measured.

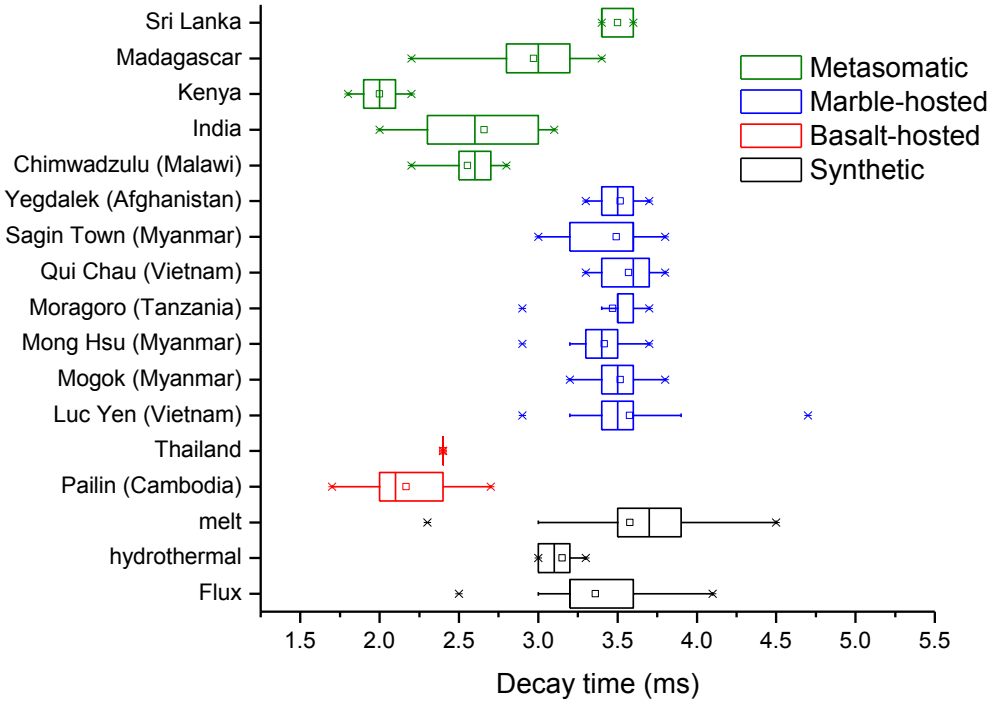

Figure 35. Boxplot graph showing the decay time parameter.

4.6 Combining parameters into area plots

The combination of two parameters in one graph can be used to create area plots as explained before. Two of these combinations result in interesting plots that will be

discussed here. The borax-treated stones were considered as a different type as their parameters resemble more those of the synthetic stones than those of the marble-hosted stones (of which they are originally part of).

The first one combines the parameters that show the best potential for making a distinction between types, namely the decay time and the 254 nm parameter. This area plot is given in Figure 33. A clear separation of the marble-hosted and the metasomatic ruby areas can be seen. The basalt-hosted rubies still show some overlap with the metasomatic rubies, but their position is significantly different from all other types. Almost all synthetic stones can be found in the top right corner of the plot, differentiating themselves from the natural rubies. Some more advanced synthetic stones with impurities to better resemble natural stones succeed in overlapping the natural ruby areas. The borax-treated rubies are indeed different from their normal marble-hosted area and are more situated in that of the synthetic rubies.

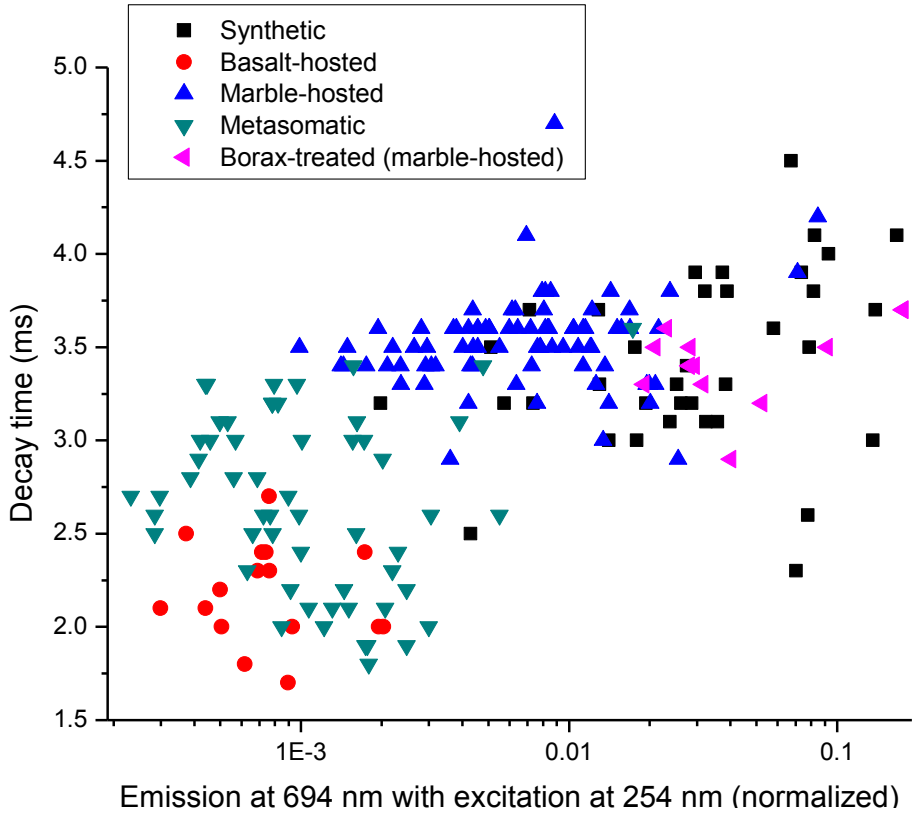

Figure 36. Area plot showing the decay time parameter in function of the intensity of the emission at 694 nm under excitation at 254 nm on a logarithmic scale.

The second plot that shows a difference between the types of rubies is the one that combines the decay time with the first Cr-Cr pair parameter. The graph is shown in Figure 34. Since the Y-axis of this second area plot is the same as that of the first one (Figure 33), these two plots look similar, but the areas have taken different shapes.

This new shape improves the separation of the basalt-hosted and metasomatic ruby areas, but the overlap of the synthetic with the marble-hosted area is increased.

Both area plots can be used together as they do not contradict each other, but rather add an extra differentiating criterion. To improve this even more, the more detailed boxplot graphs can be used to get an idea of which specific origin the gemstone could come from. Even when the origin cannot be found using all these plots and graphs, the number of possible origins may be reduced to a select few. This will already ease the work of microscopists in identification of a certain gemstone because it will already be known which inclusions to look for.

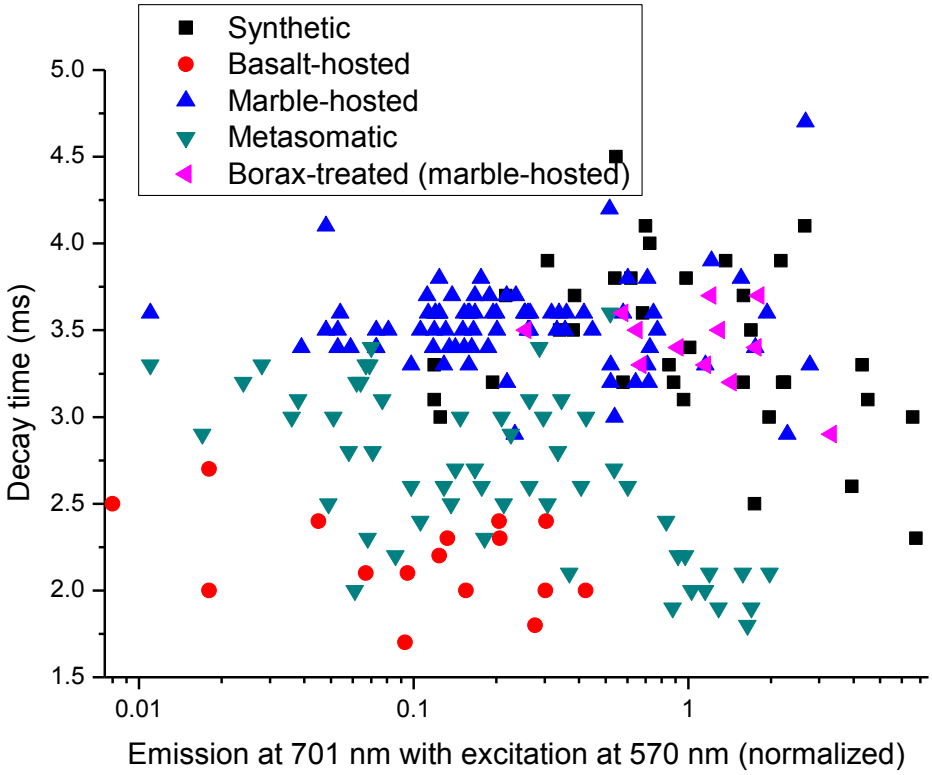

Figure 37. Area plot showing the decay time parameter in function of the intensity of the emission at 701 nm under excitation at 570 nm on a logarithmic scale.

Nederlandse samenvatting

De term *robijn* slaat op de rode variant van het mineraal korund (Al_2O_3). Dit betekent dat al de eigenschappen van korund ook eigenschappen van robijn zijn. Zo heeft robijn een hardheid van 9 op de schaal van Mohs, wat betekent dat zeer weinig materialen in staat zijn om robijn te bekrassen. Dit is naast de kleur één van de grootste troeven van robijn voor het gebruik als edelsteen.

Het mineraal krijgt de kenmerkende rode kleur doordat verschillende Al^{3+}-ionen in het kristalrooster door Cr^{3+}-ionen vervangen zijn. Dit transitiemetaalion zorgt voor de inbreng van elektronische transities in het materiaal die ervoor zorgen dat de groene en blauwe fractie van het elektromagnetisch spectrum geabsorbeerd worden. De absorptie van dit licht zorgt ervoor dat de elektronen van het Cr^{3+}-ion in een aangeslagen toestand terecht komen. Deze kunnen door de grote opsplitsing tussen de grondtoestand en de laagstgelegen aangeslagen toestand enkel door emissie van een foton terugkeren naar de grondtoestand. Het foton dat uitgezonden wordt, heeft een rode kleur. De absorptie van het groene en blauwe licht en de emissie van het rode licht zijn twee samenwerkende effecten die zorgen voor de intense rode kleur die zo uniek is voor robijn. Het is trouwens het selectief uitzenden van dit rode licht dat de interesse van de laser-industrie voor robijnen opwekte.

Natuurlijke robijnen kunnen opgedeeld worden in drie types van geologische oorsprong. Zo zijn er robijnen die in marmerlagen en in basalt teruggevonden worden. Deze twee types hebben uiteraard volledig verschillende vormingsomstandigheden. Het derde type zijn robijnen die gevormd zijn door metasomatisme, een geologisch proces waarbij een gesteente van elementsamenstelling kan veranderen door uitwisseling van ionen met een contactvloeistof onder hoge drukken en temperaturen. Naast de natuurlijke bestaan er ook synthetische robijnen. Vele methoden zijn reeds ontwikkeld en in het gebied van edelsteenvervalsing is er een constante vernieuwing aanwezig om detectie te slim af te zijn. De meeste synthetische robijnen worden geproduceerd met het Verneuil-proces, een methode die zuiver korundpoeder en kleine hoeveelheden chroomoxide volledig opsmelt en laat uitkristalliseren in een *boule.* Deze methode is sinds zijn ontdekking in het begin van de 20^{e} eeuw nauwelijks veranderd.

Het Verneuil-proces is slechts één van de verschillende methodes die het korund volledig gaan opsmelten (smelt-methodes). Andere methoden berusten eerder op het

oplossen van het materiaal in enerzijds een flux (flux-methodes) en anderzijds in water bij verhoogde drukken en temperaturen in een autoclaaf (hydrothermale methodes).

Omdat er zoveel verschillende soorten robijnen zijn en omdat de echtheid van verkochte edelstenen moet kunnen gegarandeerd worden, probeert men al jaren op een eenvoudige manier een onderscheid te maken tussen deze soorten. Hierbij wordt beroep gedaan op zowel de chemische eigenschappen van robijn als op de structurele onregelmatigheden in de steen zelf. Zo kan men met X-stralentechnieken zoals PIXE en EDXRF de samenstelling van de robijn bepalen zonder deze te beschadigen. Voor het bestuderen van onregelmatigheden, wordt een optische microscoop gebruikt om naar de insluitsels te kijken. Elke techniek heeft zijn voor- en nadelen. De eerder dure X-stralen-technieken zijn vrij accuraat maar kunnen verkleuringen van de edelstenen veroorzaken. Hier tegenover staat de niet-invasieve optische microscopie waarbij de oorsprong van de robijn niet altijd kan geïdentificeerd worden. Identificatie wordt met deze techniek al helemaal onmogelijk wanneer er geen typerende insluitsels teruggevonden kunnen worden, al is een synthetische oorsprong dan wel zeer waarschijnlijk. Om een degelijk onderscheid te kunnen maken met een microscoop is bovendien een lange opleiding en veel ervaring nodig.
Een nieuwe techniek om onderscheid te maken is dus zeker nuttig. In het kader van deze toepassingsmogelijkheid werd de optische spectroscopie getest. Concreet werden er excitatie-, emissie-, absorptie-spectra en vervaltijdmetingen opgemeten. Hiervoor werden de Edinburgh Instruments FS920 spectrofluorimeter en de Cary 5000 UV-Vis-NIR spectrophotometer gebruikt.
Deze spectra werden onderzocht op kenmerkende pieken die sterk verschillend waren van type tot type. De oorsprong van deze pieken was steeds terug te vinden in de literatuur, maar een overkoepelend samenzetten van de meetwaarden als parameters voor een soort identificatie-tool was vooralsnog niet gebeurd. De reden hiervoor is dat bij de eerste poging [Sch77] de resolutie van de opgemeten spectra nog niet hoog genoeg was om voldoende detail waar te nemen bij kamertemperatuur. Een sterke vooruitgang op technisch vlak heeft er echter voor gezorgd dat de resolutie waarmee nu gemeten wordt veel beter is. Zo kan bijvoorbeeld het doublet van de robijn-emissie zonder problemen gescheiden waargenomen worden bij kamertemperatuur. Sommige parameters werden pas later verklaard zoals Cr-Cr-paren die voor extra pieken in het emissiespectrum zorgen [Lapıac91]. Deze laatste werd eerder uit fundamentele interesse naar de invloed van de Cr^{3+}-concentratie op het luminescentie-spectrum onderzocht dan om een onderschied te kunnen maken tussen verschillende types robijnen.

Uiteindelijk bleven er drie parameters over die duidelijke verschillen vertoonden tussen verschillende types van robijnen. Deze zijn: (1) de pieken in het emissiespectrum bij 701 en 705 nm onder excitatie bij 570 nm, veroorzaakt door de Cr-Cr paren; (2) de intensiteit van de emissiepiek bij 694 nm onder excitatie bij 254 nm, genormaliseerd ten opzichte van diezelfde emissiepiek onder excitatie bij 400 of 570 nm (grootste van de twee); en (3) de vervaltijden bij 694 nm onder excitatie bij 400 nm. Boxplots die de verdeling van verschillende robijntypes weergeven voor deze parameters zijn terug te vinden in Figuren 26 , 29 en 32 respectievelijk.

De parameter veroorzaakt door de Cr-Cr-paren is opvallend groter voor de synthetische robijnen. Een van de verklaringen die hiervoor gegeven kan worden is dat de totale Cr^{3+}-concentratie in synthetische robijnen systematisch hoger zou zijn, waardoor paarvorming meer waarschijnlijk wordt dan in natuurlijke robijnen. Een andere verklaring zou kunnen zijn dat, door een minder goed mengen van de bestanddelen voor de synthese, er nog kleine zones zijn waar het Cr^{3+} in grotere concentraties voorkomt. Zelfs de langst durende synthesemethoden vormen de robijnen op een veel kortere tijd dan bij een geologisch proces voor natuurlijke robijnen. Door deze langere vormingsperiode is er veel meer diffusie van Cr^{3+} in het kristal mogelijk waardoor de verdeling beter is.

Het valt duidelijk op dat de robijnen van het basalt-type kortere vervaltijden vertonen dan de andere types. De verklaring die hiervoor gegeven kan worden is dat robijnen die op deze manier gevormd worden een hoger ijzergehalte hebben dan bijvoorbeeld robijnen die in zeer zuivere synthese-omgevingen of in ijzer-arme marmergesteentes gevormd worden. Dit aanwezige ijzer zorgt voor een *quenching*-effect dat de terugval naar het grondniveau versnelt. Robijnen van het metasomatische type hebben een ijzergehalte dat sterk afhankelijk is van de samentstelling van de contactvloeistof en het gesteente waarin het gevormd wordt. Hierdoor worden robijnen van het metasomatische type gevonden met zowel hoge als lage ijzergehaltes, afhankelijk van de locatie waar ze gevonden worden. Dit vertaalt zich in de grote variatie tussen verschillende plaatsen van herkomst binnen het metasomatische type.

De derde parameter verschilt zo sterk tussen verschillende types dat deze op een logaritmische schaal uitgedrukt kan worden. De parameter geeft de intensiteit van de emissiepiek bij 694 nm onder een excitatie bij 254 nm weer. De excitatie bij 254 nm kan toegekend worden aan de transitie van de $^4A_2$ grondtoestand naar de hoogst

gelegen $^4T_1$ aangeslagen toestand. Deze transitie is goed waar te nemen als een absorptieband in de absorptiespectra van al de robijnstalen. Het feit dat natuurlijke robijnen minder emissie vertonen bij 694 nm wanneer deze geëxciteerd worden bij 254 nm, kan toe te kennen zijn aan het feit dat deze minder zuiver zijn dan synthetische robijnen. Onzuiverheden zoals Fe^{3+} in robijn kunnen zorgen voor nieuwe energieniveau's waarnaar de energie overgedragen kan worden. De parameter is dus een maat voor de zuiverheid.

Deze drie parameters kunnen ook nog gecombineerd worden in zone-plots. In dit soort plots staan al de stalen uitgezet in functie van twee parameters. Wanneer de vervaltijd gebruikt wordt in combinatie met een van de andere twee parameters, vormen deze datapunten zones waar robijnen van een bepaald type kunnen voorkomen. Deze plots zijn terug te vinden in Figuren 36 en 37.

De boxplot grafieken en de zone-plots kunnen samen gebruikt worden om een idee te vormen over de oorsprong van een robijn op basis van slechts enkele eenvoudig op te meten parameters. Zelfs wanneer er na analyse met deze techniek nog verschillende mogelijke oorsprongen overblijven, zijn er al heel veel mogelijkheden uitgesloten. Dit beperkt het werk met de microscoop omdat reeds op voorhand geweten is naar welke insluitsels gezocht moet worden.

Table of abbreviations

A.U.	Arbitrary Units
EDXRF	Energy Dispersive X-Ray Fluorescence
IQR	Interquartile Range
NIR	Near-infrared (light)
PIXE	Particle Induced X-Ray Emission
PMT	Photomultiplier Tube
UV	Ultraviolet (light)
Vis	Visible (light)

Appendix 1: Sample names

Sample	number of stones measured	Origin
A0442	1	India
A0912	1	Mong Hsu (Myanmar) (borax-treated)
A0916	1	Mong Hsu (Myanmar) (borax-treated)
A0955	7	Qui Chau (Vietnam)
A0996	1	Myanmar
A1000	1	Verneuil (heat treated)
A1463-1468	5	Mong Hsu (Myanmar) (borax-treated)
A1545	1	Chatham
A1628	1	Verneuil (heat treated)
A1661	1	Mong Hsu (Myanmar) (borax-treated)
A1662	1	Mong Hsu (Myanmar) (borax-treated)
A1778	1	Tairus
A1781	1	Tairus
A1964	1	Verneuil
A3789	1	Thailand
A3969	1	Mong Hsu (Myanmar) (borax-treated)
A3972	1	Mong Hsu (Myanmar) (borax-treated)
A3973	1	Mong Hsu (Myanmar) (borax-treated)
A4448	1	Verneuil
A4522	1	Chatham
E001	2	Verneuil
E003	6	India
E004	2	Sri Lanka
E005	10	Kenya
G001	1	Luc Yen (Vietnam)
G002	1	Madagascar
G003	1	Mogok (Myanmar)
G004	1	Luc Yen (Vietnam)
G005	1	Madagascar
G006	1	Mogok (Myanmar)
G007	*	Pailin (Cambodia)
G008	1	Madagascar (lead glass-treated)
G009	1	Qui Chau (Vietnam)
G010	1	Sagin Town (Myanmar)
G011	2	Luc Yen (Vietnam)
G012	1	Luc Yen (Vietnam)
G014	3	Madagascar
G015	15	Madagascar
G016	3	Mogok (Myanmar)
G017	7	Mogok (Myanmar)
G018	11	Sagin Town (Myanmar)

G019	15	Pailin (Cambodia)
G020	2	Qui Chau (Vietnam)
G021	*	Qui Chau (Vietnam)
IQ01	5	India
IQ02	11	Chimwadzulu (Malawi)
IQ03	13	Luc Yen (Vietnam)
IQ04	12	Yegdalek (Afghanistan)
IQ05	10	Moragoro (Tanzania)
IQ06	*	Not specified (lead glass-treated)
IQ07	5	Mogok (Myanmar)
IQ08	2	Verneuil
IQ09	1	Chatham
IQ10	1	Lechleitner
IQ11	3	Knischka
IQ12	1	Czochralski
IQ13	2	Pinky Trade (floating zone)
IQ14	1	USA (floating zone)
IQ15	4	Ramaura
IQ16	3	Douros
IQ17	4	Kashan
IQ18	2	Pinky Trade (hydrothermal)
KB01	1	Luc Yen (Vietnam)
KB02	3	Verneuil
KB03	*	Star ruby
PT01	*	Thailand (different origin likely)
PT02	*	Myanmar
PT03	*	Star ruby
PT04	1	Verneuil

Stones with a "*" for the number of stones measured have been measured, but were not included in the box plots. This occurred either because the origin appeared to be unknown or the assumed origin seemed unlikely based on other measurements of the same origin. The star rubies are also not included as they are a completely different type of ruby that can be classified on sight.

Meaning of the letter-code in the sample labels:

- A: "Academie voor Mineralogie" (ACAM) via Guido Crauwels
- E: "Departement Geologie" (200E) via Jan Elsen
- G: Guido Crauwels
- IQ: Ivo Quintens
- KB: Koen Binnemans
- PT: Paul Tambuyser

Appendix 2: Extra Emission graphs

All extra graphs given in this appendix show the emission with excitation at 400 nm.

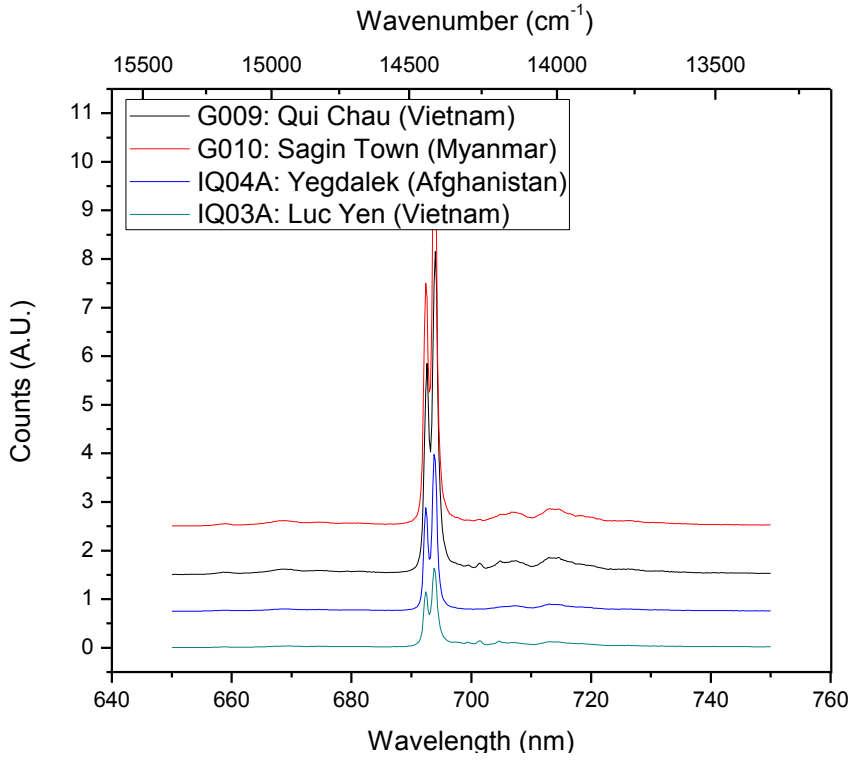

Figure 38. Extra emission spectra of marble-hosted rubies.

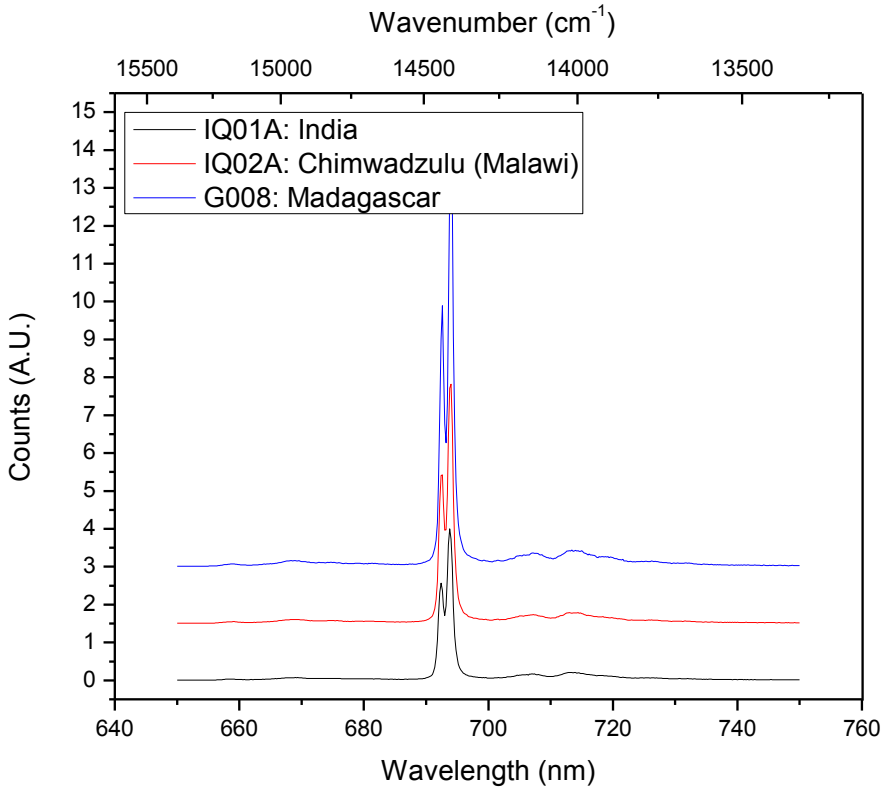

Figure 39. Extra emission spectra of metasomatic rubies.

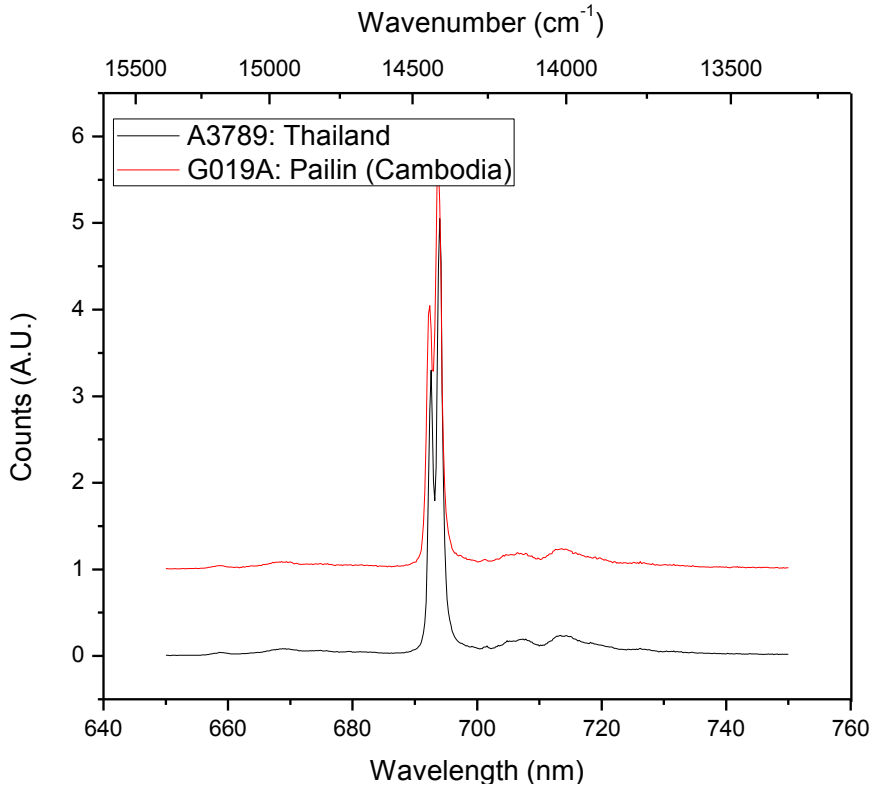

Figure 40. Extra emission spectra of basalt-hosted rubies.

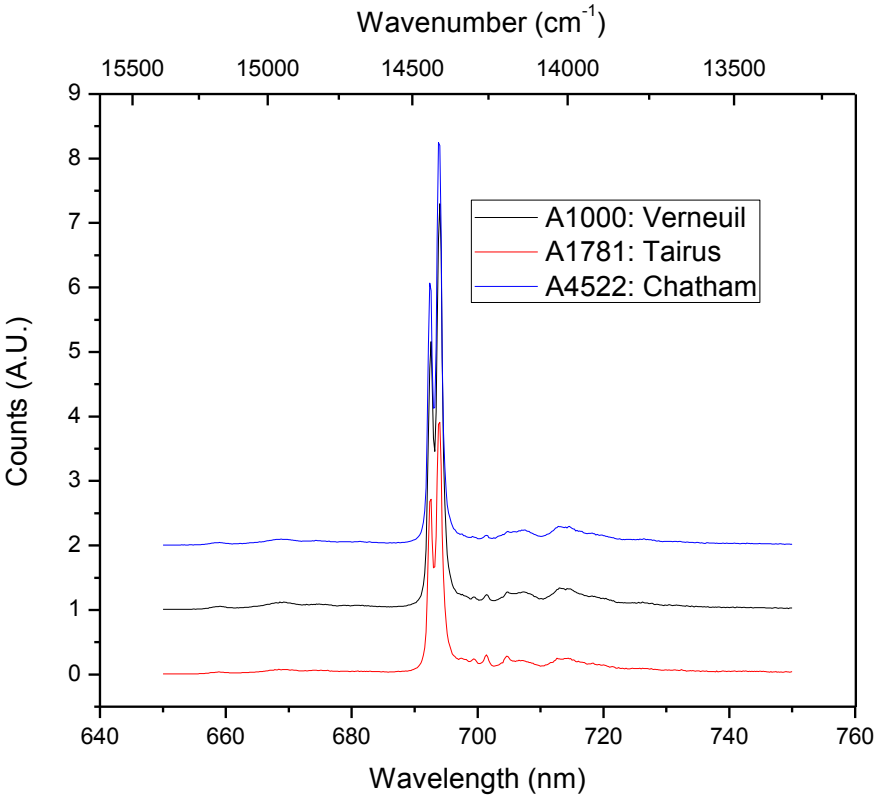

Figure 41. Extra emission spectra of synthetic rubies.

Appendix 3: Extra Excitation graphs

All extra graphs given in this appendix show the excitation measured at 694 nm.

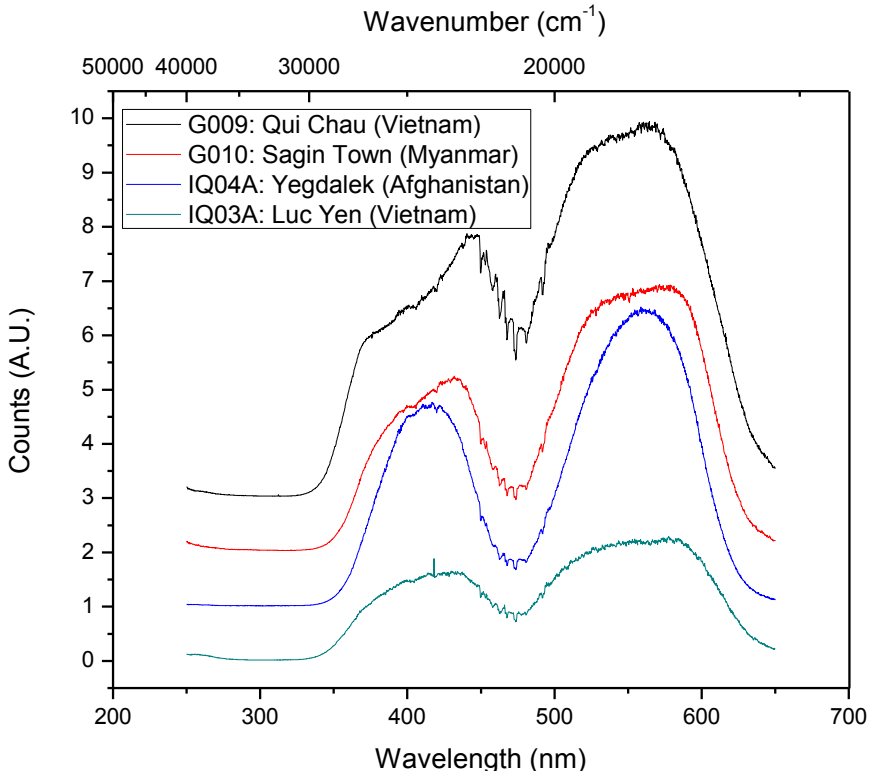

Figure 42. Extra excitation spectra of marble-hosted rubies.

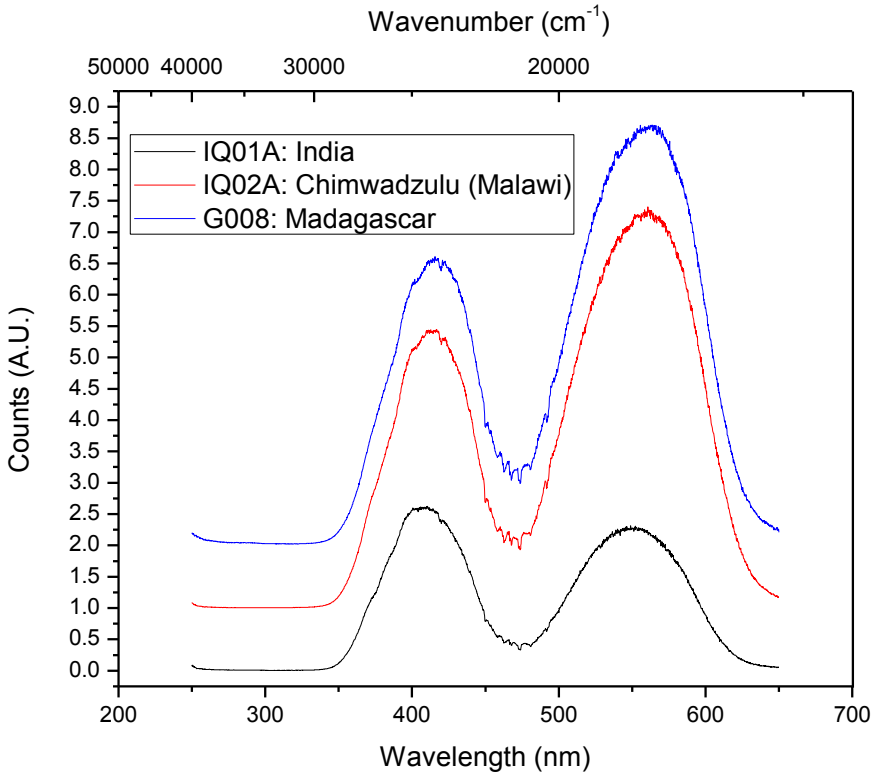

Figure 43. Extra excitation spectra of metasomatic rubies.

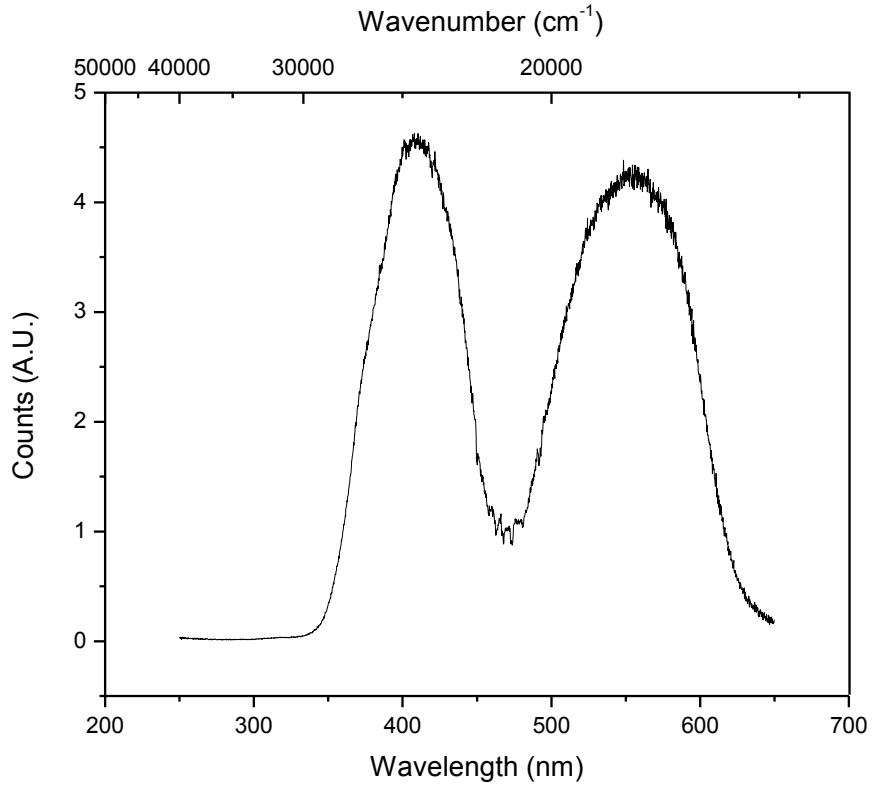

Figure 44. Excitation spectrum of G019: Pailin (Cambodia) as an example for basalt-hosted rubies.

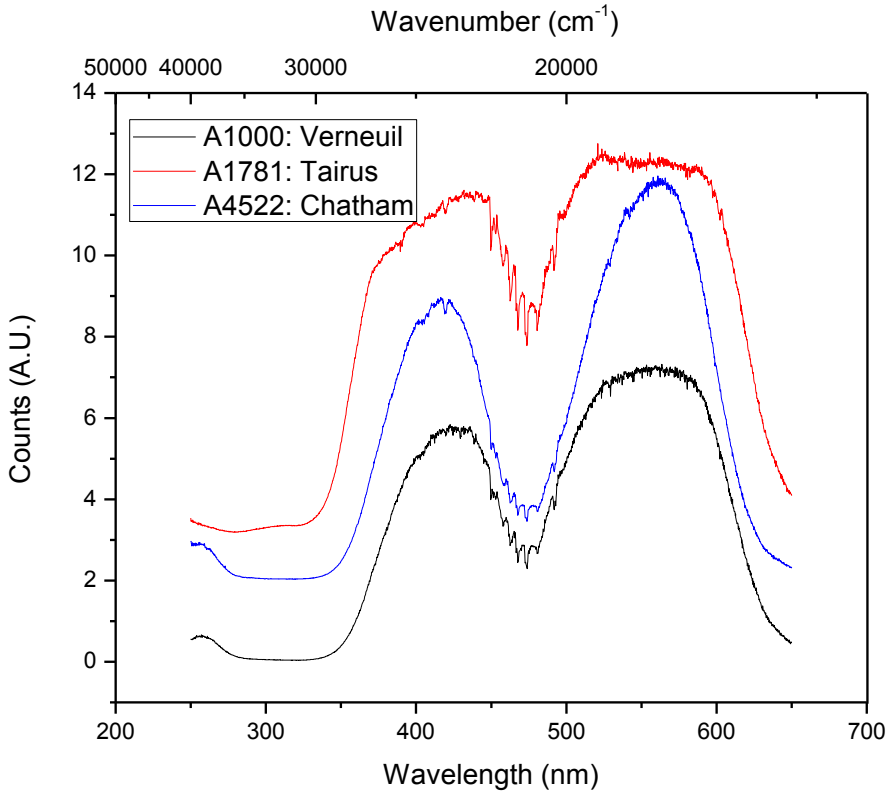

Figure 45. Extra excitation spectra of synthetic rubies.

Appendix 4: Decay time graphs

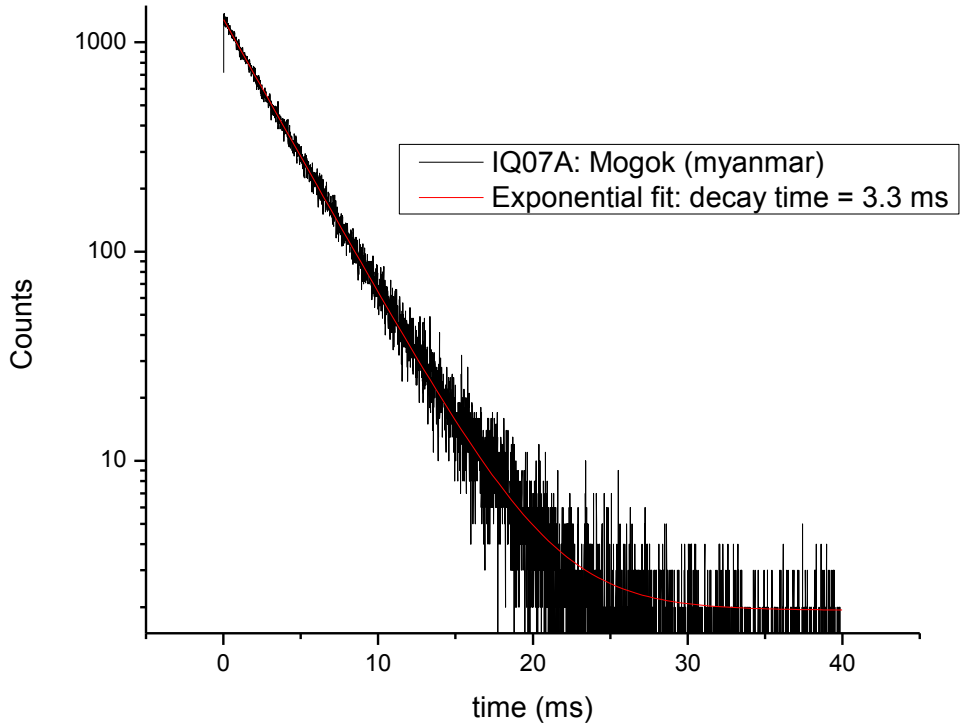

Figure 46. Decay time measurement of IQ07A: Mogok (Myanmar) fitted to equation (1) as an example for rubies with a relatively long decay time.

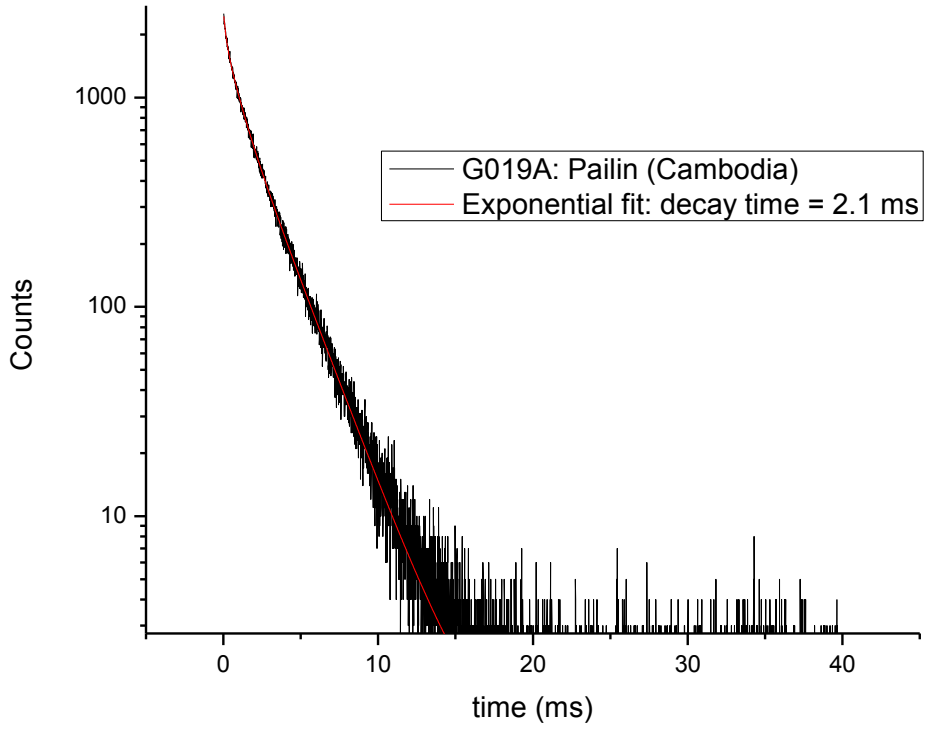

Figure 47. Decay time measurement of G019A: Pailin (Cambodia) fitted to equation (1) as an example for rubies with a relatively short decay time.

Appendix 5: Extra Absorption graphs

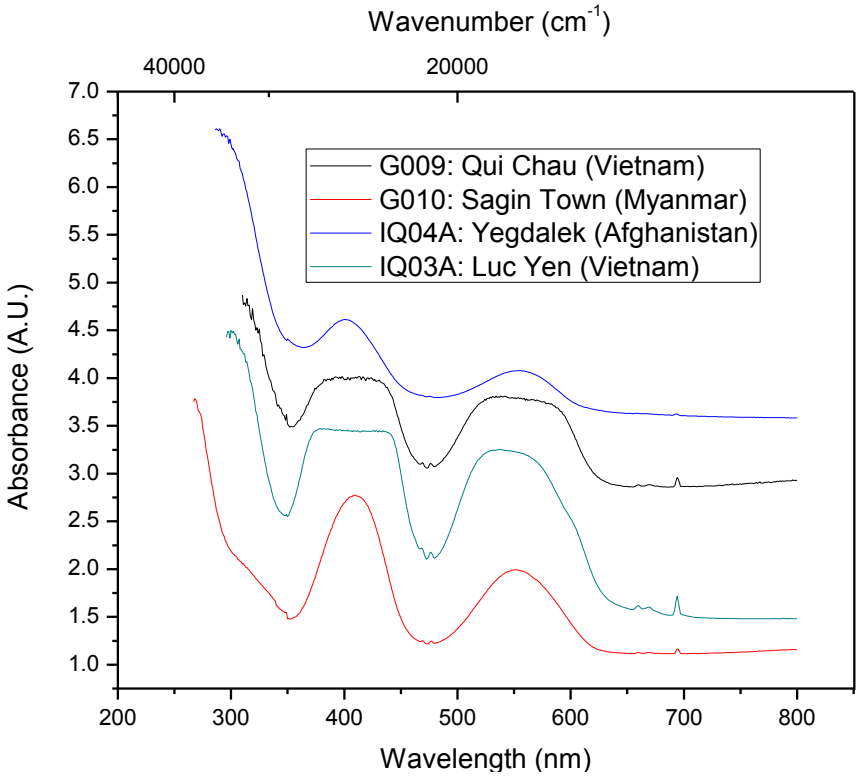

Figure 48. Extra absorption spectra of marble-hosted rubies.

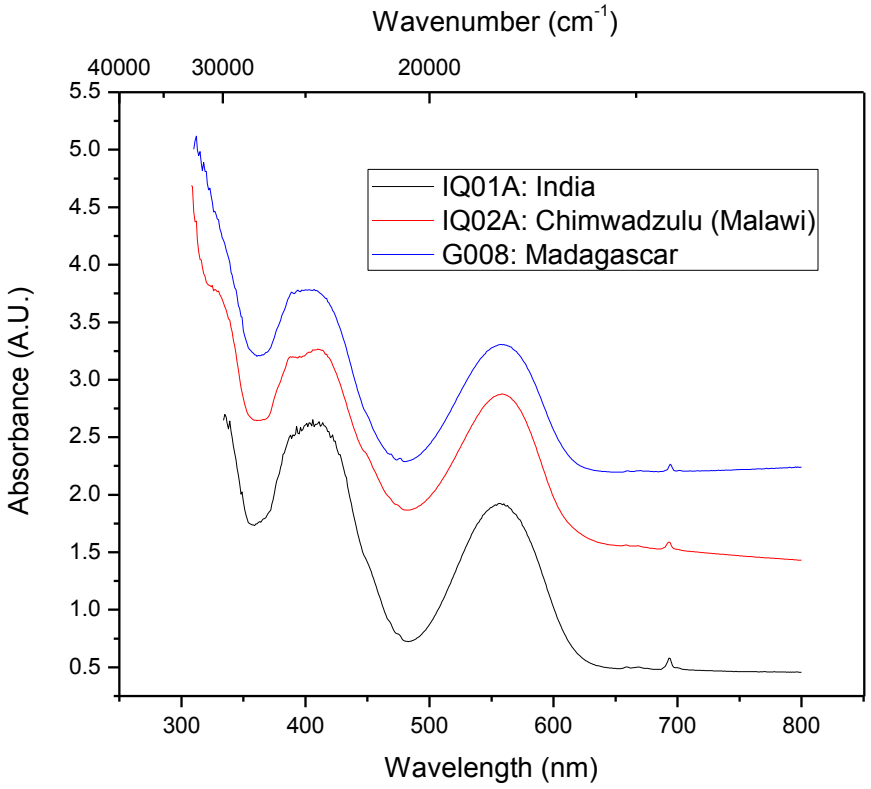

Figure 49. Extra absorption spectra of metasomatic rubies.

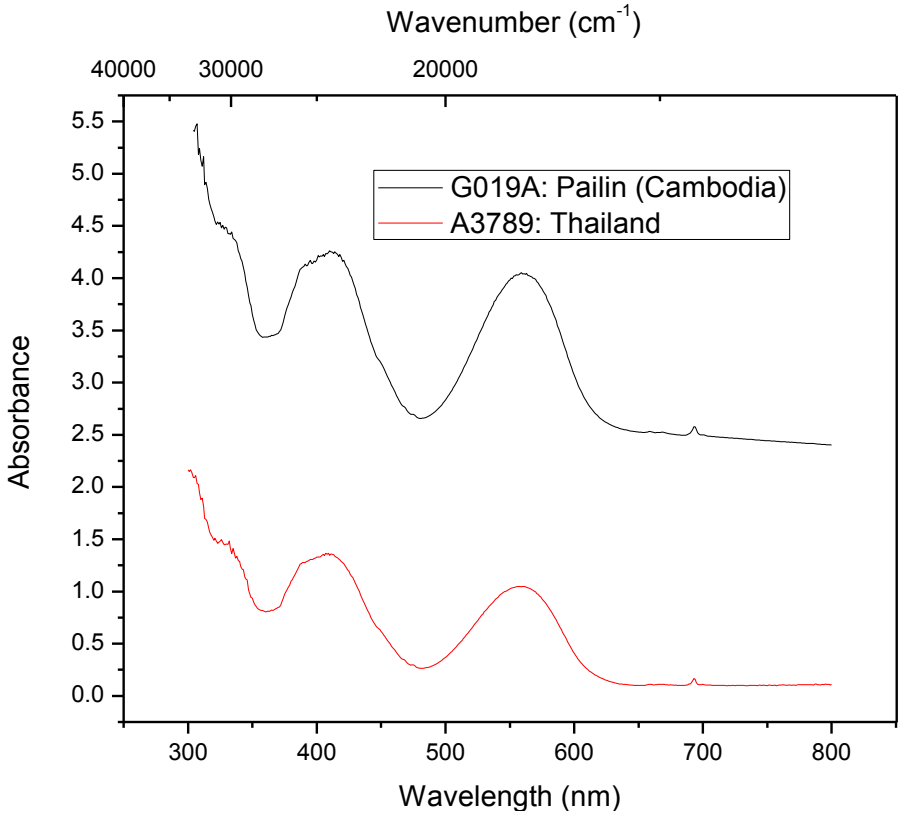

Figure 50. Extra absorption spectra of basalt-hosted rubies.

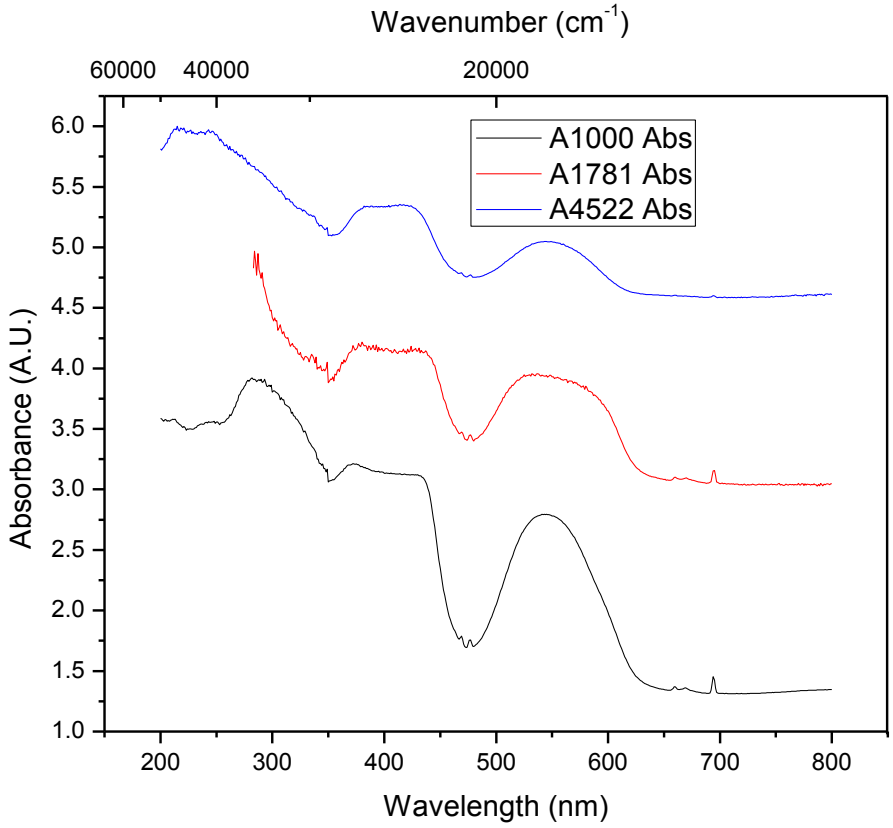

Figure 51. Extra absorption spectra of synthetic rubies.

Appendix 6: Extra Excitation-Emission maps

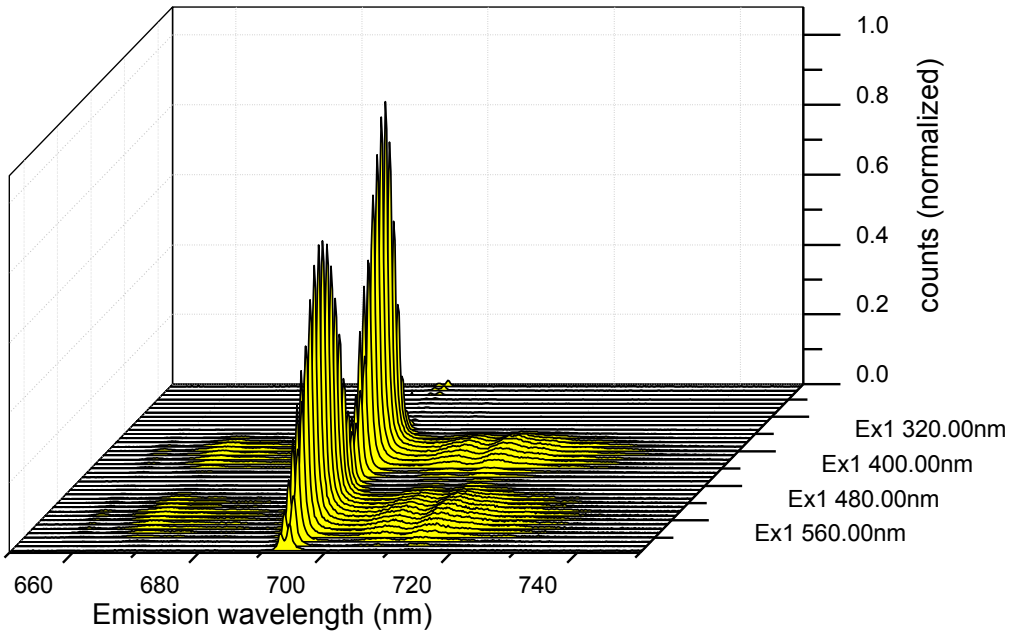

Figure 52. Excitation-Emission map of G004: Luc Yen (Vietnam), marble-hosted ruby.

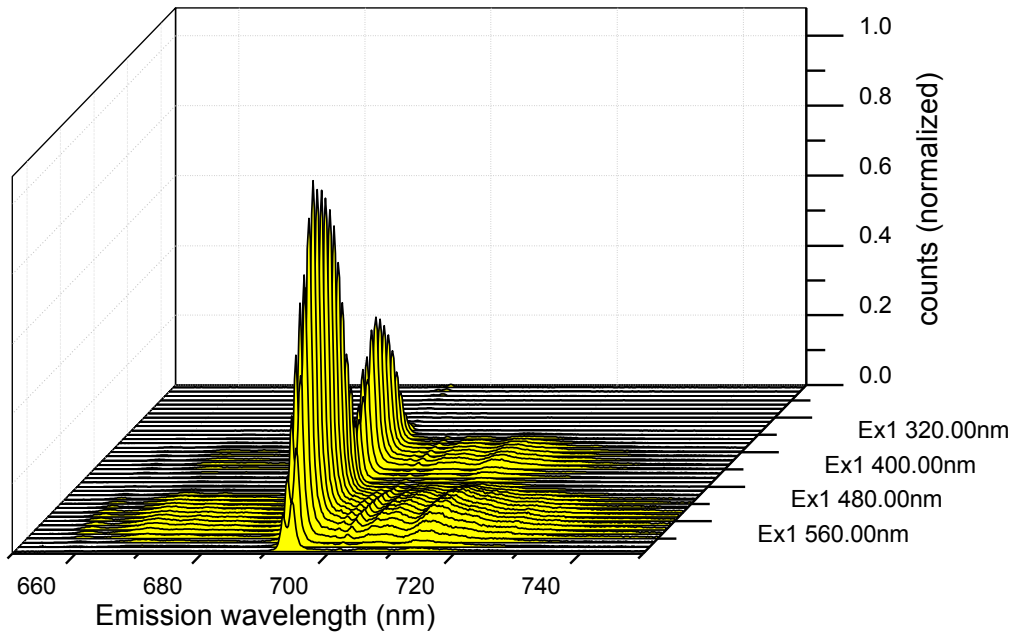

Figure 53. Excitation-Emission map of G006: Mogok (Myanmar), marble-hosted ruby.

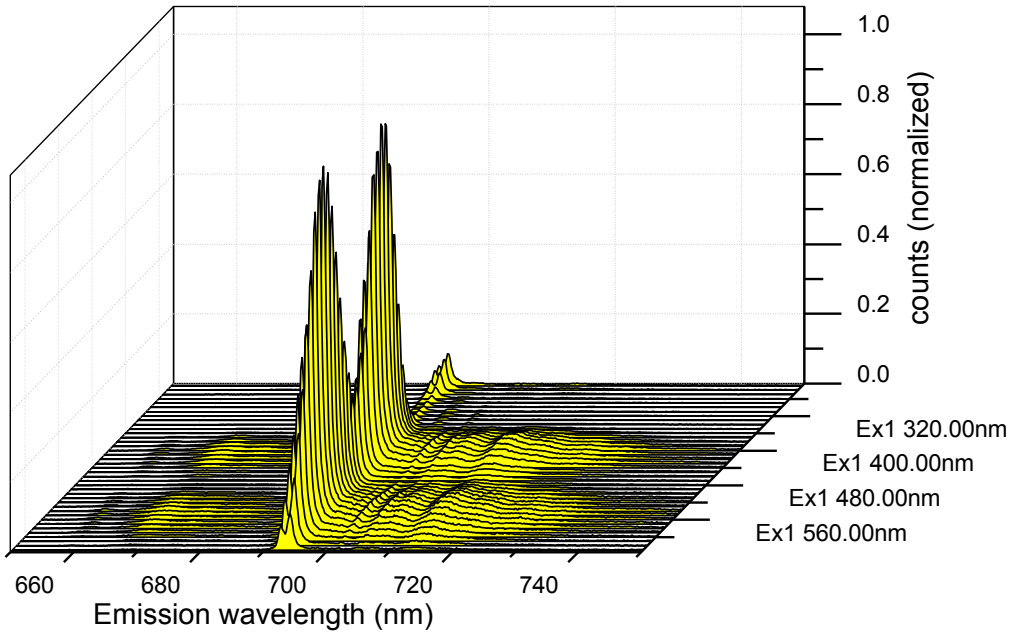

Figure 54. Excitation-Emission map of A3972: Mong Hsu (Myanmar), marble-hosted ruby, borax-treated.

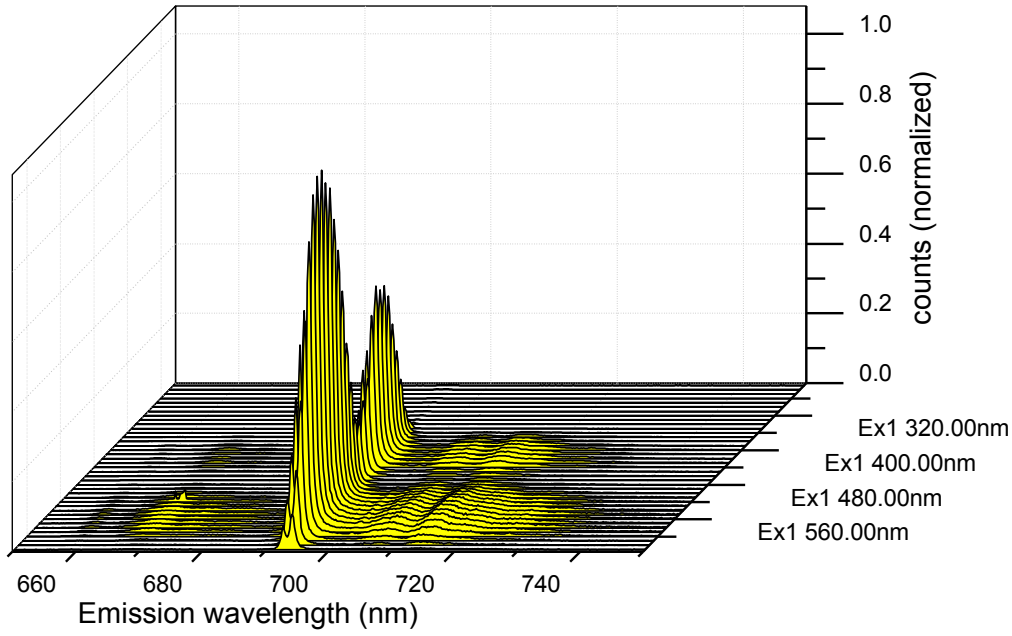

Figure 55. Excitation-Emission map of A0442: India, metasomatic ruby.

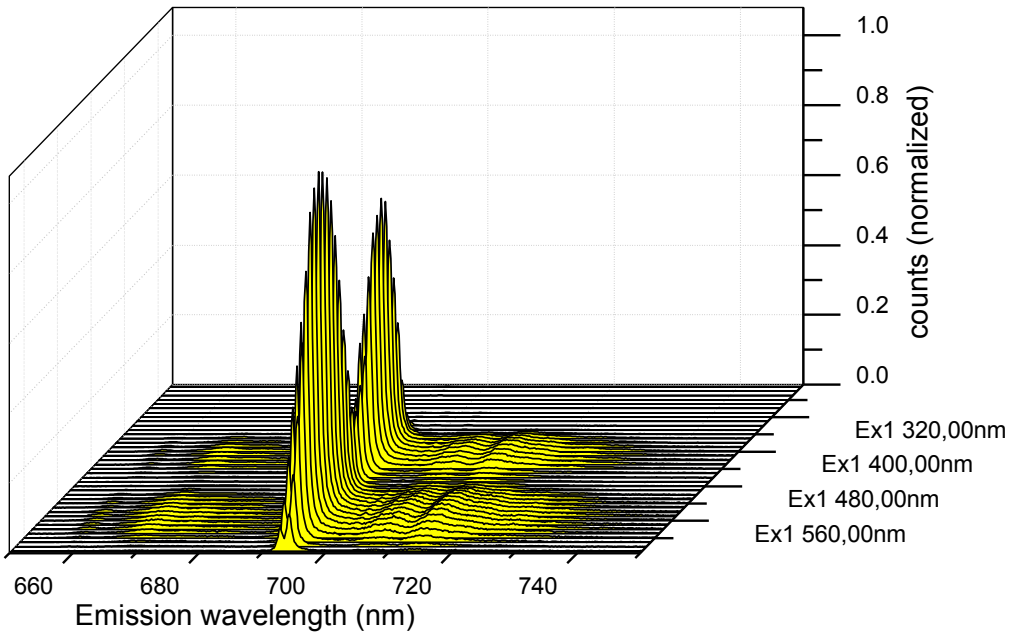

Figure 56. Excitation-Emission map of A3789: Thailand, basalt-hosted ruby.

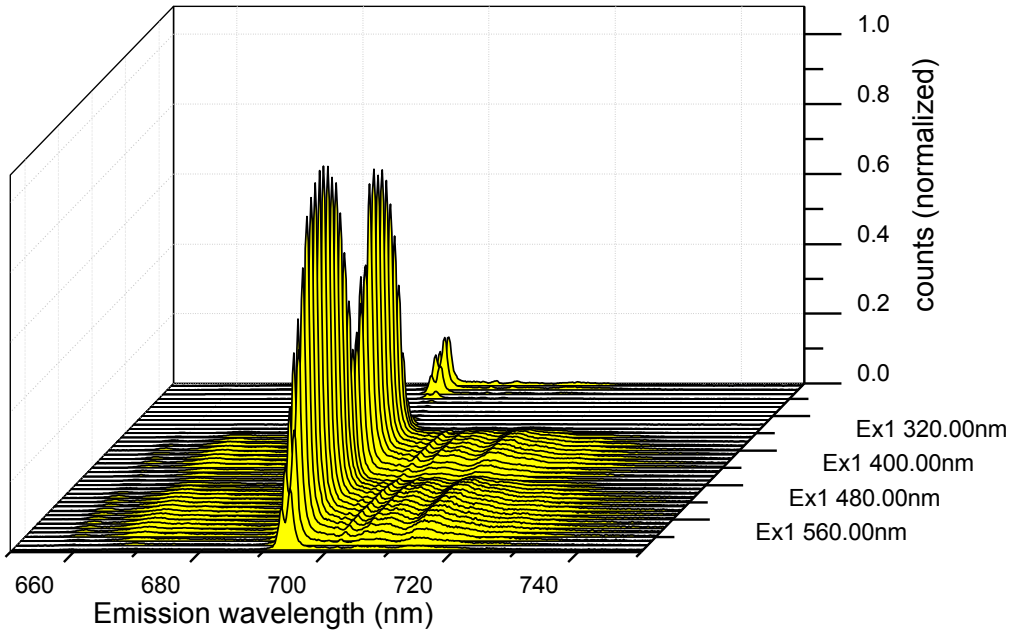

Figure 57. Excitation-Emission map of A1000: Verneuil (melt), synthetic ruby.

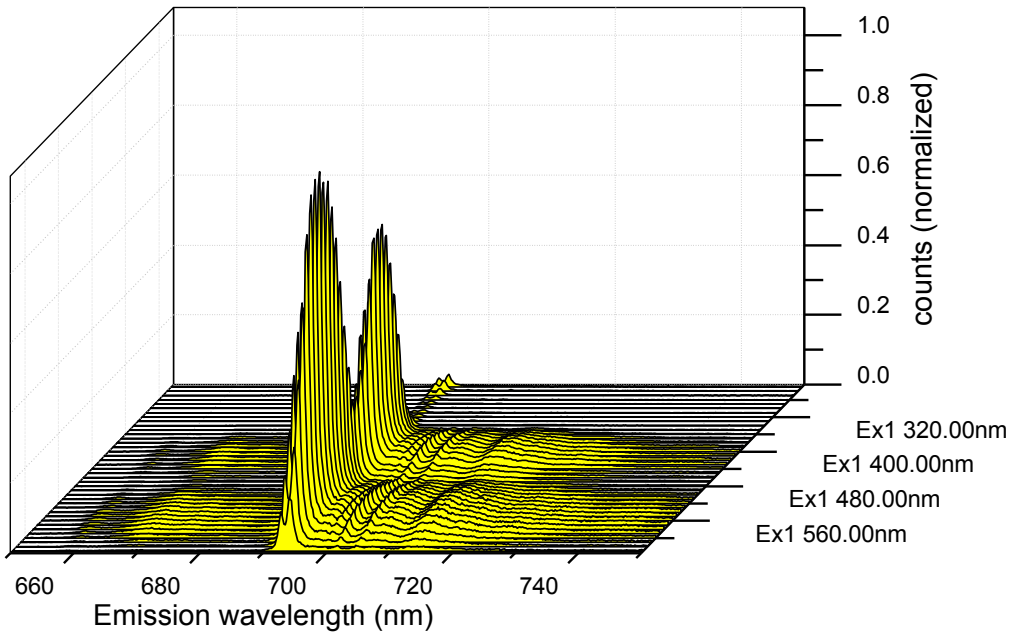

Figure 58. Excitation-Emission map of A1781: Tairus (hydrothermal), synthetic ruby.

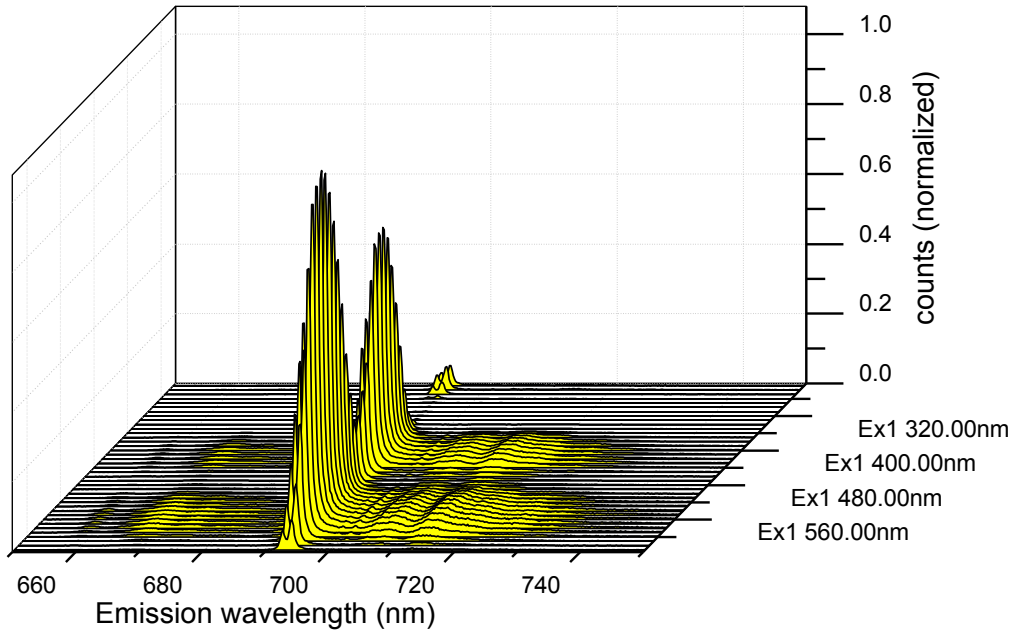

Figure 59. Excitation-Emission map of A4522: Chatham (flux), synthetic ruby.

Appendix 7: Decay time fitting results

Sample	τ1	τ1%	τ2	τ2%	τ3	τ3%	χ^2
A0442	0.91820	(8.4%)	3.15779	(91.6%)			1.391
A0912	0.62919	(1.5%	3.58567	(98.5%)			1.045
A0916	0.72709	(1.4%)	3.72482	(98.6%)			1.022
A0955A	3.42514	(100.0%)					1.036
A0955B	3.64829	(100.0%)					1.111
A0955C	3.73196	(100.0%)					1.144
A0955D	3.38925	(100.0%)					0.993
A0955E	0.90766	(1.8%)	3.59990	(98.2%)			1.048
A0955F	3.68727	(100.0%)					1.146
A0955G	0.81358	(1.7%)	3.58947	(98.3%)			1.088
A0996	3.30034	(100.0%)					1.237
A1000	3.71265	(100.0%)					1.135
A1463	1.13746	(2.2%)	3.77994	(97.8%)			2.414
A1464	0.57236	(1.0%)	3.52238	(99.0%)			1.031
A1465	0.90199	(6.6%)	2.91818	(93.4%)			1.032
A1467	0.98283	(1.9%)	3.50227	(98.1%)			1.035
A1468	0.67814	(2.3%)	3.43976	(97.7%)			1.010
A1545	3.86630	(100.0%)					2.141
A1628	4.50364	(100.0%)					1.202
A1661	0.79213	(2.5%)	3.31530	(97.5%)			1.024
A1662	1.08172	(3.4%)	3.37660	(96.6%)			0.972
A1778	1.19968	(6.4%)	3.39113	(93.6%)			1.159
A1781	1.27103	(9.0%)	3.20777	(91.0%)			1.087
A1964	0.78483	(1.5%)	2.99709	(98.5%)			0.993
A3789	0.19480	(2.0%)	1.01963	(16.8%)	2.53212	(81.2%)	1.237
A3969	0.88968	(4.0%)	3.30412	(96.0%)			0.993
A3972	0.67271	(1.5%)	3.50019	(98.5%)			1.083
A3973	1.20602	(5.3%)	3.25028	(94.7%)			1.246
A4448	1.64288	(4.6%)	4.20187	(95.4%)			1.305
A4522	3.62448	(100.0%)					1.068
E001A	3.88181	(100.0%)					1.082
E001B	4.15701	(100.0%)					1.146
E003A	0.92428	(5.8%)	3.09768	(94.2%)			0.985
E003B	0.85437	(7.1%)	3.03964	(92.9%)			0.945
E003C	0.16143	(0.8%)	1.12647	(11.7%)	2.88185	(87.5%)	1.030
E003D	0.77223	(6.0%)	2.99215	(94.0%)			0.993
E003E	0.79669	(6.4%)	3.00162	(93.6%)			1.027
E003F	0.71945	(8.2%)	2.67377	(91.8%)			0.964
E004A	0.77828	(1.4%)	3.56144	(98.6%)			0.991
E004B	0.76130	(1.2%)	3.44935	(98.8%)			1.069
E005A	0.17699	(3.9%)	0.94501	(35.0%)	2.17116	(61.1%)	0.998

E005B	0.16545	(1.7%)	0.96028	(19.9%)	2.36551	(78.4%)	0.975
E005C	0.22663	(3.2%)	0.99096	(22.2%)	2.23701	(74.6%)	0.973
E005D	0.19877	(3.4%)	0.97435	(27.2%)	2.13520	(69.4%)	0.984
E005E	0.23675	(3.3%)	1.05673	(21.3%)	2.28822	(75.4%)	0.945
E005F	0.17878	(2.8%)	0.92056	(22.8%)	2.11269	(74.4%)	0.869
E005G	0.13817	(2.3%)	0.79960	(22.0%)	2.02798	(75.7%	0.902
E005H	0.19925	(4.0%)	0.93080	(29.5%)	2.04494	(66.5%)	0.929
E005I	0.21680	(3.3%)	1.06831	(26.4%)	2.29546	(70.3%)	0.981
E005J	0.24744	(4.1%)	1.07874	(27.1%)	2.23638	(68.8%)	0.964
G001	4.68590	(100.0%)					2.375
G002	0.25241	(2.2%)	1.06675	(15.4%)	2.50804	(82.4%)	1.231
G003	3.44615	(100.0%)					1.313
G004	3.61682	(100.0%)					2.658
G005	0.19400	(1.0%)	1.00817	(12.4%)	2.67286	(86.6%)	1.040
G006	3.64512	(100.0%)					1.146
G007A	1.05061	(1.3%)	3.79345	(98.7%)			1.181
G007B	1.27919	(2.5%)	3.59717	(97.5%)			1.103
G007C	0.88360	(1.3%)	3.42002	(98.7%)			1.047
G007D	0.41546	(0.5%)	3.55347	(99.5%)			1.059
G007E	1.08427	(3.5%)	3.39327	(96.5%)			1.118
G007F	0.72145	(1.0%)	3.60594	(99.0%)			1.062
G007G	0.84597	(1.0%)	3.76524	(99.0%)			1.103
G008	0.64441	(5.0%)	2.89348	(95.0%)			1.048
G009	0.81280	(1.0%)	3.82610	(99.0%)			1.120
G010	3.62903	(100.0%)					1.150
G011A	0.89510	(1.0%)	3.62978	(99.0%)			1.105
G011B	1.30849	(1.9%)	3.65821	(98.1%)			1.035
G012	4.07624	(100.0%)					1.044
G014A	0.27694	(1.8%)	1.17697	(11.8%)	2.78579	(86.4%)	1.028
G014B	0.20433	(1.5%)	1.10708	(14.8%)	2.64099	(83.7%	1.038
G014C	0.20113	(2.6%)	1.02862	(21.6%)	2.36481	(75.8%)	1.065
G015A	0.70215	(2.0%)	3.26963	(98.0%)			1.027
G015B	0.61025	(3.6%)	3.00844	(96.4%)			0.956
G015C	0.75087	(2.1%)	3.23601	(97.9%)			0.991
G015D	0.23513	(1.5%)	1.10149	(10.3%)	2.85568	(88.2%)	0.970
G015E	0.68692	(3.5%)	3.12797	(96.5%)			1.008
G015F	0.66815	(1.5%)	3.32204	(98.5%)			1.055
G015G	0.20814	(1.2%)	1.10467	(8.9%)	2.92403	(89.9%)	1.060
G015H	0.65197	(4.1%)	3.06699	(95.9%)			0.997
G015I	0.60965	(0.9%)	3.39967	(99.1%)			1.029
G015J	0.66047	(1.9%)	3.24204	(98.1%)			1.022
G015K	0.71669	(3.7%)	3.12194	(96.3%)			0.995
G015L	0.88548	(2.5%)	3.28325	(97.5%)			1.055
G015M	0.77681	(2.5%)	3.25252	(97.5%)			1.047
G015N	0.73592	(1.7%)	3.29839	(98.3%)			1.040
G015O	0.65558	(4.3%)	3.03210	(95.7%)			1.011
G016A	3.64095	(100.0%)					1.144

G016B	1.02664	(1.2%)	3.59069	(98.8%)			1.113
G016C	1.55917	(4.0%)	3.83059	(96.0%)			1.155
G017B	0.69618	(2.0%)	3.39420	(98.0%)			0.951
G017C	3.42015	(100.0%)					1.140
G017D	0.57036	(1.0%)	3.78499	(99.0%)			1.135
G017E	3.45846	(100.0%)					1.188
G017F	3.57151	(100.0%)					1.109
G017G	3.69966	(100.0%)					1.035
G017H	0.63755	(2.5%)	3.22452	(97.5%)			0.952
G018A	3.62560	(100.0%)					1.140
G018B	3.60810	(100.0%)					1.137
G018C	3.83014	(100.0%)					1.162
G018D	3.57901	(100.0%)					1.152
G018E	3.76088	(100.0%)					1.186
G018F	0.91516	(6.0%)	3.01321	(94.0%)			1.076
G018G	3.53553	(100.0%)					1.118
G018H	3.58942	(100.0%)					1.145
G018I	3.43126	(100.0%)					1.019
G018J	0.93030	(3.5%)	3.25904	(96.5%)			1.064
G018K	0.94782	(3.2%)	3.25850	(96.8%)			0.970
G019A	0.15396	(2.3%)	0.80486	(17.5%)	2.22978	(80.2%)	0.825
G019B	0.16804	(5.3%)	0.77589	(26.7%)	1.88954	(68.0%)	0.804
G019C	0.25264	(3.6%)	1.20818	(20.4%)	2.60498	(76.0%)	1.063
G019D	0.24395	(3.8%)	1.10731	(21.9%)	2.42778	(74.3%)	1.068
G019E	0.14048	(1.0%)	0.86033	(9.6%)	2.74521	(89.4%)	0.945
G019F	0.19520	(3.8%)	0.95119	(27.8%)	2.15058	(68.4%)	1.014
G019G	0.16186	(4.5%)	0.82031	(27.7%)	2.02793	(67.8%)	0.976
G019H	0.17527	(3.5%)	0.91580	(25.2%)	2.21599	(71.3%)	0.955
G019I	0.15738	(2.0%)	0.88394	(17.8%)	2.43916	(80.2%)	0.903
G019J	0.19180	(4.2%)	0.91665	(24.7%)	2.19253	(71.1%)	0.937
G019K	0.17712	(3.6%)	0.85861	(21.8%)	2.21245	(74.6%)	0.840
G019L	0.17619	(2.5%)	0.92068	(19.5%)	2.35182	(78.0%)	0.957
G019M	0.22095	(2.6%)	1.08069	(18.8%)	2.52628	(78.6%)	1.013
G019N	0.13292	(1.4%)	0.93770	(14.9%)	2.60553	(86.7%)	0.892
G019O	0.17074	(3.3%)	0.89323	(24.0%)	2.15446	(72.7%)	0.955
G020A	0.93664	(2.8%)	3.34099	(97.2%)			1.076
G020B	1.17106	(2.7%)	3.60073	(97.3%)			1.139
G021A	1.68667	(4.7%)	3.83169	(95.3%)			1.050
G021B	0.75892	(1.0%)	3.62238	(99.0%)			1.039
G021C	0.90289	(1.1%)	3.80031	(98.9%)			0.975
G021D	0.26996	(3.2%)	1.06981	(37.4%)	2.50275	(59.4%)	0.931
G021E	3.48644	(100.0%)					0.980
G021F	0.90023	(3.3%)	3.24599	(96.7%)			1.101
G021G	0.18067	(0.5%)	0.96331	(9.3%)	2.68275	(90.2%)	0.911
G021H	1.45241	(2.0%)	3.69287	(98.0%)			1.090
IQ01A	0.20710	(3.0%)	1.05652	(18.5%)	2.54492	(78.5%)	0.997
IQ01B	0.18796	(3.6%)	0.91980	(22.4%)	2.24638	(74.0%)	0.916

IQ01C	0.21512	(4.4%)	0.98490	(26.4%)	2.20534	(69.2%)	0.967
IQ01D	0.21153	(2.7%)	1.12724	(18.5%)	2.63080	(78.8%)	1.019
IQ01E	0.20809	(3.4%)	1.01810	(20.3%)	2.46359	(76.3%)	0.975
IQ02A	0.30997	(3.2%)	1.38381	(20.4%)	2.75750	(76.4%)	1.093
IQ02B	0.24935	(2.1%)	1.25173	(15.2%)	2.81353	(82.7%)	1.043
IQ02C	0.23438	(2.0%)	1.17443	(14.0%)	2.80705	(84.0%)	1.094
IQ02D	0.21238	(1.9%)	1.07400	(13.3%)	2.71575	(84.8%)	0.973
IQ02E	0.19894	(1.1%)	1.00000	(8.6%)	2.85059	(90.3%)	1.070
IQ02F	0.21329	(1.7%)	1.05625	(13.9%)	2.67688	(84.4%)	1.068
IQ02G	0.24292	(1.7%)	1.14237	(11.8%)	2.71313	(86.5%)	1.088
IQ02H	0.21543	(2.4%)	1.17466	(14.9%)	2.64411	(82.7%)	1.048
IQ02I	0.19626	(3.0%)	0.99078	(20.6%)	2.42542	(76.4%)	0.958
IQ02J	0.23160	(2.2%)	1.11488	(16.1%)	2.61561	(81.7%)	1.023
IQ02K	0.18410	(3.0%)	0.92427	(20.6%)	2.34086	(76.4%)	0.892
IQ03A	1.08308	(3.4%)	3.33920	(96.6%)			1.133
IQ03B	1.20156	(9.3%)	2.95757	(90.7%)			0.982
IQ03C	0.74348	(2.2%)	3.19404	(97.8%)			1.001
IQ03D	0.61168	(0.8%)	3.43974	(99.2%)			1.074
IQ03E	3.45672	(100.0%)					1.057
IQ03F	3.54460	(100.0%)					1.082
IQ03G	3.50786	(100.0%)					1.031
IQ03H	3.61481	(100.0%)					1.118
IQ03I	3.38695	(100.0%)					1.069
IQ03J	3.34326	(100.0%)					0.998
IQ03K	3.47102	(100.0%)					0.988
IQ03L	3.29959	(100.0%)					0.840
IQ03M	3.40041	(100.0%)					0.974
IQ04A	3.59498	(100.0%)					1.120
IQ04B	0.91386	(1.7%)	3.48552	(98.3%)			1.100
IQ04C	3.53849	(100.0%)					1.042
IQ04D	3.59467	(100.0%)					1.088
IQ04E	3.55269	(100.0%)					1.059
IQ04F	3.67758	(100.0%)					1.075
IQ04G	3.58970	(100.0%)					1.062
IQ04H	3.42659	(100.0%)					1.056
IQ04I	3.41666	(100.0%)					1.049
IQ04J	0.61875	(1.3%)	3.29794	(98.7%)			0.993
IQ04K	3.61467	(100.0%)					1.143
IQ04L	3.38180	(100.0%)					1.026
IQ05A	3.70790	(100.0%)					1.052
IQ05B	3.56647	(100.0%)					1.103
IQ05C	3.59534	(100.0%)					1.050
IQ05D	3.52151	(100.0%)					1.073
IQ05E	3.44506	(100.0%)					0.959
IQ05F	3.46704	(100.0%)					1.029
IQ05G	3.51853	(100.0%)					1.063
IQ05H	3.51191	(100.0%)					1.054

IQ05I	3.48809	(100.0%)					1.070
IQ05J	0.71421	(3.8%)	2.87396	(96.2%)			0.853
IQ06A	0.55160	(2.0%)	3.08962	(98.0%)			0.974
IQ06B	0.53332	(2.1%)	3.02252	(97.9%)			0.901
IQ06C	0.55193	(7.0%)	2.60514	(93.0%)			0.894
IQ06D	0.54260	(10.8%)	2.19968	(89.2%)			0.812
IQ07A	3.34479	(100.0%)					1.013
IQ07B	3.49709	(100.0%)					0.969
IQ07C	3.57583	(100.0%)					1.013
IQ07D	3.29091	(100.0%)					0.967
IQ07E	3.53536	(100.0%)					0.960
IQ08A	3.80085	(100.0%)					1.144
IQ08B	3.45050	(100.0%)					1.038
IQ09	3.29922	(100.0%)					0.988
IQ10	4.02957	(100.0%)					1.073
IQ11A	3.49252	(100.0%)					0.982
IQ11B	3.65857	(100.0%)					1.051
IQ11C	4.07880	(100.0%)					1.080
IQ12	3.91183	(100.0%)					1.059
IQ13A	0.68163	(2.0%)	2.28957	(98.0%)			0.861
IQ13B	0.92568	(2.6%)	2.63828	(97.4%)			0.940
IQ14	3.50976	(100.0%)					1.006
IQ15A	0.88429	(3.3%)	3.18143	(96.7%)			0.966
IQ15B	0.98462	(4.6%)	3.19310	(95.4%)			1.018
IQ15C	0.87143	(2.1%)	3.46178	(97.9%)			1.080
IQ15D	0.65511	(2.3%)	3.16435	(97.7%)			0.949
IQ16A	0.62935	(1.6%)	3.25823	(98.4%)			1.002
IQ16B	0.68179	(10.2%)	2.53700	(89.8%)			0.863
IQ16C	1.18934	(6.3%)	3.17215	(93.7%)			1.021
IQ17A	0.66595	(1.5%)	3.26826	(98.5%)			1.088
IQ17B	0.37626	(1.2%)	3.08097	(98.8%)			0.885
IQ17C	3.22164	(100.0%)					0.975
IQ17D	3.00203	(100.0%)					0.873
IQ18A	0.70462	(2.6%)	3.04583	(97.4%)			0.897
IQ18B	0.64019	(2.2%)	3.23388	(97.8%)			0.966
KB01	3.53406	(100.0%)					1.025
KB02A	3.73597	(100.0%)					1.119
KB02B	1.95337	(10.0%)	3.87481	(90.0%)			1.124
KB02C	2.11541	(10.7%)	3.89166	(89.3%)			1.177
PT01	0.80267	(1.5%)	3.73357	(98.5%)			1.100
PT02	0.88556	(1.7%)	3.71093	(98.3%)			1.058
PT03	0.18747	(1.4%)	1.12244	(13.8%)	2.68829	(84.8%)	0.968
PT04B	1.91824	(6.2%)	3.95199	(93.8%)			1.176

Reference list

[Ano11] Anonymous, “Tanabe-Sugano diagram”, http://en.wikipedia.org/wiki/Tanabe-Sugano_diagram, Last modified on 17 March **2011**, Accessed on 7 May 2011.

[AgiTec02] Agilent Technologies, “UV-VIS-NIR Varian Cary 4000, 5000 and 6000i Spectrophotometers Preliminary Performance Data”, **2002**.

[AgiTec04] Agilent Technologies, “Info Brochure: UV-VIS-NIR Varian Cary 4000, 5000 and 6000i Spectrophotometers”, **2004**.

[Bos82] G. Bosshart, M. Sc., G.G., “Distinction of Natural and Synthetic Rubies by Ultraviolet Spectrophotometry”, *J. Gemm*., **1982**, *18*, 145-160.

[Coe92] R. R. Coenraads, “Surface features on natural rubies and sapphires derived from volcanic provinces”, *J. Gemmol*., **1992**, *23*, 151-160.

[CoeVic95] R. R. Coenraads, P. Vichit, F. L. Sutherland, “An unusual sapphire-zircon-magnetite xenoliths from the Chanthaburi gem province, Thailand”, *Mineral. Mag*., **1995**, *59*, 465-479.

[EdiIns03] Edinburgh Instruments, “Info Brochure: Steady State and Time Resolved Fluorescence Spectrometers”, **2003**.

[EdiInsXe900] Edinburgh Instruments, “Operating Instructions: Xe 900 450W Xenon Arc Lamp”, **2000**, Issue 2.

[EdiInsM300] Edinburgh Instruments, “Operating Instructions: M300 Monochromator”, **2000**, Issue 2.

[EdiInsS900] Edinburgh Instruments, “Operating Instructions: S900 Single Photon Photomultiplier Detection System”, **2000**, Issue 3.

[Elw79] D. Elwell, “Man-Made Gemstones”, *Ellis Horwood Ltd., Publishers*, Chichester, **1979**.

[GuoORe96a] J. Guo, S. Y. O’Reilly, W. L. Griffin, “Corundum from basaltic terrains: A mineral inclusion approach to the enigma”, *Contrib. Mineral. Petrol.*, **1996**, *122*, 368-386.

[GuoORe96b] J. Guo, S. Y. O’Reilly, W. L. Griffin, “Zircon inclusions in corundum megacrysts: I. Trace element geochemistry and clues to the origin of corundum megacrysts in alkali basalts”, *Geochim. Cosmochim. Acta*, **1996**, *60*, 2347-2363.

[HooThe91] D.B. Hoover, A. F. Theisen, “Fluorescence Excitation-Emission Spectra of Chromium-Containing Gems: An explanation for the effectiveness of the crossed filter method”, *Aust. Gemmol.*, **1993**, *May*, 182-186.

[Hug97] R. W. Hughes, “Ruby & Sapphire”, *RWH Publishing, Boulder*, Colorado, **1997**.

[IngCro88] J. D. Ingle, Jr., S. R. Crouch, “Spectrochemical Analysis”, *Prentice Hall, Englewood Cliffs*, New Jersey, **1988**.

[Kus66] T. Kushida, “Absorption Spectrum of Optically Pumped Ruby I. Experimental Studies of Spectrum in Excited States”, *J. Phys. Soc. Jpn*., **1966**, *21*, 1331-1341.

[LapIac91] D. Lapraz, P. Iacconi, D. Daviller, and B. Guihot, “Thermostimulated Luminescence and Fluorescence of α-Al_2O_3: Cr^{3+} Samples (Ruby)”, *Phys. Stat. Sol. (a)*, **1991**, *126*, 521-531.

[Leb11] M. Leblanc, “Classical methods of elaboration”, http://ressources.univ-lemans.fr/AccesLibre/UM/Pedago/chimie/01/divers/elaboration/elab2_2.pdf, Accessed on 21 May **2011**.

[Low60] W. Low, “Absorption Lines of Cr^{3+} in Ruby”, *J. Chem. Phys*., **1960**, *33*, 1162-1163.

[MuhFri98] S. Muhlmeister, E. Fritsch, J.E. Shigley, B. Devouard, B. M. Laurs, “Separating Natural and Synthetic Rubies on the Basis of Trace-Element Chemistry”, *Gems & Gemology*, **1998**, *summer*, 80-101.

[OkrBun76] M. Okrusch, T. E. Bunch, H. Bank, “Paragenesis and petrogenesis of a corundum-bearing marble at Hunza [Kashmir]”, *Miner. Deposita*, **1976**, *11*, 278-297.

[RalCha11] J. Ralph, I. Chau,”Mindat: Corundum”, http://www.mindat.org/min-1136.html, Accessed on 4 May **2011**.

[Sch85] K. Schmetzer, “Distinction of natural and synthetic rubies by ultraviolet absorption spectroscopy – possibilities and limitations of the method”, *Z. Dt. Gemmol. Ges.*, **1985**, *34*, 101-129.

[Sch77] D. Schwarz, “Die Bedeutung der Fluoreszenz für die Edelsteinuntersuchung”, *Uhren, Juwelen, Schmuck*, **1977**, *19*, 52-55.

[SkoWes04] D. A. Skoog, D. M. West, F. J. Holler, S. R. Crouch, “Fundamentals of Analytical Chemistry Eighth edition”, *Brooks/Cole-Thomson Learning*, Belmont, **2004**.

[Smi08] B. Smigel, “Optical Properties of Gems” http://www.bwsmigel.info/Lesson4/DE.Optical.Properties.html, Last modified in **2008**, Accessed on 7 May 2011.

[TanTan89] S. M. Tang, S. H. Tang, K. F. Mok, A. T. Retty, and T. S. Tay, “A Study of Natural and Synthetic Rubies by PIXE”, *Appl. Spectrosc*., **1989**, *43*, 219-223.

[The92] T. Themelis, “The Heat Treatment of Ruby and Sapphire”, *Gemlab Inc., Type-egraphics Inc*. USA, **1992**.

[ToyObi98] T. Toyoda, T. Obikawa, T. Shigenari, “Photoluminescence Spectroscopy of Cr^{3+} in ceramic Al_2O_3”, *Mater. Sci. Eng. B*, **1998**, *54*, 33-37.